View metadata, citation and similar papers at core.ac.uk

brought to you by CORE

provided by Università degli Studi di Napoli Federico II Open Archive

UNIVERSITÀ DEGLI STUDI DI NAPOLI FEDERICO II

UNIVERSITÀ DEGLI STUDI DI NAPOLI FEDERICO II

PH.D. THESIS IN

INFORMATION TECHNOLOGY AND ELECTRICAL ENGINEERING

EQUALIZATION OF CPM SIGNALS OVER DOUBLY-SELECTIVE AERONAUTICAL CHANNELS

IVAN IUDICE

TUTOR: PROF. GIACINTO GELLI

XXIX CICLO

SCUOLA POLITECNICA E DELLE SCIENZE DI BASE
DIPARTIMENTO DI INGEGNERIA ELETTRICA E TECNOLOGIE DELL'INFORMAZIONE

Between Ulysses and Achilles,
looking for the beautiful mind

Acknowledgments

Firstly, I would like to express my sincere gratitude to my tutor Prof. Giacinto Gelli for the continuous support of my Ph.D. work and related research, for his patience, motivation, and precious advice. His guidance helped me in all the time of research and writing of this thesis.

My sincere thanks also go to Prof. Francesco Verde and Prof. Donatella Darsena, who allowed me to appreciate the value of working in a collaborative research team.

Moreover, I would like to thank my thesis reviewers, Prof. Stefano Marano and Prof. Stefano Buzzi, for their insightful comments that allowed me to improve my thesis work.

I would like to thank the Italian Aerospace Research Centre (CIRA), which gave access to the laboratories and research facilities, and allowed to increase my knowledge by funding my Ph.D. course. I wish to extend my thanks to all of my colleagues at CIRA who always endured me before deadlines.

I would like to express my appreciation to my friends who have never doubted me and my abilities.

Last but most, I would like to express my sincerest thanks to my parents Lucio and Rosina, and my girlfriend Mariavincenza, for their encouragement, support and unconditional love.

Thank you all!

Ivan Iudice
Electronics and Communications Laboratory
CIRA - Italian Aerospace Research Centre
April 2017

Contents

List of Figures

List of Tables

List of acronyms

ABER	Average Bit-Error Rate
AG	Air-Ground
ARTM	Advanced Range TeleMetry
ASA	Airport Surface Area
ATM	Air Traffic Management
AWGN	Additive White Gaussian Noise
BEM	Basis Expansion Model
CCCF	Cyclic Conjugate Cross-Correlation Function
CCF	Cyclic Cross-Correlation Function
CCM	Cyclic Correlation Matrix
CLT	Central Limit Theorem
CNPC	Control and Not-Payload Communications
CPFSK	Continuous-Phase Frequency Shift Keying
CPM	Continuous-Phase Modulated
DFS	Discrete Fourier Series
FDE	Frequency Domain Equalization
FM	Frequency Modulation
FOT	Fraction-Of-Time

FSK	Frequency-Shift Keying
FRESH	FREquency-SHift
FQPSK	Feher Quadrature Phase-Shift Keying
OQPSK	Offset Quadrature Phase-Shift Keying
SOQPSK	Shaped Offset Quadrature Phase-Shift Keying
GMSK	Gaussian Minimum-Shift Keying
GO	Geometrical Optics
GWSSUS	Gaussian Wide-Sense Stationary Uncorrelated Scattering
ICAO	International Civil Aviation Organization
IRIG	Inter-Range Instrumentation Group
ISI	InterSymbol Interference
LTI	Linear Time-Invariant
LTV	Linear Time-Varying
LOS	Line-Of-Sight
MIMO	Multiple-Input Multiple-Output
ML	Maximum-Likelihood
MMSE	Minimum Mean Square Error
MSE	Mean Square Error
NLOS	Non-Line-Of-Sight
NRZ-L	Non-Return-to-Zero-Level
OFDM	orthogonal frequency domain modulation
PAM	Pulse Amplitude Modulation
PCM	Pulse-Code Modulation
PDF	Probability Distribution Function
PDP	Power Delay Profile

PTV	Periodically Time-Varying
RPAS	Remotely Piloted Aircraft System
SESAR	Single European Sky ATM Research
SNR	Signal-to-Noise Ratio
SOS	Second Order Statistic
TDL	Tapped-Delay Line
TV	Time-Varying
UAS	Unmanned Aerial System
UTD	Uniform Theory of Diffraction
VA	Viterbi Algorithm
VCO	Voltage Controlled Oscillator
VHF	Very High Frequency
WiMAX	Worldwide interoperability for Microwave Access
WLTV	Widely Linear Time-Varying
WSSUS	Wide-Sense Stationary Uncorrelated Scattering
ZF	Zero-Forcing

Basic notations

T	Symbol interval duration
T_{c}	Sampling period
N	Oversampling factor
R_{b}	Bit-rate
$\mathbb{B}$	Set of binary numbers $\{0,1\}$
$\mathbb{R}$	Set of real numbers
$\mathbb{Z}$	Set of integer numbers
f_{c}	Carrier frequency
c_0	Velocity factor in a vacuum
λ_c	Wave-length in a vacuum
$\mathscr{E}$	Radio-frequency passband energy
$\mathscr{E}_{\mathrm{b}}$	Energy per bit
$(m)^+$	$\max(m,0)$
$\mathbb{C}^n$	Vector-space of all n-column vector with complex elements
$\mathbb{R}^n$	Vector-space of all n-column vector with real elements
$\mathbb{C}^{n\times m}$	Vector-space of all the $n \times m$ matrices with complex elements

$\mathbb{R}^{n\times m}$	Vector-space of all the $n \times m$ matrices with real elements
$\mathbf{0}_n$	n-column zero vector
$\mathbf{O}_{n\times m}$	$n \times m$ zero matrix
$\mathbf{I}_n$	$n \times n$ identity matrix
$\text{diag}\,[\mathbf{A}_{11}, \mathbf{A}_{22}, \ldots, \mathbf{A}_{nn}]$	Block diagonal matrix wherein $\{\mathbf{A}_{ii}\}_{i=0}^{n}$ are the block diagonal entries
$\mathbf{J}_n$	$\text{diag}\left[1, -1, 1, \ldots, (-1)^{n-1}\right]$
$\{\mathbf{A}\}_{i_1,i_2}$	(i_1+1, i_2+1)th element of matrix $\mathbf{A} \in \mathbb{C}^{n\times m}$, with $i_1 \in \{0,1,\ldots,n-1\}$ and $i_2 \in \{0,1,\ldots,m-1\}$
$j \triangleq \sqrt{-1}$	Imaginary unit
f_{D}	Doppler frequency
$(\cdot)^*$	Complex conjugate
$(\cdot)^{\text{T}}$	Transpose of a matrix
$(\cdot)^{\text{H}}$	Hermitian (conjugate transpose) of a matrix
$(\cdot)^{-1}$	Inverse of a matrix
$(\cdot)^{-}$	Generalized $\{1\}$-inverse[1] of a matrix
$\otimes$	Kronecker product
$\lceil\cdot\rceil$	The smallest following integer
$(\cdot)_R$	The modulo-R operation
$\mathbb{E}\,[\cdot]$	Ensemble averaging
$\sum_{n=n_1}^{n_2} a_n \equiv 0$	For all $\{a_n\}_{n\in\mathbb{Z}}$, if $n_2 < n_1$, with $n_1, n_2 \in \mathbb{Z}$
$\prod_{n=n_1}^{n_2} a_n \equiv 1$	For all $\{a_n\}_{n\in\mathbb{Z}}$, if $n_2 < n_1$, with $n_1, n_2 \in \mathbb{Z}$

[1] According to the terminology of [7], a generalized $\{1\}$-inverse of a matrix $\boldsymbol{A}$ is a matrix $\boldsymbol{X}$ satisfying $\boldsymbol{AXA} = \boldsymbol{A}$.

Chapter 1

Introduction to aeronautical communications

In this chapter, the technological background of the thesis is introduced. In particular, in Sec. 1.1 we provide a short introduction to wireless communications in an aeronautical context, whereas in Sec. 1.2 we discuss how emerging *unmanned aerial systems* (UASs) determined a major breakthrough in requirements and design of aeronautical data-links. In Sec. 1.3, some typical modulation formats or "waveforms" used for telemetry aeronautical links are introduced. Section 1.4 discusses the impact of the aeronautical communication channels on the employed signaling solutions. Finally, in Sec. 1.5, the original contributions and organization of the thesis are summarized.

1.1 Introduction

Communication technologies have always been one of the fundamental milestones of the aeronautical environment, as well as one of its biggest challenges. Despite the continuous increase of demand for high performance, the aviation context is strongly reluctant to move toward new technologies, thus one of the goals is to fulfill the new requirements by an incremental approach, that is, by updating some parts of the existing (legacy) systems.

A modern aircraft communication system might encompass, in addition to VHF radio, two digital data-links, which are mainly used to backup the pilot

activities:

- *payload data-link*, which is used to transmit in downlink the mission data (e.g., a video stream);
- *telemetry data-link*, which is used to transmit in downlink the parameters representing the state of the avionic system.

In general, due to the presence of the pilot onboard, such data-links do not have strong constraints on communication performances. However, aerial vehicles are used today in many different applications, including monitoring of critical environments, remote sensing, and emergency communications. Such applications might require huge performances in terms of data-rate, nevertheless it is essential to preserve the robustness of data-link. Furthermore, the growing number of applications makes it difficult to manage the frequency spectrum, requiring that the bandwidth occupancy be kept to a minimum.

Regardless of applications, the exponential increase in the number of civilian aerial vehicles has pushed some institutions to explore new solutions for improved *air traffic management* (ATM) systems, which in turn needs significant improvements in communication technologies (see [21]). Two projects have been recently started to evolve the ATM systems: the SESAR project [2] in Europe, and the NextGen [1] one in USA, under the supervision of the *International Civil Aviation Organization* (ICAO). All of the proposed communication solutions are derived from terrestrial networks such as WiMAX and LTE, which are based on multi-carrier modulation methods or *orthogonal frequency domain modulation* (OFDM).

However, one of the big paradoxes of aviation industry, which is an high-technological domain, resides in its difficulty to move toward new technologies in communications. This reluctance arises mainly because changing communication standards would require replacing all preexistent infrastructures, thus, during transition, the goal is to assure the needed requirements by still using the legacy communication standards proposed for telemetry some decades ago.

1.2 Unmanned aerial systems communications

The UAS scenario has significantly changed the aeronautical communication framework, by introducing [44] specific requirements about data-rate and re-

liability. Indeed, whereas payload data-links for UASs still require high data-rates, *control and not-payload communications* (CNPC) data-links (including telemetry, command, and control) require in addition high reliability and low latency, since they must support real-time remote aircraft driving.

As an example, let us consider a UAS flying in *remotely piloted aircraft system* (RPAS) mode, wherein the ground pilot may need to see, with low latency, the aircraft telemetry data, and/or images coming from a camera installed on the vehicle, to correctly pilot it. Managing such huge amounts of data, the CNPC communication system has to satisfy much higher data-rate requirements, with severe latency constraints.

Modulation and coding techniques to be used in UAS scenarios are not fully standardized yet. Techniques compliant to the IRIG-106 telemetry standard [71], based on PCM/FM (see Sec. 1.3), are often used for the CNPC channel of medium-to-large dimension UASs, such as, e.g., the General Atomics MQ-1 Predator [8], whereas GMSK-based (see Chap. 2) chips are installed on smaller vehicles.

1.3 Waveforms

Continuous phase modulated (CPM) signals (see [3]) are widely employed for telemetry data transmission in aeronautical applications, due to their many advantages, such as constant envelope properties, spectral efficiency, and noise robustness. Indeed, the IRIG-106 telemetry standard [71] adopts different CPM modulation techniques, starting from legacy PCM/FM and SOQPSK, to the advanced multi-*h* ARTM one.

Pulse code modulation (PCM)*/frequency modulation* (FM), also refereed to as filtered *continuous-phase frequency-shift keying* (CPFSK) or CPM-1REC (see Chap. 2), has been the most popular telemetry modulation since around 1970. The RF signal is typically generated by filtering the baseband *non-return-to-zero-level* (NRZ-L) signal and then frequency modulating a *voltage-controlled oscillator* (VCO).

Frequency and phase modulation exhibit several desirable features, but they might not be sufficient to cope with the required bandwidth efficiency, especially for higher bit-rates. When a better bandwidth efficiency is required, the standard methods for telemetry data transmission are the Feher patented

quadrature phase-shift keying (FQPSK-B and FQPSK-JR), the *shaped offset quadrature phase-shift keying* (SOQPSK-TG), and the *Advanced Range Telemetry* (ARTM) CPM.

FQPSK represents an optimized modulation scheme derived from *offset quadrature phase-shift keying* (OQPSK). The main characteristics of FQPSK-B are described in [22], whereas FQPSK-JR is a cross-correlated, constant envelope, spectrum shaped variant of FQPSK that utilizes the time domain wavelet functions defined in [48], with some exceptions on the transition functions (see [71]).

SOQPSK is a family of constant envelope CPM waveforms defined by T. Hill (see [36, 81, 29]), and it is uniquely defined in terms of impulse excitation of a frequency pulse shaping filter function (see [71]).

Finally, ARTM CPM is a quaternary signaling scheme in which the frequency pulses are shaped for spectral containment purposes. The modulation index alternates at the symbol rate between two values (multi-h CPM, see Chap. 2) to improve the likelihood that the transmitted data be faithfully recovered, and the frequency impulse response for ARTM CPM is a three symbol long raised cosine, i.e., CPM-3RC (see Chap. 2).

1.4 Aeronautical communication channel

The knowledge of the communication channel is crucial not only to design an efficient digital communication link, but also to assess its performance and reliability in the desired operational environment.

Wireless communication channels are characterized by many different physical effects that are combined at the receiver (see [65, 45]):

1. *Path loss*: it is caused by dissipation of the power radiated by the transmitter.

2. *Shadowing*: it is caused by obstacles between the transmitter and receiver that absorb power; when the obstacle absorbs all the power, the signal is blocked.

3. *Multipath*: it is caused by the constructive and destructive addition of signal components travelling over different paths.

4. *Doppler*: it is caused by the relative motion of the transmitter, the receiver, and the location of reflectors.

Variations due to path loss and shadowing occur over relatively large distances, and are sometimes referred to as *large-scale* propagation effects or local mean attenuation (see [33]); they are well represented using deterministic models based on *geometrical optics* (GO) or *Uniform Theory of Diffraction* (UTD) (see [4]), and can be counteracted simply by increasing the transmitted signal power.

Instead, variations due to multipath and Doppler occur over very short distances, on the order of the signal wavelength, so these variations are sometimes referred to as *small-scale* propagation effects or multipath *fading*, which are usually described using statistical models (see [33]). Such effects need more complicated strategies to improve system performances, e.g., equalization, diversity, coding, and *multiple-input multiple-output* (MIMO) techniques.

During the different states of a flight, the aircraft passes through different environmental conditions that influence the air-ground communication channel, by introducing all of the cited effects. Traditional coding and diversity techniques can be used mainly to counteract the effects of non-dispersive channels, i.e., frequency-flat channels; furthermore, mechanical constraints often preclude mounting of multiple antennas on the aircraft. To counteract time dispersion introduced by frequency-selective channels, therefore, one can either adopt multicarrier modulation formats or, when single-carrier modulations are employed, resort to *channel equalization* techniques

1.5 Thesis contribution and organization

In this thesis, we focus on receiver synthesis for single-carrier aeronautical communication data-links employing CPM modulation over doubly-selective (i.e., both in time and frequency) wireless communication channels. Since CPM is a non-linear digital modulation method with memory, simple linear equalization techniques cannot be directly used. In many cases, one can leverage on the so-called *Laurent representation* [50] to obtain a more manageable expression of the CPM signal to be equalized.

Most of the techniques already proposed to equalize CPM signals in the aeronautical environment [66] and in other applications [70, 61, 72], are based

on *frequency-domain equalization* (FDE). However, FDE is not a computationally advantageous strategy when the channel is rapidly time-varying, such as the aeronautical one. Thus, our goal is to design efficient and low-complexity time-varying equalizers, by exploiting all of the CPM signal features, in order to compensate for the effects due to the rapidly time-varying aeronautical channels. For instance, since CPM signal may exhibit noncircular or improper features, the so-called *widely-linear* signal processing, a generalization of linear processing which jointly elaborates a signal and its comples conjugate, can significantly increase performances.

In particular, in this thesis, we presented the following original contributions:

1. The application of the *basis expansion model* (BEM) to a typical aeronautical communication channel is considered and validated by computer simulations (see Chap. 3).

2. The second-order statistical characterization of the pseudosymbols arising from Laurent representation of CPM signal is introduced and discussed in Chap. 2, showing that some mathematical inconsistencies can be overcome by adopting a one-sided signal model;

3. *Linear time-varying* (LTV) *zero forcing* (ZF) and *minimum mean square error* (MMSE) receiver structures for CPM signals operating over doubly-selective channels are proposed and implemented by using the BEM model for the channel; their performances are tested by simulations (see Chap. 4)

4. *Widely-linear time-varying* (WLTV) ZF and MMSE receiver structures for improper CPM signals operating over doubly-selective channels are proposed and implemented by using the BEM model; their performances are tested by simulations (see Chap. 4) and shown to be largely superior than those of their linear counterparts.

The thesis is organized as follows:

Chapter 2 introduces the main features of the CPM signals, including their linear (Laurent) representation; the second-order statistics of the CPM signal

are also derived, which are needed to implement equalization strategies optimizing quadratic cost functions.

Chapter 3 deals with the characterization of the aeronautical wireless channel, presenting some models proposed in the open literature; furthermore, the deterministic BEM approach is introduced for the parsimonious representation of a doubly-selective wireless channel, and its applicability to the aeronautical context is assessed by means of numerical simulations.

Chapter 4 represents the core of the thesis, wherein the problem of receiving a CPM signal over a doubly-selective channel is tackled. After introducing the overall system model, ZF and MMSE time-varying equalizers are synthesized, in both linear and widely-linear versions. Exploiting the BEM approach, frequency-shift (FRESH) versions of the proposed equalizers are derived. Finally, performances of the proposed algorithms are assessed by Monte Carlo computer simulations.

Chapter 5 draws some conclusions, summarizes the obtained results, and proposes future work guidelines.

Chapter 2

Continuous-phase modulated signals

In this chapter, the main features and mathematical models of the *continuous-phase modulated* (CPM) signal are introduced and discussed. Section 2.1 introduces the classical CPM signal model and its linear (Laurent) representation, wherein the signal is obtained as a superposition of time-limited amplitude-modulated pulses. In Sec. 2.3, leveraging on Laurent representation, the *second-order statistics* (SOS) of the CPM signal are evaluated. Finally, in Sec. 2.4 a compact analysis of the cyclic second-order statistics of the CPM signal is reported.

2.1 CPM signal model

CPM waveforms belong to the class of non-linear digital modulation methods, wherein the phase of the modulated signal is constrained to be continuous. This constraint results in a phase or frequency modulator that has memory.

A conventional M-ary frequency-shift keying (FSK) signal is generated by shifting the carrier to reflect the digital information that is being transmitted (see [65]). Switching from one frequency to another one can be accomplished by means of $M = 2^K$ separate oscillators tuned to the desired frequencies and selecting one of the M frequencies according to the particular K-bit symbol to be transmitted in a signal interval of duration $T = KT_b$ seconds,

where $R_\mathrm{b} = 1/T_b$ is the source bit-rate. However, switching from one oscillator output to another in subsequent signaling interval results in relatively large spectral sidelobes outside the main spectral band of the signal; consequently, this method exhibits a large band occupancy.

To avoid the use of signals having large spectral side lobes, in CPM modulation the information-bearing signal modulates a carrier whose frequency and phase is changed continuously. The resulting signal is phase-continuous, and it has memory because the phase of the carrier in every signaling interval depends on the phase value at the end of the previous signaling intervals.

The continuous-time ($t \in \mathbb{R}$) CPM signal with carrier frequency f_c can be expressed (see [65]) as

$$s_\mathrm{a}(t) = \Re[x_\mathrm{a}(t)e^{j2\pi f_c t}] = \sqrt{\frac{2\mathscr{E}}{T}}\cos[2\pi f_c t + \phi_\mathrm{a}(t)] \tag{2.1}$$

where $x_\mathrm{a}(t)$ is the complex envelope:

$$x_\mathrm{a}(t) = \sqrt{\frac{2\mathscr{E}}{T}}\exp[j\phi_\mathrm{a}(t)] \tag{2.2}$$

and $\phi_\mathrm{a}(t)$ represents the time-varying phase:

$$\phi_\mathrm{a}(t) = 2\pi \sum_{k=-\infty}^{+\infty} h_k a_k q_\mathrm{a}(t-kT) \tag{2.3}$$

In (2.3), $\{a_k\}_{k\in\mathbb{Z}}$ is the sequence of M-ary information symbols, usually selected from the alphabet $\mathscr{A} \triangleq \{\pm 1, \pm 3, \ldots, \pm(M-1)\}$, $\{h_k\}_{k\in\mathbb{Z}}$ is a sequence of *modulation indices*,

$$q_\mathrm{a}(t) \triangleq \int_{-\infty}^{t} f_\mathrm{a}(u)\,du \tag{2.4}$$

is the *phase response* pulse, and $f_\mathrm{a}(t)$ is the *frequency response* pulse satisfying the following conditions:

1. $f_\mathrm{a}(t) \equiv 0$ for each $t \notin [0, LT]$,
2. $f_\mathrm{a}(t) = f_\mathrm{a}(LT - t)$
3. $\displaystyle\int_{-\infty}^{LT} f_\mathrm{a}(u)\,du = q_\mathrm{a}(LT) = 1/2$

LREC	$f_{\mathrm{a}}(t) = \begin{cases} \dfrac{1}{2LT} & 0 \le t \le LT \\ 0 & \text{otherwise} \end{cases}$
LRC	$f_{\mathrm{a}}(t) = \begin{cases} \dfrac{1}{2LT}\left[1-\cos\left(\frac{2\pi t}{LT}\right)\right] & 0 \le t \le LT \\ 0 & \text{otherwise} \end{cases}$
GMSK	$f_{\mathrm{a}}(t) = \dfrac{Q\left[2\pi B\left(t-\frac{T}{2}\right)\right] - Q\left[2\pi B\left(t+\frac{T}{2}\right)\right]}{\sqrt{\log 2}}$

Table 2.1: Commonly used CPM pulse shapes.

where $L \geq 1$ is an integer representing the length of the frequency response, expressed in symbol periods.

When $h_k = h$ for all $k \in \mathbb{Z}$, the modulation index is fixed for all symbols (*single-h* CPM); instead, when the modulation index varies from one symbol to another, the signal is called *multi-h* CPM (see [65]). In such a case, the sequence $\{h_k\}_{z\in\mathbb{Z}}$ is typically allowed to vary in a cyclic manner through a finite set of indices. For the sake of simplicity, in the following $\mathscr{E} = T/2$ will be assumed in (2.2). Three popular pulse shapes are given in Tab. 2.1 (see, e.g., [65]). LREC denotes a rectangular pulse of duration LT; if $L = 1$, it results in a so-called CPFSK signal. LRC denotes a raised cosine pulse of duration LT. In Gaussian minimum-shift keying (GMSK), the frequency response pulse assumes a Gaussian shape with bandwidth parameter B, which represents the -3 dB bandwidth of the Gaussian pulse; we observe that the pulse duration increases as the bandwidth of the pulse decreases. In practical applications, the pulse is usually truncated to some specified fixed duration. GMSK with $BT = 0.3$ is used in GSM systems.

2.2 Linear representation of CPM signals

When h is not an integer and the symbol alphabet is binary, i.e., $M = 2$, the signal (2.2) can be expressed (see [50, 41]) as a superposition of $Q \triangleq 2^{L-1}$

PAM waveforms:

$$x_{\mathrm{a}}(t) = \sum_{q=0}^{Q-1} \sum_{n=-\infty}^{+\infty} s_{q,n}\, c_{\mathrm{a},q}(t-nT) \tag{2.5}$$

where the following *non-linear* functions of $\{a_k\}_{k\in\mathbb{Z}}$:

$$s_{q,n} \triangleq \exp\left[j\pi h \left(\sum_{\ell=-\infty}^{n} a_\ell - \sum_{\ell=0}^{L-1} a_{n-\ell}\beta_{q,\ell} \right) \right] \tag{2.6}$$

are referred to as the *pseudo-symbols*. For $\ell \in \{1,2,\ldots,L-1\}$, the parameter $\beta_{q,\ell} \in \{0,1\}$ is the ℓth bit of the radix-2 representation of $q \in \{0,1,\ldots,Q-1\}$, i.e., $q = \sum_{\ell=1}^{L-1} 2^{\ell-1}\beta_{q,\ell}$, whereas $\beta_{q,0}$ is always zero for all $q \in \{0,1,\ldots,Q-1\}$, and $c_{\mathrm{a},q}(t)$ is a real-valued pulse (see [50] for its detailed expression) obeying $c_{\mathrm{a},q}(t) \equiv 0$, for each $t \notin [0, L_q T]$, with $L_q \triangleq \min_{\ell\in\{0,1,\ldots,L-1\}}[L(2-\beta_{q,\ell})] \leq L+1$. Model (2.5) is also referred to as the *Laurent* or *AMP representation* of a CPM signal.

As an example, Fig. 2.1 shows the phase response (top) of the CPM-LREC signal with $L = 3$ and $h = 0.7$, and the first 4 components of its Laurent representation (bottom). Moreover, Fig. 2.2 shows the phase response (top) of the CPM-GMSK signal with $L = 4$, $B = 0.25/T$ and $h = 0.5$, and the first 4 components of its Laurent representation (bottom).

It is noteworthy that when $L = 1$ (*full-response* CPM) one has $Q = 1$, that is, there is only one PAM component in (2.5). On the other hand, when $L > 1$ (*partial-response* CPM), it results that, for smooth phase response pulses (e.g., the CPM-GMSK signal of Fig. 2.2), the power of $x_{\mathrm{a}}(t)$ is mainly contained in the first PAM component, i.e., the one associated with $c_{\mathrm{a},0}(t)$, which exhibits moreover the longest duration.

Note that the decomposition into PAM waveforms can be extended to multilevel ($M > 2$) CPM signaling, by expressing the M-ary symbol sequence in terms of binary subsequences (see [57]). Moreover the pathological case of integer h can be dealt with by viewing $x_{\mathrm{a}}(t)$ as the product of CPM signals with rational modulation indices (see [57]), or using special representations (see [58, 42]). Therefore, generalization of the considered analysis to $M > 2$ and/or integer h can be carried out with straightforward modifications.

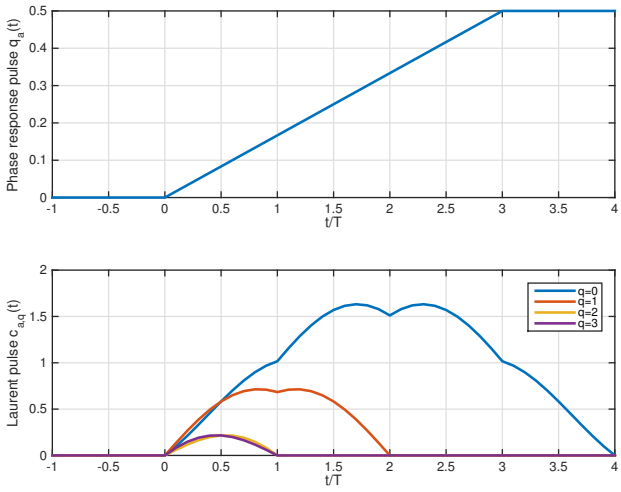

Figure 2.1: Phase response $q_{\mathrm{a}}(t)$ (top) and the first 4 corresponding Laurent pulses (bottom) $c_{\mathrm{a},q}(t)$ of CPM-LREC signal with $L = 3$ and $h = 0.7$.

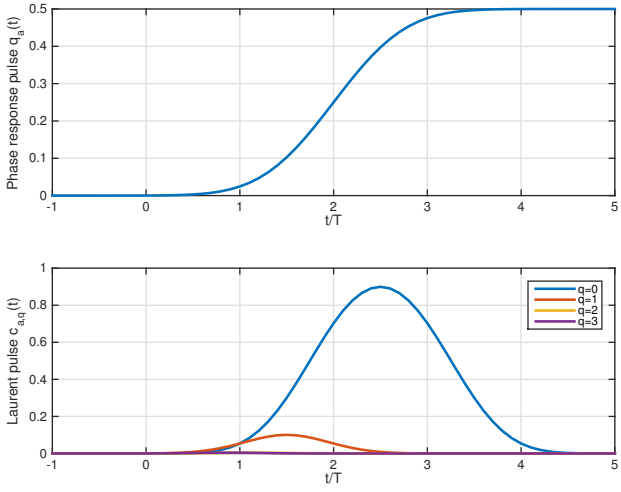

Figure 2.2: Phase response $q_{\mathrm{a}}(t)$ (top) and the first 4 corresponding Laurent pulses (bottom) $c_{\mathrm{a},q}(t)$ of CPM-GMSK signal with $L = 4$, $BT = 0.25$, and $h = 0.5$.

2.3 Second-order statistics of CPM signals

Equalization of frequency- and time-selective channels is often carried out by means of linear filtering, aimed at providing an estimate of the transmitted symbols. Many linear filters, such as the widespread *minimum mean square error* (MMSE) filter, are based on quadratic cost criteria, whose design require knowledge of the second-order statistics (SOS) of the transmitted signal. It is noteworthy that SOS characterization of a complex signal requires (see [59],[63]) evaluation of both its *autocorrelation* $R_{xx}(t,\tau) = \mathbb{E}\left[x_{\mathrm{a}}(t)x_{\mathrm{a}}^{*}(t-\tau)\right]$ as well as its *conjugate correlation function* $R_{xx^{*}}(t,\tau) = \mathbb{E}\left[x_{\mathrm{a}}(t)x_{\mathrm{a}}(t-\tau)\right]$.

The autocorrelation function of a CPM signal has been evaluated in [50] as:

$$\begin{aligned} R_{xx}(t,\tau) = \sum_{q_1=0}^{Q-1}\sum_{q_2=0}^{Q-1}\sum_{m=-\infty}^{+\infty} R_{s_{q_1}s_{q_2}}(m) \\ \times \sum_{n=-\infty}^{+\infty} c_{\mathrm{a},q_1}(t-nT)\,c_{\mathrm{a},q_2}(t-nT+mT-\tau) \end{aligned} \tag{2.7}$$

where $R_{s_{q_1}s_{q_2}}(m) \triangleq \mathbb{E}\left[s_{q_1,n}s_{q_2,n-m}^{*}\right]$ is the cross-correlation function of the pseudo-symbols, which does not depend on n. It turns out that

$$R_{s_{q_1}s_{q_2}}(m) = [\cos(\pi h)]^{\Delta_{q_1q_2}(m)} \tag{2.8}$$

where $\Delta_{q_1q_2}(m)$ is given (see [50]) by

$$\begin{aligned} \Delta_{q_1q_2}(m) =& |m| + \sum_{\ell=0}^{L-1}\left(\beta_{q_1,\ell}+\beta_{q_2,\ell}\right) \\ &+ 2\left(\sum_{\ell=0}^{\min(m-1,L-1)}\beta_{q_1,\ell} + \sum_{\ell=0}^{\min(-m-1,L-1)}\beta_{q_2,\ell}\right. \\ &\left. + \sum_{\ell=(m)^{+}}^{\min(L+m-1,L-1)}\beta_{q_2,\ell-m}\beta_{q_1,\ell}\right) \end{aligned} \tag{2.9}$$

It can be noted that, for any $L \geq 1$, the function $R_{xx}(t,\tau)$ given by (2.7) is periodic in t with period T, hence the CPM signal exhibits, in general, *wide-sense cyclostationarity* (see [25]) with *cycle frequencies* integer multiples of $1/T$.

Evaluation of the conjugate correlation function has not been carried out in [50]. It is straightforward to show that

$$R_{xx^*}(t,\tau) = \sum_{q_1=0}^{Q-1}\sum_{q_2=0}^{Q-1}\sum_{m=-\infty}^{+\infty}\sum_{n=-\infty}^{+\infty} R_{s_{q_1}s^*_{q_2}}(n,m) \times c_{\mathrm{a},q_1}(t-nT)c_{\mathrm{a},q_2}(t-nT+mT-\tau) \tag{2.10}$$

where $R_{s_{q_1}s^*_{q_2}}(n,m) \triangleq \mathbb{E}[s_{q_1,n}s_{q_2,n-m}]$ is the conjugate cross-correlation function of the pseudo-symbols.

In [58] evaluation of second- and higher-order statistics for CPM signals has been carried out in the *fraction-of-time* (FOT) probability framework where, however, some problems of convergence of infinite products arising in the conjugate case are solved by introducing an annoying "undetermined constant" c_∞ that can assume values ± 1. We show herein that the problems of convergence can be overcome by assuming, as it happens in practical cases, that the CPM signal evolves starting from a finite time-epoch, i.e., $t = 0$, instead of $t = -\infty$.

2.3.1 One-sided CPM signal model

If the CPM signal evolves starting from a finite time-epoch, it can be modeled as a one-sided random process [34]: the associated model can be simply obtained by setting $a_n = 0$ and $s_{q,n} = 0$, for all $n < 0$, and $x_\mathrm{a}(t) = 0$, for all $t < 0$, in all the previous equations. For instance, the one-sided version of (2.6) is

$$s_{q,n} = \exp\left[j\pi h\left(\sum_{\ell=0}^{n} a_\ell - \sum_{\ell=0}^{L-1} a_{n-\ell}\beta_{q,\ell}\right)\right] u(n) \tag{2.11}$$

where $u(n)$ represents the step function, defined as

$$u(n) = \begin{cases} 1 & n \geq 0 \\ 0 & \text{otherwise} \end{cases} \tag{2.12}$$

Since (2.7) and (2.10) depend on the cross-correlation functions of the pseudo-symbols, we will evaluate both the cross-correlation function and the conjugate cross-correlation function of the pseudo-symbols for the one-sided model. We

will particularly show that, in this case, the conjugate cross-correlation function can be evaluated without mathematical inconsistencies.

Bearing in mind (2.11), it can be proven with straightforward calculations that the cross-correlation function of pseudo-symbols is given by

$$R_{s_{q_1}s_{q_2}}(n,m) = [\cos(\pi h)]^{\Delta^{+}_{q_1q_2}(n,m)}\, u\left[n-(m)^{+}\right] \tag{2.13}$$

where $\Delta^{+}_{q_1q_2}(n,m) \triangleq \Delta_{q_1q_2}(m) + \widetilde{\Delta}_{q_1q_2}(n,m)$, i.e., the first term is the same of (2.9), and the second one is

$$\begin{aligned}\widetilde{\Delta}_{q_1q_2}(n,m) = \sum_{\ell=n+1}^{\min(L+m-1,L-1)} & 2\beta_{q_2,\ell-m}\beta_{q_1,\ell} \\ & - \sum_{\ell=n+1}^{L-1}\beta_{q_1,\ell} - \sum_{\ell=n-m+1}^{L-1}\beta_{q_2,\ell}\end{aligned} \tag{2.14}$$

Note that for all $n \geq L-1+(m)^{+}$, $\widetilde{\Delta}_{q_1q_2}(n,m) = 0$, i.e., the cross-correlation function of the one-sided version of pseudo-symbols turns out to be the same of (2.8) after a small transient.

Moreover, based on (2.11), it can be inferred with straightforward calculations that the conjugate cross-correlation function of pseudo-symbols assumes the following form:

$$\begin{aligned}R_{s_{q_1}s^{*}_{q_2}}(n,m) = & \prod_{\ell=0}^{m-1}\cos[\pi h(1-\beta_{q_1,\ell})] \prod_{\ell=0}^{-m-1}\cos[\pi h(1-\beta_{q_2,\ell})] \\ & \times \prod_{\ell=(m)^{+}}^{\min[n,L+m-1-(m)^{+}]}\cos\left[\pi h\left(2-\beta_{q_1,\ell}-\beta_{q_2,\ell-m}\right)\right] \\ & \times \prod_{\ell=L-m}^{\min(n-m,L-1)}\cos\left[\pi h\left(2-\beta_{q_2,\ell}\right)\right] \\ & \times \prod_{\ell=L+m}^{\min(n,L-1)}\cos\left[\pi h\left(2-\beta_{q_1,\ell}\right)\right] \\ & \times [\cos(2\pi h)]^{\max[0,n-L+1-(m)^{+}]}\, u\left[n-(m)^{+}\right]\end{aligned} \tag{2.15}$$

Note that, for all $n \geq L-1+(m)^{+}$, (2.15) can be factorized as

$$R_{s_{q_1}s^{*}_{q_2}}(n,m) = R^{+}_{s_{q_1}s^{*}_{q_2}}(m)\,[\cos(2\pi h)]^{n} \tag{2.16}$$

in which

$$\begin{aligned} R^{+}_{s_{q_1}s^{*}_{q_2}}(m) = &\prod_{\ell=0}^{m-1}\cos[\pi h(1-\beta_{q_1,\ell})]\prod_{\ell=0}^{-m-1}\cos[\pi h(1-\beta_{q_2,\ell})] \\ &\times\prod_{\ell=(m)^{+}}^{L+m-1-(m)^{+}}\cos\left[\pi h\left(2-\beta_{q_1,\ell}-\beta_{q_2,\ell-m}\right)\right] \\ &\times\prod_{\ell=L-m}^{L-1}\cos\left[\pi h\left(2-\beta_{q_2,\ell}\right)\right]\prod_{\ell=L+m}^{L-1}\cos\left[\pi h\left(2-\beta_{q_1,\ell}\right)\right] \\ &\times\left[\cos(2\pi h)\right]^{-L+1-(m)^{+}} \end{aligned} \tag{2.17}$$

It is apparent from (2.16) that for $h \neq 1/2+k$, with $k \in \mathbb{Z}$, the conjugate cross-correlation function vanishes as n increases, i.e., the one-sided CPM signal is asymptotically *circular* or *proper* (see [59, 63]). Instead, when $h = 1/2+k$, with $k \in \mathbb{Z}$, the CPM signal exhibits asymptotically *noncircular* or *improper* features, thus it might be convenient to obtain the relationship between the pseudo-symbols and their complex conjugates.

With straightforward manipulations, we note that considering $h = 1/2+k$, with $k \in \mathbb{Z}$, (2.11) can be expressed as

$$s_{q,n} = j^{n+1+N_q^{(1)}}(-1)^{N_q^{(1)}+k\left[n+1+N_q^{(1)}\right]}\prod_{\ell=0}^{n}a_\ell\prod_{\ell=0}^{L-1}a_{n-\ell}^{\beta_{q,\ell}} \tag{2.18}$$

with $N_q^{(1)} \triangleq \sum_{\ell=0}^{L-1}\beta_{q,\ell}$ representing the number of ones of the radix-2 representation of $q \in \{0,1,\ldots,Q-1\}$. From (2.18), the relationship between the pseudo-symbols[1] and their complex conjugates can be obtained as

$$\begin{aligned} s^{*}_{q,n} &= (-j)^{n+1+N_q^{(1)}}(-1)^{N_q^{(1)}+k\left[n+1+N_q^{(1)}\right]}\prod_{\ell=0}^{n}a_\ell\prod_{\ell=0}^{L-1}a_{n-\ell}^{\beta_{q,\ell}} \\ &= (-1)^{n+1+N_q^{(1)}}j^{n+1+N_q^{(1)}}(-1)^{N_q^{(1)}+k\left[n+1+N_q^{(1)}\right]}\prod_{\ell=0}^{n}a_\ell\prod_{\ell=0}^{L-1}a_{n-\ell}^{\beta_{q,\ell}} \\ &= (-1)^{n+1+N_q^{(1)}}s_{q,n} \end{aligned} \tag{2.19}$$

for $h = 1/2+k$, with $k \in \mathbb{Z}$, and $q \in \{0,1,\ldots,Q-1\}$.

[1]Note that only for improper or non-circular signals the complex conjugate is proportional to the signal iself.

2.4 Second-order cyclic statistics of CPM signals

With reference to the one-sided CPM signal model, one observe that the pseudo-symbols exhibit in general time-varying (with n) cross-correlations [see (2.13) and (2.16)]. Such time-varying features cannot be estimated in practice unless a specific model for time variations is assumed. Indeed, practical techniques estimate correlations by evaluating time averages of sampled data: for one-sided processes, such time averages must be evaluated only for $n \geq 0$.

When statistical time variations are described by a periodic or almost periodic model, they can be conveniently measured by defining the (discrete-time) *cyclic cross-correlation function* (CCCF) at cycle frequency $\alpha \in \mathbb{R}$:

$$R^{\alpha}_{s_{q_1}s_{q_2}}(m) \triangleq \lim_{N\to+\infty} \frac{1}{N} \sum_{n=0}^{N-1} R_{s_{q_1}s_{q_2}}(n,m) e^{-j2\pi\alpha n} \tag{2.20}$$

Indeed, a practical estimator of (2.20) can be built by considering the time-average of $s_{q_1,n} s^*_{q_2,n-m}$ over a finite sample-size, i.e., as

$$\widehat{R}^{\alpha}_{s_{q_1}s_{q_2}}(m) \triangleq \frac{1}{N} \sum_{n=0}^{N-1} s_{q_1,n}\, s^*_{q_2,n-m} e^{-j2\pi\alpha n} \tag{2.21}$$

It is clear that $\widehat{R}^{\alpha}_{s_{q_1}s_{q_2}}(m)$ is an asymptotically (for $N \to +\infty$) unbiased estimator of $R^{\alpha}_{s_{q_1}s_{q_2}}(m)$; under mild conditions (see [43, 16]), it can be proven that it is also a consistent estimator.

To obtain the theoretical expression of $R^{\alpha}_{s_{q_1}s_{q_2}}(m)$, eq. (2.13) must be substituted in (2.20). Let us analyze the convergence of the limit in (2.20):

$$\begin{aligned} \sum_{n=0}^{N-1} R_{s_{q_1}s_{q_2}}(n,m) e^{-j2\pi\alpha n} = & \sum_{n=0}^{L-2+(m)^+} R_{s_{q_1}s_{q_2}}(n,m) e^{-j2\pi\alpha n} \\ & + \sum_{n=L-1+(m)^+}^{N-1} R_{s_{q_1}s_{q_2}}(m) e^{-j2\pi\alpha n} \end{aligned} \tag{2.22}$$

in which $R_{s_{q_1}s_{q_2}}(m) \triangleq [\cos(\pi h)]^{\Delta_{q_1 q_2}(m)}$.

First, we demonstrate that the first term is limited, then its contribution to the time average is null. Indeed one has:

$$\left| \sum_{n=0}^{L-2+(m)^+} R_{s_{q_1}s_{q_2}}(n,m) e^{-j2\pi\alpha n} \right| \leq \sum_{n=0}^{L-2+(m)^+} \left| R_{s_{q_1}s_{q_2}}(n,m) \right| \tag{2.23}$$

Observing that $\left|R_{s_{q_1}s_{q_2}}(n,m)\right| \leq 1$, it can be inferred that

$$\lim_{N\to+\infty}\frac{1}{N}\left|\sum_{n=0}^{L-2+(m)^+} R_{s_{q_1}s_{q_2}}(n,m)e^{-j2\pi\alpha n}\right| \leq \lim_{N\to+\infty}\frac{1}{N}[L-1+(m)^+] = 0 \quad (2.24)$$

Therefore, since the first term in (2.22) is a finite summation of limited elements, it does not contribute to the evaluation of the time average.

The second term in (2.22) can be rewritten as

$$\begin{aligned}\sum_{n=L-1+(m)^+}^{N-1} R_{s_{q_1}s_{q_2}}(m)e^{-j2\pi\alpha n} &= \sum_{n=0}^{N-1} R_{s_{q_1}s_{q_2}}(m)e^{-j2\pi\alpha n} \\ &\quad - \sum_{n=0}^{L-2+(m)^+} R_{s_{q_1}s_{q_2}}(m)e^{-j2\pi\alpha n}\end{aligned} \quad (2.25)$$

where the second term does not contribute to the time average for the same reason of the first term in (2.22) [see (2.23) and (2.24)], whereas the first one assumes the form

$$\begin{aligned}\sum_{n=0}^{N-1} R_{s_{q_1}s_{q_2}}(m)e^{-j2\pi\alpha n} &= R_{s_{q_1}s_{q_2}}(m)\sum_{n=0}^{N-1} e^{-j2\pi\alpha n} \\ &= R_{s_{q_1}s_{q_2}}(m)\frac{\sin(\pi\alpha N)}{\sin(\pi\alpha)}e^{-j\pi\alpha(N-1)}\end{aligned} \quad (2.26)$$

from which it can be inferred that (see[2] [15])

$$\begin{aligned}R^{\alpha}_{s_{q_1}s_{q_2}}(m) &= R_{s_{q_1}s_{q_2}}(m)\lim_{N\to+\infty}\frac{1}{N}\frac{\sin(\pi\alpha N)}{\sin(\pi\alpha)}e^{-j\pi\alpha(N-1)} \\ &= R_{s_{q_1}s_{q_2}}(m)\sum_{i=-\infty}^{\infty}\delta(\alpha-i)\end{aligned} \quad (2.27)$$

for all $\alpha \in \mathbb{R}$, where $\delta(x)$ represents the Dirac delta function.

Following similar reasoning, the *cyclic conjugate cross-correlation function* (CCCF) at cycle frequency $\alpha \in \mathbb{R}$ can be defined as

$$R^{\alpha}_{s_{q_1}s^*_{q_2}}(m) \triangleq \lim_{N\to+\infty}\frac{1}{N}\sum_{n=0}^{N-1} R_{s_{q_1}s^*_{q_2}}(n,m)e^{-j2\pi\alpha n} \quad (2.28)$$

[2] A rigorous proof of (2.27) can be given by interpreting the convergence in the space of distributions (see eg. [24]).

To obtain its expression, eq. (2.15) and (2.16) must be substituted in (2.28). Let us analyze the convergence of the limit in (2.28):

$$\begin{aligned}\sum_{n=0}^{N-1} R_{s_{q_1}s^*_{q_2}}(n,m)e^{-j2\pi\alpha n} = &\sum_{n=0}^{L-2+(m)^+} R_{s_{q_1}s^*_{q_2}}(n,m)e^{-j2\pi\alpha n} \\ &+ R^+_{s_{q_1}s^*_{q_2}}(m)\sum_{n=L-1+(m)^+}^{N-1}[\cos(2\pi h)]^n e^{-j2\pi\alpha n}\end{aligned} \tag{2.29}$$

The first term in (2.29) does not contribute to the time average (2.28) for the same reason of the first term in (2.22) [see (2.23) and (2.24)], and the sum in the second term assumes the form

$$\begin{aligned}\sum_{n=L-1+(m)^+}^{N-1}[\cos(2\pi h)]^n e^{-j2\pi\alpha n} = &\sum_{n=0}^{N-1}[\cos(2\pi h)]^n e^{-j2\pi\alpha n} \\ &- \sum_{n=0}^{L-2+(m)^+}[\cos(2\pi h)]^n e^{-j2\pi\alpha n}\end{aligned} \tag{2.30}$$

in which the second term does not contribute to the time average (2.28) for the same reason expressed above. Bearing in mind the previous considerations, eq. (2.28) can be expressed as

$$R^{\alpha}_{s_{q_1}s^*_{q_2}}(m) = R^+_{s_{q_1}s^*_{q_2}}(m)\lim_{N\to+\infty}\frac{1}{N}\sum_{n=0}^{N-1}[\cos(2\pi h)]^n e^{-j2\pi\alpha n} \tag{2.31}$$

With reference to (2.31), two distinct cases must be discussed, according to the value of h:

- when $|\cos(2\pi h)| < 1$, $R^{\alpha}_{s_{q_1}s^*_{q_2}}(m) = 0$ for all $m \in \mathbb{Z}$;
- when $\cos(2\pi h) = -1$, i.e., $h = 1/2 + k$ for all $k \in \mathbb{Z}$, the sums in (2.31) assume the following form:

$$\begin{aligned}\sum_{n=0}^{N-1}[\cos(2\pi h)]^n e^{-j2\pi\alpha n} &= \sum_{n=0}^{N-1}(-1)^n e^{-j2\pi\alpha n} \\ &= \sum_{n=0}^{N-1} e^{-j2\pi(\alpha-1/2)n} \\ &= \frac{\sin[\pi(\alpha-1/2)N]}{\sin[\pi(\alpha-1/2)]}e^{-j\pi(\alpha-1/2)(N-1)}\end{aligned} \tag{2.32}$$

Therefore, substituting (2.32) in (2.31), the CCCF can be expressed as

$$\begin{aligned} R^{\alpha}_{s_{q_1}s^*_{q_2}}(m) &= R^{+}_{s_{q_1}s^*_{q_2}}(m) \lim_{N\to+\infty} \frac{1}{N} \frac{\sin[\pi(\alpha-1/2)N]}{\sin[\pi(\alpha-1/2)]} e^{-j\pi(\alpha-1/2)(N-1)} \\ &= R^{+}_{s_{q_1}s^*_{q_2}}(m) \sum_{i=-\infty}^{\infty} \delta\left(\alpha-1/2-i\right) \end{aligned} \tag{2.33}$$

for all $\alpha \in \mathbb{R}$, and $h = 1/2+k$ with $k \in \mathbb{Z}$.

Looking at the first two products in (2.17) for $h = 1/2+k$ with $k \in \mathbb{Z}$, it is simple to infer that

$$\prod_{\ell=0}^{m-1} \cos[\pi h(1-\beta_{q_1,\ell})] \prod_{\ell=0}^{-m-1} \cos[\pi h(1-\beta_{q_2,\ell})] = \prod_{\ell=0}^{m-1} \beta_{q_1,\ell} \prod_{\ell=0}^{-m-1} \beta_{q_2,\ell} \tag{2.34}$$

Due to $\beta_{q,0} = 0$ for all $q \in \{0,1,\ldots,Q-1\}$, eq. (2.17) is zero for all $m \neq 0$. Then, considering $h = 1/2+k$ with $k \in \mathbb{Z}$, and $m = 0$, the third products in (2.17) assume the form

$$\prod_{\ell=0}^{L-1} \cos\left[\pi h\left(2-\beta_{q_1,\ell}-\beta_{q_2,\ell}\right)\right] = \prod_{\ell=0}^{L-1} (\beta_{q_1,\ell}+\beta_{q_2,\ell}-1) \tag{2.35}$$

Note that if $\exists \ell \in \{0,1,\ldots,L-1\}$ such that $\beta_{q_1,\ell} \neq \beta_{q_2,\ell}$, the products in (2.35) are null. The last assertion is equivalent to say that

$$\forall q_1,q_2 \in \{0,1,\ldots,Q-1\} : q_1 \neq q_2 \Rightarrow \prod_{\ell=0}^{L-1} (\beta_{q_1,\ell}+\beta_{q_2,\ell}-1) = 0 \tag{2.36}$$

Based on previous observation, the CCCF at cycle frequency $\alpha \in \mathbb{R}$ can be finally expressed as

$$R^{\alpha}_{s_{q_1}s^*_{q_2}}(m) = \begin{cases} \delta_m \delta_{q_1-q_2} \sum_{i=\infty}^{+\infty} \delta\left(\alpha-\frac{1}{2}-i\right)(-1)^{1-N^{(1)}_{q_1}} & h = 1/2+k, k \in \mathbb{Z} \\ 0 & \text{otherwise} \end{cases} \tag{2.37}$$

where δ_n is the Kronecker delta function, i.e., $\delta_n = 1$ for $n = 0$ and zero otherwise.

Chapter 3

Aeronautical time-varying channels

This chapter deals with characterization of the aeronautical wireless channel. In Sec. 3.1 and Sec. 3.2 some aeronautical channel models proposed in literature are described, with particular emphasis on the model proposed by Erik Haas in [35] (Haas model). In Sec. 3.4, the *Basis Expansion Model* (BEM) approach is introduced for the parsimonious representation of a doubly-selective channel. Finally, in Sec. 3.5 the BEM approach is applied to the Haas model and numerical simulations are carried out to validate the usefulness of the approach.

3.1 Aeronautical channel modeling

As it is well known, the wireless physical medium has fundamental effects on communication signaling and its reliability, hence accurate characterization of the channel is vital to reliable CNPC design and performance.

The problem of developing effective channel models for wireless communications in aeronautical environment is considered in many works. In [54], a comprehensive review of the existing literature is presented, dealing with the problem of modeling the wireless channel in aeronautical environments, with particular emphasis on UAS applications. In [35] a fairly complete description of the *air-ground* (AG) channel in terms of a statistical *tapped-delay line*

(TDL) model has been proposed by Erik Haas. In particular the aeronautical channel is classified as belonging to several scenarios: parking, taxiing, en-route, and takeoff/landing, with the parking and taxiing scenarios actually denoting ground-to-ground channels for use on *airport surface areas* (ASAs). Although the relevant models are developed for VHF band, in [55] and [68] it is shown that they represent a worst case for the ASA channel also in C-band.

The model proposed in [35] is based on the classical *wide-sense stationary uncorrelated scattering* (WSSUS) framework originally developed by Paul Bello in [6], wherein the complex baseband wireless channel is modeled as a *linear time-varying* (LTV) system characterized by its impulse response $h_{\mathrm{a}}(t,\tau)$, where t and τ represent the time-instant and the time-delay respectively; moreover, the function $h_{\mathrm{a}}(t,\tau)$ is modeled as a complex two-dimensional random process.

The WSSUS model is based on the superposition of uncorrelated echos, and assumes that the resulting impulse response is wide-sense stationary. As long as the number of multipath components is large, we can invoke the *Central Limit Theorem* (CLT) to prove that $h_{\mathrm{a}}(t,\tau)$ is distributed as a complex Gaussian process (GWSSUS). In this case, its statistical characterization is fully describerd by the mean, the autocorrelation, and the cross-correlation of the in-phase and quadrature-phase components, or, equivalently, from its *scattering function* $P(\tau, f_{\mathrm{D}})$, which depends on the time-delay τ (due to the-multipath effects) and the *Doppler frequency* f_{D} (due to mobility).

In [67], a stochastic model is proposed to approximate a frequency-selective GWSSUS channel, mostly suited for Monte Carlo simulations. Following this model, also cited in [38, 62], the channel impulse response can be obtained (see [35, 67]) as the sum of P echoes:

$$h_{\mathrm{a}}(t,\tau) = \lim_{P\to+\infty} \frac{1}{\sqrt{P}} \sum_{p=1}^{P} e^{j\theta_p} e^{j2\pi f_{\mathrm{D}p} t} \delta(\tau - \tau_p) \tag{3.1}$$

wherein the p-th path is characterized by a phase θ_p, a delay τ_p and a Doppler shift $f_{\mathrm{D}p}$, all modeled as continuous random variables; note that the factor $1/\sqrt{P}$ enforces the average power to be unity. In [38] it is shown that the scattering function $P(\tau, f_{\mathrm{D}})$ associated to a model like (3.1) is proportional to the joint *probability distribution function* (PDF) $p(\tau, f_{\mathrm{D}})$ of the random variables τ_q and $f_{\mathrm{D}q}$.

In practice, for Monte Carlo simulations, we first generate P values of τ_p and $f_{\mathrm{D}p}$ according to the desired $p(\tau, f_{\mathrm{D}})$, as well as P values of the phase θ_p uniformly distributed in $[0, 2\pi)$: using these values we generate a channel realization using (3.1).

The number of paths has to be about $P = 25$ in order to obtain a good representation of the fading channel, if the parameter set $\{\tau_p, f_{\mathrm{D}p}, \theta_p\}_{p=1}^{P}$ is generated once before the simulation starts. However, about $P = 7 \div 10$ paths are sufficient, if new parameter sets are generated from time to time, given the same statistics (see [45, 38]).

3.2 Aeronautical channel scenarios

As discussed in [35], the different conditions during the flight of an aircraft lead to different channel scenarios. These scenarios are characterized by the type of fading, the Doppler, and the delays in the system. All of the scenarios described by Haas, except for parking, consider an LTV channel composed by a deterministic LOS path that has to be summed to the multiple NLOS (diffuse) random components as defined in (3.1). Typically the LOS path must be separately taken into account. Haas discusses the statistical properties of all the variables involved in the model, furthermore he provides typical values of the parameters to be used to simulate the communication channel in the aeronautical framework, for all the considered scenarios (see Tab. 3.1).

3.2.1 *En-route* scenario

The en-route scenario applies when the aircraft is flying and it is engaged in ground-air or air-air communication. Ground-air communication is referred to the link between a base station on the ground and an aircraft, whereas air-air communication is related to the link between two flying aircrafts. Typically, the resulting multipath channel consists of a LOS path as well as a cluster of reflected, delayed paths. Therefore, the scenario may be characterized by a two-ray model composed by a deterministic direct path and an unique diffuse component, modeled as a Rayleigh process, delayed by $\tau_{\max}$. Due to the high speed of the aircraft, en-route channels are characterized by high Doppler shifts. Furthermore, since the scattered components are typically not isotrop-

	Parking scenario	**Taxi scenario**	**Arrival scenario**	**En-Route scenario**
Aircraft velocity $v\,[\mathrm{m/s}]$	5.5 $0\ldots5.5$	15.0 $0\ldots15$	150.0 $25\ldots150$ typ. 85	440.0 (620.0) $17\ldots440$ typ. 250
Maximum delay $\tau_{\max}\,[\mathrm{s}]$	$7.0\cdot10^{-6}$	$0.7\cdot10^{-6}$	$7.0\cdot10^{-6}$	$33.0\cdot10^{-6}$ $(66.0\cdot10^{-6})$ $6\cdot10^{-6}\ldots200\cdot10^{-6}$
Number of echo paths $N\,[\#]$	20	20	20	20
Rice factor $K_{\mathrm{Rice}}\,[\mathrm{dB}]$	–	6.9	15.0 $9\ldots20$	15.0 $2\ldots20$
$f_{\mathrm{DLOS}}/f_{\mathrm{Dmax}}$ factor	–	0.7	1.0	1.0
Start angle of beam $\phi_{\mathrm{a_L}}\,[\mathrm{deg}]$	0.0	0.0	-90.0	178.25
End angle of beam $\phi_{\mathrm{a_H}}\,[\mathrm{deg}]$	360.0	360.0	$+90.0$	181.75
Exponential or two-ray delay	exp	exp	exp	two-ray
Slope time $\tau_{\mathrm{slope}}\,[\mathrm{s}]$	$1.0\cdot10^{-6}$	$1/9.2\cdot10^{-6}$	$1.0\cdot10^{-6}$	–

Table 3.1: Set of typical aeronautical scenarios for simulations (see [35]).

ically distributed, i.e., the beamwidth of the scattered components is rather small (about $\beta = 3.5^o$), the resulting Doppler spectrum is only a part[1] of the classical 2-D isotropic Doppler density function derived by Jakes in [45].

3.2.2 *Takeoff/Landing* scenario

In this phase the aircraft is typically engaged in ground-air communication; it already has left its cruising speed and altitude, and is about to land (landing), or vice versa (takeoff). In this scenario there is still a LOS component, but there will be also some moderate NLOS scattered components, mainly from buildings at the airport itself, which can be modeled by a Rayleigh process. Also in this case the scatterers are not uniformly distributed, since the diffuse components arrive from preferred directions (back/front of the aircraft during takeoff/landing, respectively). The beamwidth of the scattered components is broader ($\beta = 180^o$) than in the en-route environment, but typically narrower than in the taxi environment shown in the following. The distribution of delays is likely to switch from a two-ray scenario toward a typical rural environment, this requires that the PDP be modeled as an exponentially decreasing function.

3.2.3 *Taxiing* scenario

The taxiing scenario applies when the aircraft is on the ground and it is traveling toward or from the ground base station. This scenario is characterized by low mobility, i.e., slow fading. Furthermore it can be assumed that the scatterers are uniformly distributed around the aircraft ($\beta = 360^o$), i.e., a Jakes distribution of Doppler is obtained. The Doppler and delay power spectra and the *Rice factor*, defined in the following, are based on the recommendations for rural (non-hilly) areas.

3.2.4 *Parking* scenario

The parking scenario applies when the aircraft is on the ground and it is traveling at very slow speed close to the base station, or it is parked at the terminal. The Doppler and delay power spectra are based on the recommendations for

[1] Jakes assumes in [45] that the scattering sources are uniformly distributed in $[0, 2\pi)$.

urban (non-hilly) areas, thus we apply the Jakes model for Doppler and an exponentially distributed PDP. Note that the LOS path is assumed to be blocked in this scenario.

3.3 Discrete-time representation of the Haas models

In this section the discrete-time version of the general Haas model (3.1) is introduced. Let T_c denote the sample time, the channel can be expressed as

$$h(k,\ell) \triangleq h_a(kT_c, \ell T_c) = h_{\text{LOS}}(k,\ell) + h_{\text{NLOS}}(k,\ell) \tag{3.2}$$

where, $\forall k,\ell \in \mathbb{Z}$, $h_{\text{LOS}}(k,\ell)$ is the deterministic LOS component, wheraes $h_{\text{NLOS}}(k,\ell)$ is the stochastic NLOS one.

Based on [35], the LOS component can be written as

$$h_{\text{LOS}}(k,\ell) \triangleq a\, e^{j2\pi f_{\text{DLOS}} kT_c}\, \delta(\ell) \tag{3.3}$$

where f_{DLOS} represents the Doppler frequency of the LOS path, and

$$a = \sqrt{\frac{K_{\text{Rice}}}{K_{\text{Rice}}+1}} \tag{3.4}$$

is the amplitude of the LOS path, with K_{Rice} representing the so-called *Rice factor*, i.e., the power ratio between the LOS and the NLOS components.

Furthermore, the NLOS contribution can be written as

$$h_{\text{NLOS}}(k,\ell) \triangleq \frac{c}{\sqrt{N}} \sum_{n=1}^{N} e^{j(\theta_n + 2\pi f_{\text{D}_n} kT_c)} \text{sinc}\left(\ell - \frac{\tau_n}{T_c}\right) \tag{3.5}$$

where

$$c = \sqrt{\frac{1}{K_{\text{Rice}}+1}} \tag{3.6}$$

represents the standard deviation of the NLOS contribution, $\theta_n \sim \mathscr{U}(0,2\pi)$ is the uniform phase of the nth path. In (3.5), the Doppler frequency f_{D_n} of the nth path can be obtained from the uniform random variable $u_n \sim \mathscr{U}(0,1)$ using the following expression:

$$f_{\text{D}n} = f_{\text{D}\max} \cos[\phi_{a_L} + (\phi_{a_H} - \phi_{a_L})u_n] \tag{3.7}$$

with ϕ_{a_L} and ϕ_{a_H} representing, respectively, the lower- and upper-limits of the angular diffuse components beam, and the maximum Doppler frequency $f_{\mathrm{D}\max}$ can be evaluated as

$$f_{\mathrm{D}\max} = \frac{v}{\lambda_c} = \frac{v}{c_0} f_{\mathrm{c}} \,. \tag{3.8}$$

Moreover, τ_n denotes the time-delay of the nth path which can be generated from the uniform random variable $u_n \sim \mathscr{U}(0,1)$ as

$$\tau_n = -\tau_{\mathrm{slope}} \log \left[1 - u_n \left(1 - e^{-\tau_{\max}/\tau_{\mathrm{slope}}} \right) \right] \tag{3.9}$$

with $\tau_{\max}$ representing the maximum time-delay of the diffuse paths, whereas τ_{slope} describes the behavior of the time-delay distribution.

For a given Rice factor K_{Rice}, equations (3.4) and (3.6) impose that the power at the output of the channel remains unchanged, i.e., $\mathbb{E}\left[|h_a(t,\tau)|^2|\right] = a^2 + c^2 = 1$. Furthermore when $K_{\mathrm{Rice}} = 0$ (Rayleigh fading), one obtains $a = 0$ and $c = 1$, whereas for $K_{\mathrm{Rice}} \to \infty$ (AWGN channel), one obtains $a = 1$ and $c = 0$, respectively.

Typical values that will be used to simulate the main aeronautical scenarios are shown in [35] and reported in Tab. 3.1.

3.4 The BEM approach

Many channel models, as well as the classical WSSUS one, are based on time varying gains modeled as low-pass Gaussian processes. Such models correctly represent the channel when there is an moderate-to-large number of scatterers. Recently, deterministic models based on the *basis expansion model* (BEM) have been proposed (see [32, 73]), which have been shown to be more efficient than the stochastic ones when a small number of scatterers is involved.

According to the BEM approach, the time-varying channel coefficients are expressed as superposition of suitable time-varying base functions (e.g., complex exponentials) with time-invariant coefficients. In this way, one obtains parsimonious models (i.e., described by a reasonable number of parameters) that can be used to conveniently represent rapidly time-varying channels.

The discrete-time expression of the input-output relationship through an

LTV channel $h(k,\ell)$ is

$$r(k) = \sum_{\ell=-\infty}^{+\infty} h(k,\ell)s(k-\ell) \tag{3.10}$$

where $s(k)$ and $r(k)$ represent the input and output signals, respectively, and $k \in \mathbb{Z}$. Under the BEM approach, the impulse response of the LTV channel is expressed, for any $\ell \in \mathbb{Z}$, in terms of a suitable set of base functions $\{u_q(k)\}_{q=0,1,\ldots,Q-1}$ (see [37]):

$$h(k,\ell) = \sum_{q=0}^{Q-1} c_q(\ell)u_q(k) \tag{3.11}$$

where the coefficients of the representation $c_q(\ell)$ depend on $\ell \in \mathbb{Z}$ but are independent of $k \in \mathbb{Z}$.

Typical sets of base functions are the complex exponentials (CE-BEM, see [32]) and the discrete prolate spheroidal sequences (DPS-BEM, see [82]). Both CE-BEM (with a suitable frequency sampling) and DPS-BEM are able to accurately represent the stochastic Jakes model.

Substituting the BEM representation (3.11) in (3.10), one obtains

$$r(k) = \sum_{q=0}^{Q-1} u_q(k) \sum_{\ell=-\infty}^{+\infty} c_q(\ell)s(k-\ell) \tag{3.12}$$

The resulting model is a *SIMO channel model*, wherein the time-varying channel is described by a filter-bank composed by Q time-invariant filters with impulse response $c_q(\ell)$, with $q \in \{0,1,\ldots,Q-1\}$ and $\ell \in \mathbb{Z}$. In the CE-BEM case, the structure (3.12) is reminiscent of FRESH filtering (see [25]).

3.4.1 CE-BEM

In CE-BEM model (see [5]), the impulse response $h_{\mathrm{BEM}}(k,\ell)$ of the channel, with $k \in \mathscr{K} \triangleq \{k_0, k_0+1, k_0+K-1\}$ and $\ell \in \mathbb{Z}$, is expressed as

$$h_{\mathrm{BEM}}(k,\ell) = \sum_{q=-Q_{\mathrm{h}}/2}^{Q_{\mathrm{h}}/2} h_q(\ell)e^{j\frac{2\pi}{P}kq} \tag{3.13}$$

where K represents the length of the observation time window, and P and Q_{h} are design parameters. In particular, if one chooses $P = K$, the CE-BEM model

is said to be *critically sampled*; instead, it is proven that *oversampled* CE-BEM models, i.e., with $P > K$, represent very well the Jakes channel (see [69]). Typical design choices are $P = 2K$ and $Q_{\rm h} = 2\lceil f_{\rm D\max} P T_{\rm c} \rceil$.

Note that (3.13) can be compactly rewritten as

$$h_{\rm BEM}(k,\ell) = \mathbf{e}^{\rm T}(k)\mathbf{h}(\ell) \tag{3.14}$$

where $\mathbf{e}(k) \triangleq \left[e^{j\frac{2\pi}{P}\left(-\frac{Q_{\rm h}}{2}\right)k}, e^{j\frac{2\pi}{P}\left(-\frac{Q_{\rm h}}{2}+1\right)k}, \ldots, e^{j\frac{2\pi}{P}\frac{Q_{\rm h}}{2}k}\right]^{\rm T} \in \mathbb{C}^{Q_{\rm h}+1}$, and $\mathbf{h}(\ell) \triangleq \left[h_{-Q_{\rm h}/2}(\ell), h_{-Q_{\rm h}/2+1}(\ell), \ldots, h_{Q_{\rm h}/2}(\ell)\right]^{\rm T} \in \mathbb{C}^{Q_{\rm h}+1}$.

If we assume that the channel has finite-length impulse response, i.e., $h_{\rm BEM}(k,\ell) \neq 0$ only for $\ell \in \{0,1,L_{\rm h}-1\}$, the $L_{\rm h}$ relationships described by (3.14) can be expressed in matrix forma as

$$\mathbf{h}_{\rm BEM}^{\rm T}(k) = \mathbf{e}^{\rm T}(k)\,\mathbf{H} \tag{3.15}$$

where $\mathbf{h}_{\rm BEM}(k) \triangleq [h_{\rm BEM}(k,0), h_{\rm BEM}(k,1), \ldots, h_{\rm BEM}(k,L_{\rm h}-1)]^{\rm T} \in \mathbb{C}^{L_{\rm h}}$, with $k \in \mathscr{K}$, and

$$\mathbf{H} \triangleq \begin{bmatrix} h_{-Q_{\rm h}/2}(0) & h_{-Q_{\rm h}/2}(1) & \cdots & h_{-Q_{\rm h}/2}(L_{\rm h}-1) \\ h_{-Q_{\rm h}/2+1}(0) & h_{-Q_{\rm h}/2+1}(1) & \cdots & h_{-Q_{\rm h}/2+1}(L_{\rm h}-1) \\ \vdots & \vdots & \ddots & \vdots \\ h_{Q_{\rm h}/2}(0) & h_{Q_{\rm h}/2}(1) & \cdots & h_{Q_{\rm h}/2}(L_{\rm h}-1) \end{bmatrix} \in \mathbb{C}^{(Q_{\rm h}+1)\times L_{\rm h}} \tag{3.16}$$

Finally, collecting the data for all k values, we obtain the linear system

$$\mathbf{H}_{\rm BEM} = \mathbf{E}\,\mathbf{H} \tag{3.17}$$

where $\mathbf{H}_{\rm BEM} \triangleq [\mathbf{h}_{\rm BEM}(k_0), \mathbf{h}_{\rm BEM}(k_0+1), \ldots, \mathbf{h}_{\rm BEM}(k_0+K-1)]^{\rm T} \in \mathbb{C}^{K\times L_{\rm h}}$, and $\mathbf{E} \triangleq [\mathbf{e}(k_0), \mathbf{e}(k_0+1), \ldots, \mathbf{e}(k_0+K-1)]^{\rm T} \in \mathbb{C}^{K\times(Q_{\rm h}+1)}$.

To evaluate the coefficients of the BEM representation, i.e., the matrix $\mathbf{H}$, one can resort the following least-square optimization:

$$\widehat{\mathbf{H}} = \arg\min_{\mathbf{H}} \|\mathbf{H}_{\rm LTV} - \mathbf{E}\mathbf{H}\|^2 \tag{3.18}$$

where

$$\mathbf{H}_{\rm LTV} \triangleq \begin{bmatrix} h(k_0,0) & \cdots & h(k_0,L_{\rm h}-1) \\ \vdots & \ddots & \vdots \\ h(k_0+K-1,0) & \cdots & h(k_0+K-1,L_{\rm h}-1) \end{bmatrix} \tag{3.19}$$

whose solution can be expressed as (see [7])

$$\widehat{\mathbf{H}} = \mathbf{E}^{-}\mathbf{H}_{\mathrm{LTV}} = \mathbf{E}^{\mathrm{H}}[\mathbf{E}\mathbf{E}^{\mathrm{H}}]^{-1}\mathbf{H}_{\mathrm{LTV}} \tag{3.20}$$

3.5 Numerical results

In the following we report some Matlab simulations aimed at showing the goodness-of-fit of the CE-BEM approach (see [5]) to represent the models proposed by Haas (see [35]).

We considered a communication system working at the carrier frequency $f_{\mathrm{c}} = 2.375$ GHz (S-band). For each scenario, we used an observation window of length $K = \left\lceil \frac{3}{f_{\mathrm{D}\max} T_{\mathrm{c}}} \right\rceil$, i.e., three-times the coherence time of the channel, whereas we set the sample time as $T_{\mathrm{c}} = \tau_{\max}/50$ for en-route scenario and $T_{\mathrm{c}} = \tau_{\max}/10$ for all the other ones. All simulations have been carried out with $P = 2K$ and $Q_{\mathrm{h}} = 2\lceil f_{\mathrm{D}\max} P T_{\mathrm{c}} \rceil$.

To evaluate the accuracy of the BEM representation we used the mean-square error, for all $k \in \mathscr{K}$ and $\ell \in \{0, 1, \ldots, L_{\mathrm{h}} - 1\}$, with respect to the true Haas channel, defined as

$$\mathrm{MSE}(k,\ell) \triangleq \mathbb{E}\left[\|h(k,\ell) - h_{\mathrm{BEM}}(k,\ell)\|^2\right] \tag{3.21}$$

where the statistical mean has been estimated on 10 realizations of the channel.

3.5.1 Parking scenario

Figure 3.1 reports a single realization of the Haas channel, furthermore, to better observe its behavior, we show in Fig. 3.2 a cut of the same realization for $k = 0$.

In Fig. 3.3, the MSE (expressed in dB) of the BEM representation is shown; the representation error is very small for all $k \in \mathscr{K}$ and $\ell \in \{0, 1, \ldots, L_{\mathrm{h}} - 1\}$. Figure 3.4 plots an estimate of the power delay profile of the Haas model (top) and the same for the BEM approximation (bottom), whereas Fig. 3.5 plots an estimate of the Doppler spectrum of the Haas channel (top) followed by the Doppler spectrum of its BEM approximation (bottom). Note that the BEM approach provides a very good representation of the delay and Doppler profiles of the channel model.

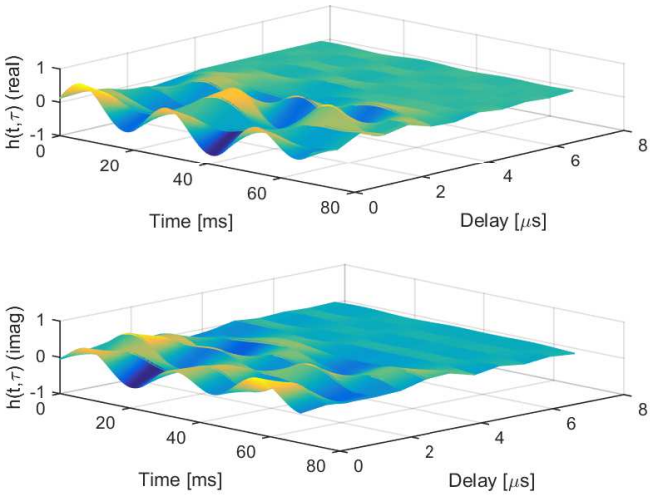

Figure 3.1: Parking scenario – real part (top) and imaginary part (bottom) of one realization of the channel.

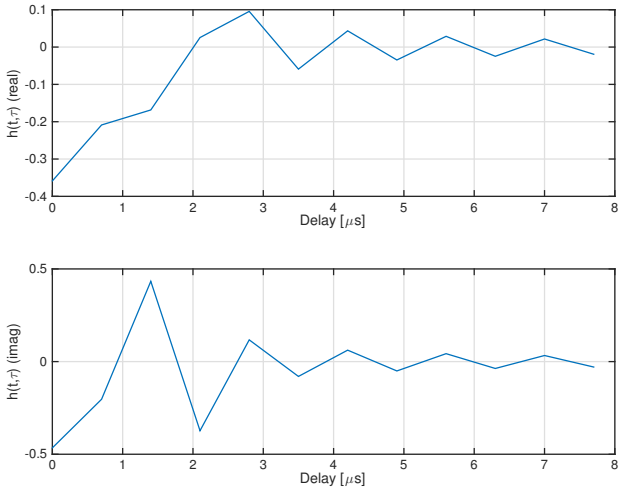

Figure 3.2: Parking scenario – real part (top) and imaginary part (bottom) of one realization of the channel, with $k = 0$.

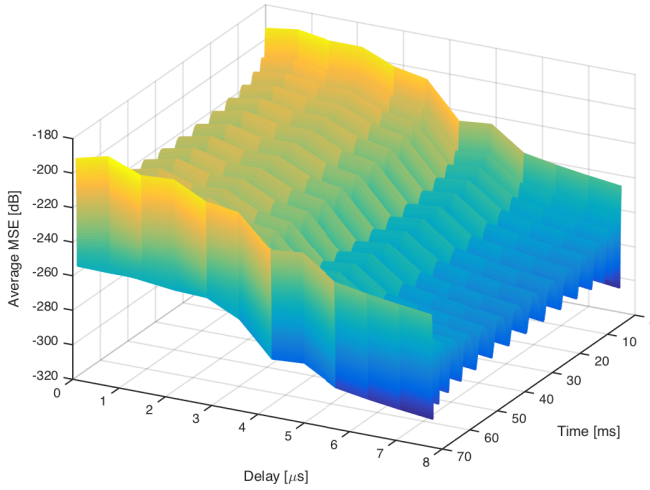

Figure 3.3: Parking scenario – mean-square error of BEM representation.

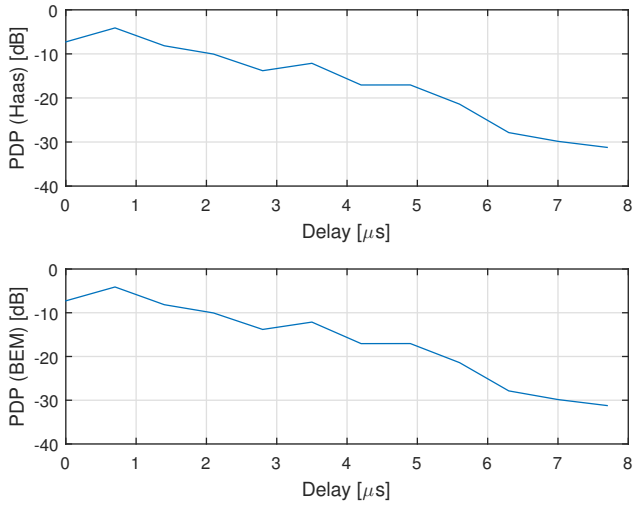

Figure 3.4: Parking scenario – power delay profile of the Haas channel (top) and of the BEM representation (bottom).

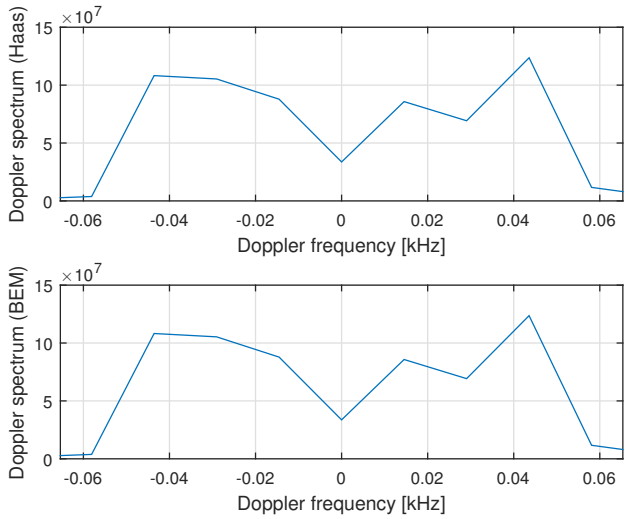

Figure 3.5: Parking scenario – Doppler power spectrum of the Haas channel (top) and of the BEM representation (bottom).

3.5.2 Taxiing scenario

In Fig. 3.6, a single realization of the Haas channel (taxiing scenario) is reported; furthermore we show in Fig. 3.7 the same realization for $k = 0$.

Figure 3.8 plots the MSE (expressed in dB) of the BEM representation expressed in dB. The representation error is again very small for all $k \in \mathscr{K}$ and $\ell \in \{0, 1, \ldots, L_{\mathrm{h}} - 1\}$. Figure 3.9 plots an estimate of the power delay profile of the Haas model (top) and of its BEM approximation (bottom), whereas Fig. 3.10 plots an estimate of the Doppler spectrum of the Haas channel (top) followed by the Doppler spectrum of its BEM approximation (bottom). The obtained behaviors are again indistinguishable, thus assuring that the BEM approach provide a very accurate representation of the delay and Doppler profiles of the channel model.

3.5.3 Takeoff/Landing scenario

In Fig. 3.11, a single realization of the Haas channel is reported, with the real part (top) and the imaginary one (bottom). Furthermore, we show in Fig. 3.12

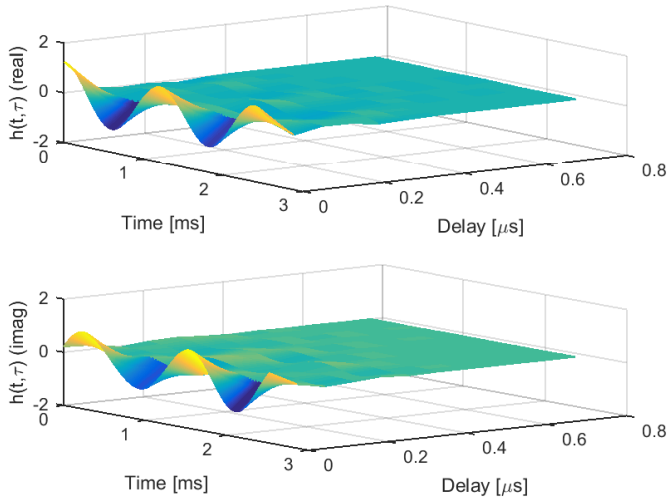

Figure 3.6: Taxiing scenario – real part (top) and imaginary part (bottom) of one realization of the channel.

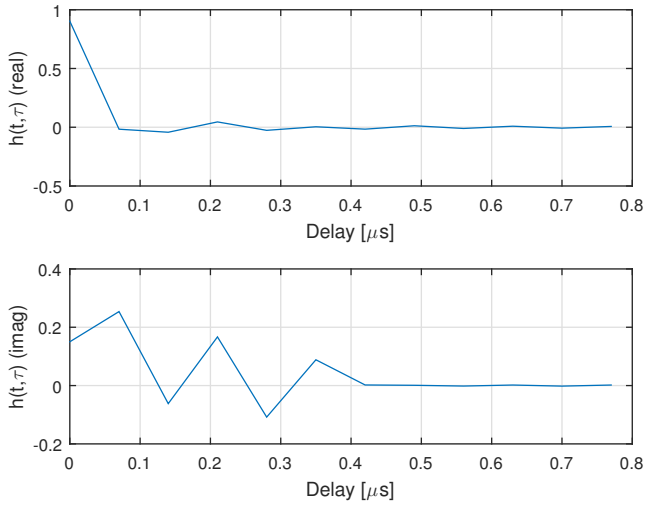

Figure 3.7: Taxiing scenario – real part (top) and imaginary part (bottom) of one realization of the channel, with $k = 0$.

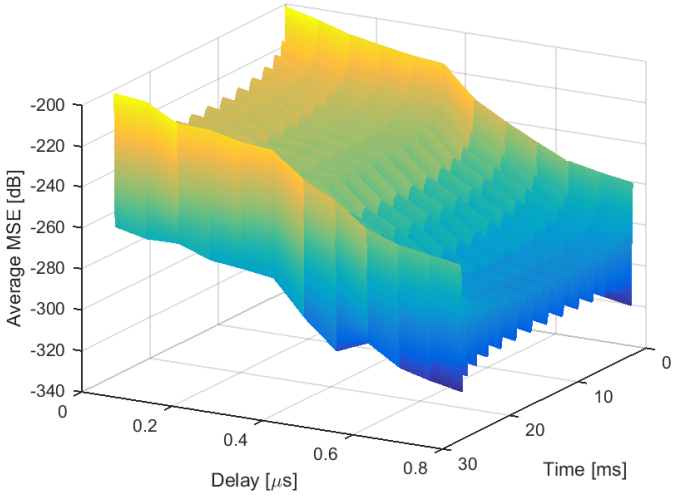

Figure 3.8: Taxiing scenario – mean-square error of BEM representation.

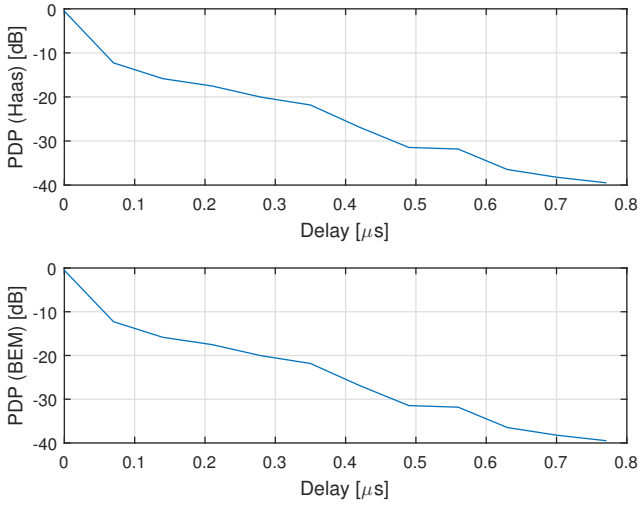

Figure 3.9: Taxiing scenario – power delay profile of the Haas channel (top) and of the BEM representation (bottom).

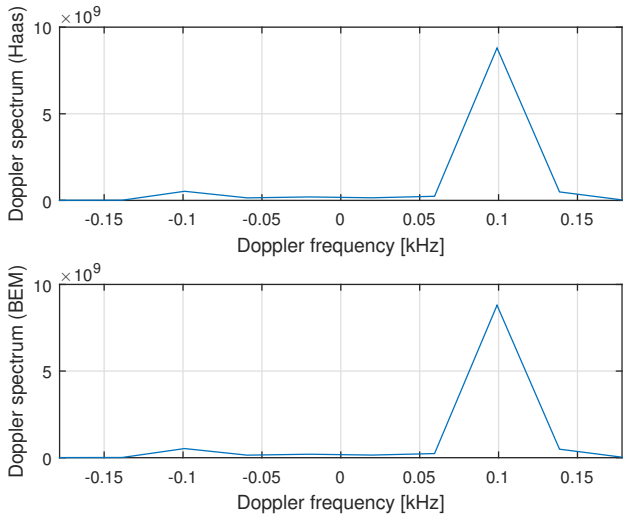

Figure 3.10: Taxiing scenario – Doppler power spectrum of the Haas channel (top) and of the BEM representation (bottom).

a cut of the same realization for $k = 0$.

In Fig. 3.13, the MSE of the BEM representation is reported, expressed in dB. The plot shows that the approximation error is very small for all $k \in \mathscr{K}$ and $\ell \in \{0, 1, \ldots, L_{\mathrm{h}} - 1\}$. Figure 3.14 reports an estimate of the power delay profile of the Haas model (top) and the its BEM approximation (bottom), whereas Fig. 3.15 reports an estimate of the Doppler spectrum of the Haas channel (top) followed by the Doppler spectrum of its BEM approximation (bottom). The BEM approximation is very accurate because the delay and Doppler profiles of the channel model are again indistinguishable.

3.5.4 En-route scenario

In Figs. 3.16–3.20 the results obtained in the en-route scenario are reported. In particular, in Fig. 3.16 we show a single realization of the Haas channel (real part on top and imaginary part on the bottom), whereas in Fig. 3.17 the details of the same representation for $k = 0$ are reported. In Fig. 3.18 the MSE error of the BEM representation with respect to the Haas model is reported; the BEM approximation provides again very good results. Finally in Figs. 3.19–3.20

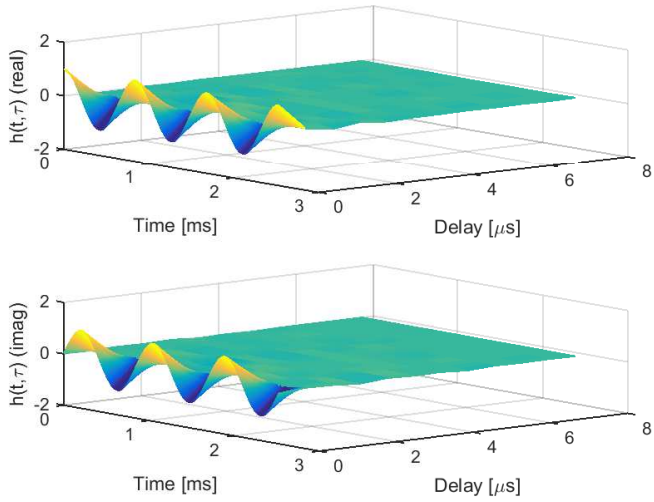

Figure 3.11: Arrival scenario – real part (top) and imaginary part (bottom) of one realization of the channel.

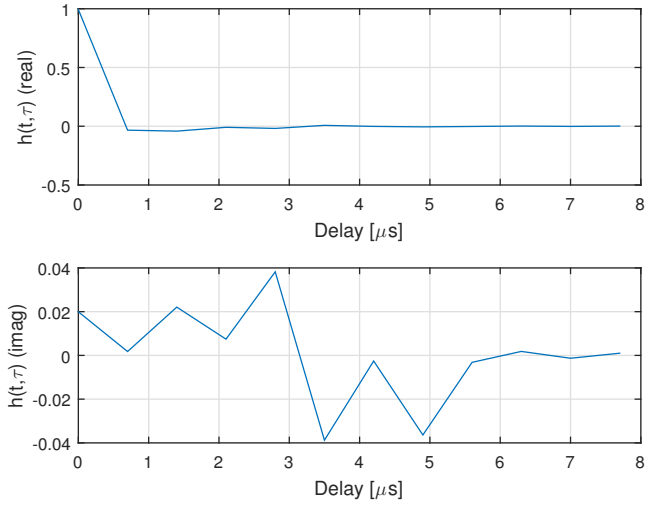

Figure 3.12: Arrival scenario – real part (top) and imaginary part (bottom) of one realization of the channel, with $k = 0$.

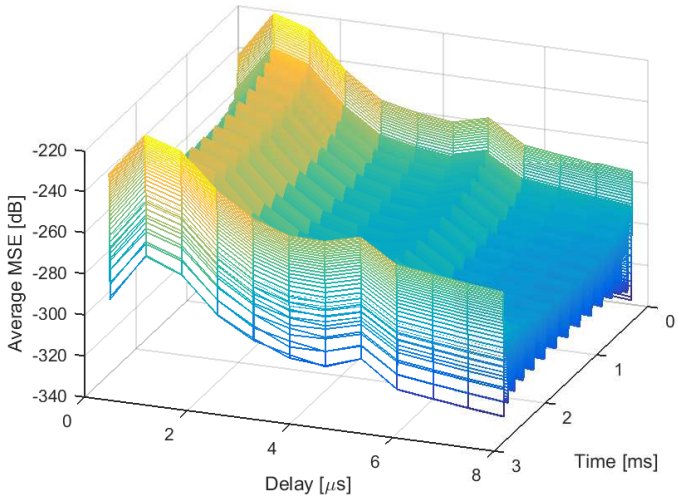

Figure 3.13: Arrival scenario – mean-square error of BEM representation.

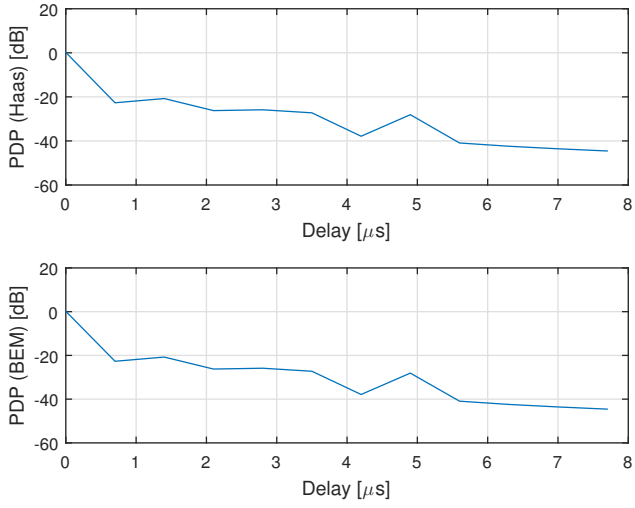

Figure 3.14: Arrival scenario – power delay profile of the Haas channel (top) and of the BEM representation (bottom).

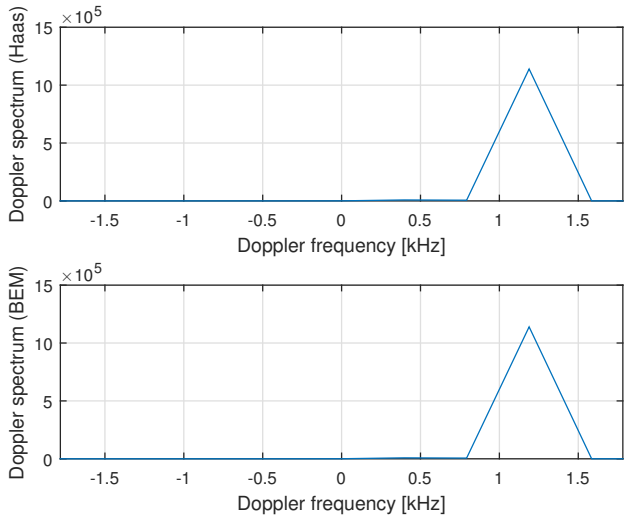

Figure 3.15: Arrival scenario – Doppler power spectrum of the Haas channel (top) and of the BEM representation (bottom).

we show, respectively, the power delay profile and the Doppler spectrum of the Haas model (top) and its BEM representation (bottom). The behaviors are indistinguishable again, thus we can say that the BEM approximation is able to represent very accurately all the aeronautical channel models proposed by Haas in [35].

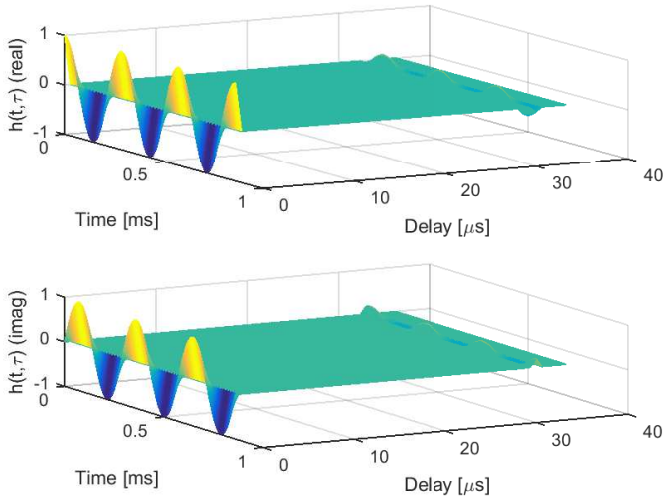

Figure 3.16: En-route scenario – real part (top) and imaginary part (bottom) of one realization of the channel.

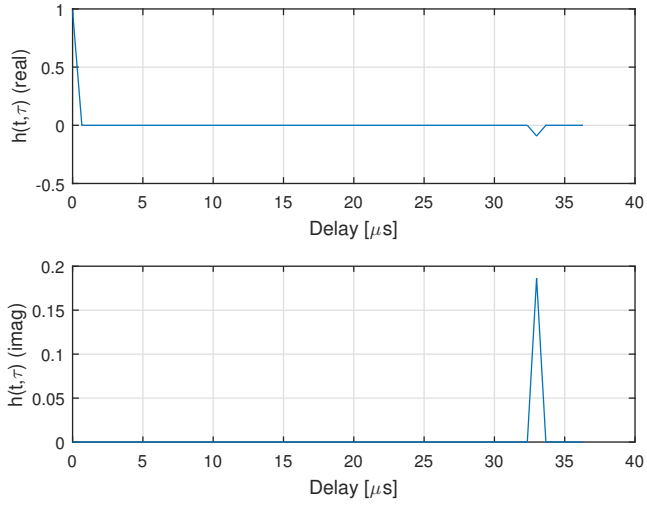

Figure 3.17: En-route scenario – real part (top) and imaginary part (bottom) of one realization of the channel, with $k = 0$.

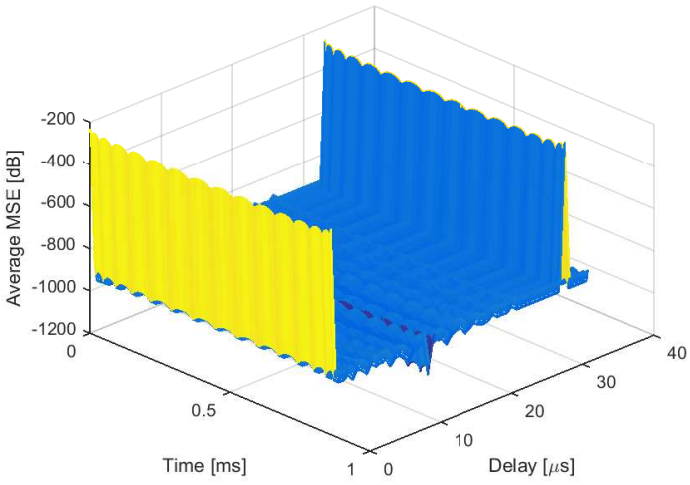

Figure 3.18: En-route scenario – mean-square error of BEM representation.

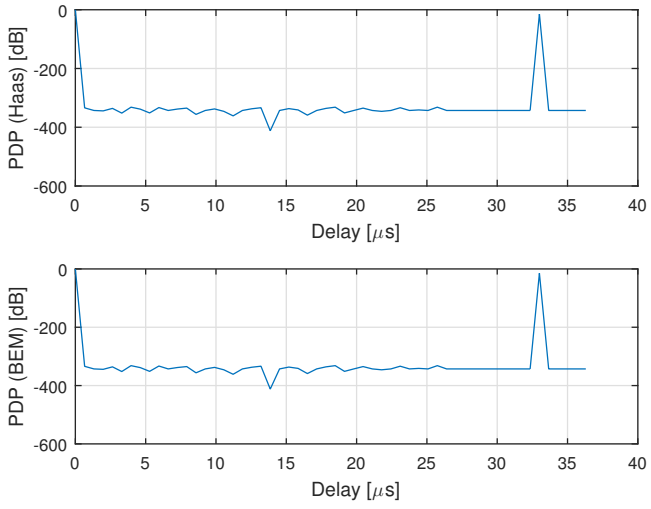

Figure 3.19: En-route scenario – power delay profile of the Haas channel (top) and of the BEM representation (bottom).

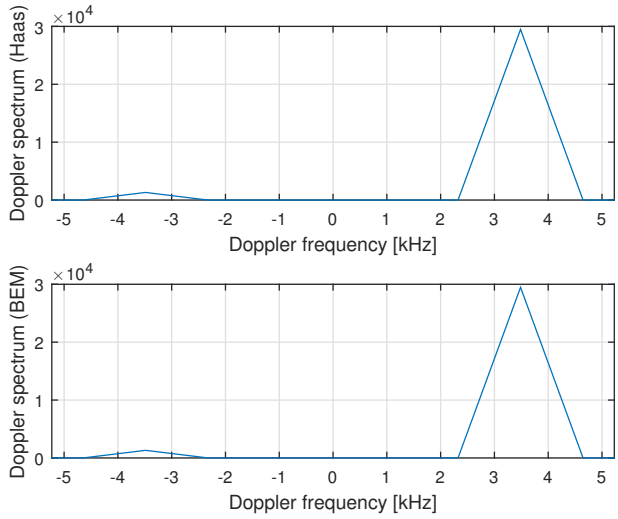

Figure 3.20: En-route scenario – Doppler power spectrum of the Haas channel (top) and of the BEM representation (bottom).

Chapter 4

Time-varying equalization for CPM signals

In this chapter, the problem of receiving a CPM signal over a doubly-selective channel is tackled. Section 4.1 contains a brief introduction to techniques used for receiving CPM signals over doubly-selective channels, whereas Sec. 4.2 describes the system model. In Sec. 4.3 both *zero-forcing* (ZF) and *minimum mean square error* (MMSE) LTV equalizers are synthesized, whereas in Sec. 4.4 their *widely-linear* versions are proposed for non-circular CPM signals. In Sec. 4.5 and 4.6, we introduce simplified implementations of the equalizer and decision rule, respectively, whereas in Sec. 4.7, by exploiting the BEM model for the doubly-selective channel, convenient *frequency-shift* (FRESH) versions of the proposed equalizers are derived. Finally, the performance analysis of the proposed receivers is carried out by Monte Carlo computer simulations in Sec. 4.8.

4.1 Introduction

Since CPM modulation has memory, its main drawback is the high computational complexity of the optimal *maximum-likelihood* (ML) detection strategy. This issue can be partially overcome by exploiting the inherent trellis structure of CPM and resorting to the *Viterbi algorithm* (VA) [65]. However, in aeronautical communications, due to the high-speed of the aircrafts, the wire-

less channel might exhibit joint frequency and time selectivity: when CPM is employed over such *doubly-selective* channels, even optimal ML detection by means of Viterbi algorithm becomes prohibitive, due to the huge number of states of the trellis and the need to perform fast channel estimation and tracking.

Several approaches aimed at reducing the complexity of the ML receiver have been proposed, mostly suited for time-invariant channels. A popular approach considered in [70, 61, 72] performs preliminary frequency-domain channel equalization to mitigate the effects of *intersymbol interference* (ISI), allowing thus the subsequent VA to work in an almost ISI-free setting, albeit with colored noise. However, frequency-domain equalization is not a computationally advantageous strategy when the channel is rapidly time-varying, since in this case the channel cannot be diagonalized by a channel-independent transformation of the received data [5, 79, 78].

Herein we take a different approach, by designing *linear time-varying* (LTV) or *widely-linear time-varying* (WLTV) equalizers to mitigate channel ISI. The proposed equalizers leverage on the well-known Laurent decomposition of a CPM signal shown in Chap. 2 to perform *time-varying* (TV) equalization in the time domain. The overall receiver is composed by two stages: the first stage performs LTV or WLTV equalization, allowing one to extract the pseudo-symbols; the second stage performs a simple recursive inversion to obtain the symbol sequence from the pseudo-symbols. The obtained structure, although suboptimal, allows one to equalize rapidly time-varying and dispersive channels with an affordable complexity.

We also propose a method to eventually tackle ill-conditioning problems inherent to the equalizer synthesis and reduce the complexity of the time domain equalizers, as well as a simple recursive decision rule to extract the symbols from the pseudo-symbols. Moreover, by exploiting the BEM model for the doubly-selective channel described in Sec. 3.4, we derive convenient *frequency-shift* (FRESH) versions of the proposed equalizers, showing that they can be implemented as a parallel bank of *linear time-invariant* (LTI) filters having, as input signals, different frequency-shifted versions of the received data.

4.2 System model

Let us consider a wireless communication system employing a binary partial-response[1] one-sided CPM modulation format with baud-rate $1/T$, $\mathscr{E} = T/2$ and modulation index $h \notin \mathbb{Z}$, whose complex envelope, recalling (2.2) and (2.3), is given by

$$x_{\mathrm{a}}(t) = \exp\left[j2\pi h \sum_{i=0}^{+\infty} a_i q_{\mathrm{a}}(t - iT) \right] \tag{4.1}$$

By means of Laurent representation, the signal (4.1) can also be expressed as

$$x_{\mathrm{a}}(t) = \sum_{q=0}^{Q-1} \sum_{i=0}^{+\infty} s_{q,i} c_{\mathrm{a},q}(t - iT) \tag{4.2}$$

where, for all $i \in \mathbb{Z}$, $s_{q,i}$ and $c_{\mathrm{a},q}(t)$ are, respectively, the qth pseudo-symbol and the qth Laurent pulse [see Sec. 2.2].

To obtain a compact discrete model for the overall communication system, we assume that the CPM signal given by (4.1) or (4.2) is well represented (see [53]) by its samples $x(k) \triangleq x_{\mathrm{a}}(kT_{\mathrm{c}})$ taken with rate $1/T_{\mathrm{c}} \triangleq N/T$, with $N > 1$ denoting the *oversampling factor*. In particular, we will find it convenient to resort to the following[2] *polyphase decomposition* of $x(k)$ with respect to N:

$$x^{(\eta)}(\ell) \triangleq x(\ell N + \eta) = x_{\mathrm{a}}(\ell T + \eta T_{\mathrm{c}}) = \sum_{q=0}^{Q-1} \sum_{i=0}^{+\infty} s_{q,i} c_q^{(\eta)}(\ell - i) \tag{4.3}$$

where (4.2) has been taken into account, and $c_q^{(\eta)}(\ell) \triangleq c_{\mathrm{a},q}(\ell T + \eta T_{\mathrm{c}})$.

The CPM signal given by (4.1) or (4.2) is up-converted to *radio-frequency* (RF) and transmitted over a wireless channel; the received distorted signal, corrupted by AWGN, is filtered and sampled. Denoting with $h_{\mathrm{a}}(t, \tau)$ the overall time-varying channel impulse response (including also the effects of transmit/receive filters), we assume that:

(a-4.1) the channel spans L_{h} symbol periods in τ, i.e., $h_{\mathrm{a}}(t, \tau) \equiv 0$ for $\tau \notin [0, L_{\mathrm{h}} T]$.

[1] For the sake of simplicity, our design assumes a binary single-h partial-response CPM signal, with $h \notin \mathbb{Z}$. Extensions to non-binary and/or multi-h CPM signals are less tractable and will be the subject of further investigations.

[2] Remember that since $x_{\mathrm{a}}(t)$ is a one-sided signal, $x(k) = x_{\mathrm{a}}(kT_{\mathrm{c}}) \equiv 0$ for all $k < 0$.

The complex envelope of the received signal, at the output of the receiver filter, can be expressed as

$$r_{\mathrm{a}}(t) = \sum_{\ell=0}^{+\infty} \sum_{\eta=0}^{N-1} x^{(\eta)}(\ell)\, h_{\mathrm{a}}(t, t-\ell T-\eta T_{\mathrm{c}}) + v_{\mathrm{a}}(t) \tag{4.4}$$

where $v_{\mathrm{a}}(t)$ represents filtered AWGN, whereas $x^{(\eta)}(\ell)$ samples are given by (4.3). Hence, assuming perfect symbol synchronization, the received signal given by (4.4) is sampled at time instants $t_{k,n} \triangleq kT + nT_{\mathrm{c}}$, with $k \in \mathbb{Z}$ and $n \in \{0,1,\ldots,N-1\}$, thus obtaining $r^{(n)}(k) \triangleq r_{\mathrm{a}}(t_{k,n})$ represented by the following polyphase decomposition with respect to N:

$$r^{(n)}(k) = \sum_{\ell=0}^{L_{\mathrm{h}}} \sum_{\eta=0}^{N-1} h^{(n)}(k, \ell N+n-\eta) x^{(\eta)}(k-\ell) + v^{(n)}(k) \tag{4.5}$$

where $h^{(n)}(k,\ell) \triangleq h(kN+n,\ell)$, and the discrete-time channel $h(k,\ell) \triangleq h_{\mathrm{a}}(kT_{\mathrm{c}}, \ell T_{\mathrm{c}})$, due to **(a-4.1)**, is a causal *finite impulse response* (FIR) system of order $NL_{\mathrm{h}}+1$, i.e., $h(k,\ell) \equiv 0$ for $\ell \notin \{0,1,\ldots,NL_{\mathrm{h}}\}$, and $v^{(n)}(k) \triangleq v_{\mathrm{a}}(t_{k,n})$.

The following customary assumptions will be considered in the sequel:

(a-4.2) the information-bearing symbols $a_i \in \{\pm 1\}$ are modeled as a sequence of independent and identically distributed (i.i.d.) zero-mean random variables, with $\mathbb{E}\left[a_i^2\right] = 1$;

(a-4.3) the noise samples $\{v^{(n)}(k)\}_{n=0}^{N-1}$ are modeled as mutually independent zero-mean random variables, with variance $\sigma_v^2 \triangleq \mathbb{E}\left[|v^{(n)}(k)|^2\right]$, statistically independent of a_i for each $i \in \mathbb{Z}$.

We further assume that:

(a-4.4) the noise variance σ_v^2 is either exactly known at the receiver or it is estimated by using data-aided or non-data aided algorithm (see [9]).

Collecting N consecutive samples (4.5) into the vector $\mathbf{r}(k) \triangleq [r^{(0)}(k), r^{(1)}(k), \ldots, r^{(N-1)}(k)]^{\mathrm{T}} \in \mathbb{C}^N$, the model in (4.5) can be compactly expressed as

$$\mathbf{r}(k) = \sum_{\ell=0}^{L_{\mathrm{h}}} \mathbf{H}_{\ell}(k)\mathbf{x}(k-\ell) + \mathbf{v}(k) \tag{4.6}$$

where the (i_1+1, i_2+1)th element of the time-varying matrix $\mathbf{H}_{\ell}(k) \in \mathbb{C}^{N\times N}$ is given by $\{\mathbf{H}_{\ell}(k)\}_{i_1,i_2} = h^{(i_1)}(k, \ell N+i_1-i_2)$, for $i_1, i_2 \in \{0,1,\ldots,N-1\}$, and $\mathbf{x}(k) \triangleq [x^{(0)}(k), x^{(1)}(k), \ldots, x^{(N-1)}(k)]^{\mathrm{T}} \in \mathbb{C}^N$.

To further expand (4.6), observe that due to the support properties of $c_{\mathrm{a},q}(t)$, eq. (4.3) can be expressed as

$$x^{(\eta)}(k) = \sum_{q=0}^{Q-1} \sum_{i=k-L_q+1}^{k} s_{q,i} c_q^{(\eta)}(k-i) = \sum_{q=0}^{Q-1} \sum_{i=0}^{L_q-1} s_{q,k-i} c_q^{(\eta)}(i) \tag{4.7}$$

thus $\mathbf{x}(k)$ in (4.6) can be compactly rewritten as

$$\mathbf{x}(k) = \sum_{q=0}^{Q-1} \mathbf{C}_q \mathbf{s}_q(k) \tag{4.8}$$

where, for $i_1, i_2 \in \{0,1,\ldots,N-1\}$, the (i_1+1, i_2+1)th element of the matrix $\mathbf{C}_q \in \mathbb{R}^{N \times L_q}$ is given by $\{\mathbf{C}_q\}_{i_1,i_2} = c_q^{(i_1)}(i_2)$, and $\mathbf{s}_q(k) \triangleq [s_{q,k}, s_{q,k-1}, \ldots, s_{q,k-L_q+1}]^{\mathrm{T}} \in \mathbb{C}^{L_q}$.

Finally, by exploiting (4.8), the received vector (4.6) can be expressed as

$$\mathbf{r}(k) = \sum_{\ell=0}^{L_{\mathrm{h}}} \mathbf{H}_\ell(k) \sum_{q=0}^{Q-1} \mathbf{C}_q \mathbf{s}_q(k-\ell) + \mathbf{v}(k) \tag{4.9}$$

4.3 LTV equalization

To compensate for the deleterious effects induced by time- and frequency-selectivity of the transmission channel, we consider a front-end causal LTV block equalizer of order $L_{\mathrm{e}} > 0$, whose input-output relationship is given by

$$\mathbf{y}(k) = \widetilde{\mathbf{F}}^{\mathrm{H}}(k) \tilde{\mathbf{z}}(k) \tag{4.10}$$

for $k \in \mathbb{Z}$, where $\widetilde{\mathbf{F}}(k) \in \mathbb{C}^{N(L_{\mathrm{e}}+1) \times Q}$ collects all the equalizer parameters, and the input vector, based on (4.9), is given by

$$\tilde{\mathbf{z}}(k) \triangleq \begin{bmatrix} \mathbf{r}(k) \\ \mathbf{r}(k-1) \\ \vdots \\ \mathbf{r}(k-L_{\mathrm{e}}) \end{bmatrix} = \widetilde{\mathbf{H}}(k) \sum_{q=0}^{Q-1} \widetilde{\mathbf{C}}_q \tilde{\mathbf{b}}_q(k) + \tilde{\mathbf{w}}(k) = \widetilde{\mathbf{H}}(k) \widetilde{\mathbf{C}} \tilde{\mathbf{b}}(k) + \tilde{\mathbf{w}}(k) \tag{4.11}$$

where $\tilde{\mathbf{b}}_q(k) \triangleq [s_{q,k}, s_{q,k-1}, \ldots, s_{q,k-L_\mathrm{a}-L_\mathrm{q}+1}]^\mathrm{T} \in \mathbb{C}^{L_\mathrm{a}+L_\mathrm{q}}$, with $L_\mathrm{a} = L_\mathrm{e} + L_\mathrm{h}$, $\widetilde{\mathbf{C}}_q \in \mathbb{R}^{N(L_\mathrm{a}+1)\times(L_\mathrm{a}+L_\mathrm{q})}$ is a block matrix defined as[3]

$$\widetilde{\mathbf{C}}_q \triangleq \begin{bmatrix} \mathbf{C}_q & \mathbf{0}_N & \cdots & \mathbf{0}_N \\ \mathbf{0}_N & \mathbf{C}_q & \cdots & \mathbf{0}_N \\ \vdots & \ddots & \ddots & \vdots \\ \mathbf{0}_N & \cdots & \mathbf{0}_N & \mathbf{C}_q \end{bmatrix} \tag{4.12}$$

matrix $\widetilde{\mathbf{H}}(k) \in \mathbb{C}^{N(L_\mathrm{e}+1)\times N(L_\mathrm{a}+1)}$ is defined as

$$\widetilde{\mathbf{H}}(k) \triangleq \begin{bmatrix} \mathbf{H}_0(k) & \cdots & \mathbf{H}_{L_\mathrm{h}}(k) & \mathbf{O}_{N\times N} & \cdots & \mathbf{O}_{N\times N} \\ \mathbf{O}_{N\times N} & \mathbf{H}_0(k-1) & \cdots & \mathbf{H}_{L_\mathrm{h}}(k-1) & \cdots & \mathbf{O}_{N\times N} \\ \vdots & \ddots & \ddots & \ddots & \ddots & \vdots \\ \mathbf{O}_{N\times N} & \cdots & \mathbf{H}_0(k-L_\mathrm{e}) & \mathbf{H}_1(k-L_\mathrm{e}) & \cdots & \mathbf{H}_{L_\mathrm{h}}(k-L_\mathrm{e}) \end{bmatrix} \tag{4.13}$$

and $\tilde{\mathbf{w}}(k) \triangleq [\mathbf{v}^\mathrm{T}(k), \mathbf{v}^\mathrm{T}(k-1), \ldots, \mathbf{v}^\mathrm{T}(k-L_\mathrm{e})]^\mathrm{T}$. Moreover, we have defined in (4.11) $\widetilde{\mathbf{C}} \triangleq [\widetilde{\mathbf{C}}_0, \widetilde{\mathbf{C}}_1, \ldots, \widetilde{\mathbf{C}}_{Q-1}] \in \mathbb{R}^{N(L_\mathrm{a}+1)\times(QL_\mathrm{a}+L_\mathrm{c})}$, with $L_\mathrm{c} \triangleq \sum_{q=0}^{Q-1} L_\mathrm{q}$, and $\tilde{\mathbf{b}}(k) \triangleq [\tilde{\mathbf{b}}_0^\mathrm{T}(k), \tilde{\mathbf{b}}_1^\mathrm{T}(k), \ldots, \tilde{\mathbf{b}}_{Q-1}^\mathrm{T}(k)]^\mathrm{T} \in \mathbb{C}^{QL_\mathrm{a}+L_\mathrm{c}}$.

Our aim is to obtain a reliable estimate of the pseudo-symbols block $\mathbf{s}(k-d) \triangleq [s_{0,k-d}, s_{1,k-d}, \ldots, s_{Q-1,k-d}]^\mathrm{T} \in \mathbb{C}^Q$, with $d \in \{0, 1, \ldots, L_\mathrm{a}+1\}$ denoting a suitable equalization delay. In the following, we will present two common strategies to this end, i.e., the ZF and MMSE ones.

4.3.1 LTV-ZF equalizer

Ideally, in the absence of noise, perfect or *zero-forcing* (ZF) recovery can be obtained by using a time-varying ZF equalizer (see [79]). Imposing the ZF condition $\mathbf{y}(k) = \mathbf{s}(k-d)$ leads to the following system of linear equations:

$$\widetilde{\mathbf{F}}^\mathrm{H}(k)\widetilde{\mathbf{H}}(k)\widetilde{\mathbf{C}} = \mathbf{E}_d^\mathrm{T} \tag{4.14}$$

[3]Note that, due to the time-varying assumption for the channel, the matrix $\widetilde{\mathbf{H}}(k)$ loses its typical Toeplitz structure.

with

$$\mathbf{E}_d \triangleq \begin{bmatrix} \mathbf{e}_{d,0} & \mathbf{0}_{L_0+L_\mathrm{a}} & \cdots & \mathbf{0}_{L_0+L_\mathrm{a}} & \mathbf{0}_{L_0+L_\mathrm{a}} \\ \mathbf{0}_{L_1+L_\mathrm{a}} & \mathbf{e}_{d,1} & \cdots & \mathbf{0}_{L_1+L_\mathrm{a}} & \mathbf{0}_{L_1+L_\mathrm{a}} \\ \vdots & \vdots & \ddots & \vdots & \vdots \\ \mathbf{0}_{L_{Q-2}+L_\mathrm{a}} & \mathbf{0}_{L_{Q-2}+L_\mathrm{a}} & \cdots & \mathbf{e}_{d,Q-2} & \mathbf{0}_{L_{Q-2}+L_\mathrm{a}} \\ \mathbf{0}_{L_{Q-1}+L_\mathrm{a}} & \mathbf{0}_{L_{Q-1}+L_\mathrm{a}} & \cdots & \mathbf{0}_{L_{Q-1}+L_\mathrm{a}} & \mathbf{e}_{d,Q-1} \end{bmatrix} \in \mathbb{B}^{(QL_\mathrm{a}+L_\mathrm{c})\times Q} \quad (4.15)$$

where $\mathbf{e}_{d,q} \triangleq [\overbrace{0,0,\ldots,0}^{d},1,\overbrace{0,0,\ldots,0}^{L_q+L_\mathrm{a}-d-1}]^\mathrm{T} \in \mathbb{B}^{L_q+L_\mathrm{a}}$, for all $q \in \{0,1,\ldots,Q-1\}$.

The system of linear equation in (4.14) is consistent (see [7]) if and only if $\widetilde{\mathbf{C}}^\mathrm{T}\widetilde{\mathbf{H}}^\mathrm{H}(k)[\widetilde{\mathbf{C}}^\mathrm{T}\widetilde{\mathbf{H}}^\mathrm{H}(k)]^{-}\mathbf{E}_d = \mathbf{E}_d$, for all $k \in \mathbb{Z}$.

If the matrix $\widetilde{\mathbf{H}}(k)\widetilde{\mathbf{C}} \in \mathbb{C}^{N(L_\mathrm{e}+1)\times(QL_\mathrm{a}+L_\mathrm{c})}$ is full-column rank, i.e., $\mathrm{rank}[\widetilde{\mathbf{H}}(k)\widetilde{\mathbf{C}}] = QL_\mathrm{a}+L_\mathrm{c}$, for all $k \in \mathbb{Z}$, it results that $\widetilde{\mathbf{C}}^\mathrm{T}\widetilde{\mathbf{H}}^\mathrm{H}(k)[\widetilde{\mathbf{C}}^\mathrm{T}\widetilde{\mathbf{H}}^\mathrm{H}(k)]^{-} = \mathbf{I}_{QL_\mathrm{a}+L_\mathrm{c}}$, for all $k \in \mathbb{Z}$, and, then, the system in (4.14) turns out to be consistent irrespective of the equalization delay d. In this case, the *minimal norm* solution of the system in (4.14) is (see, e.g., [7]) given by

$$\widetilde{\mathbf{F}}_{\mathrm{ZF}}(k) = \widetilde{\mathbf{H}}(k)\widetilde{\mathbf{C}}\left[\widetilde{\mathbf{C}}^\mathrm{T}\widetilde{\mathbf{H}}^\mathrm{H}(k)\widetilde{\mathbf{H}}(k)\widetilde{\mathbf{C}}\right]^{-1}\mathbf{E}_d \quad (4.16)$$

Since the condition $\mathrm{rank}[\widetilde{\mathbf{H}}(k)\widetilde{\mathbf{C}}] = QL_\mathrm{a}+L_\mathrm{c}$, for all $k \in \mathbb{Z}$, assures the consistency of the system in (4.14) and, thus, the existence of the WLTV-ZF equalizer, it seems natural to investigate the rank properties of $\widetilde{\mathbf{H}}(k)\widetilde{\mathbf{C}}$.

A *necessary* condition is that $QL_\mathrm{a}+L_\mathrm{c} = Q(L_\mathrm{e}+L_\mathrm{h})+L_\mathrm{c} \leq N(L_\mathrm{e}+1)$, from which

$$L_\mathrm{e} \geq \frac{QL_\mathrm{h}+L_\mathrm{c}-N}{N-Q} \quad (4.17)$$

Note that, since $\mathrm{rank}(\mathbf{AB}) \leq \min[\mathrm{rank}(\mathbf{A}),\mathrm{rank}(\mathbf{B})]$, for all $\mathbf{A} \in \mathbb{C}^{n\times p}$ and $\mathbf{B} \in \mathbb{C}^{p\times m}$, $\widetilde{\mathbf{C}}$ has to be full-column rank, i.e., $\mathrm{rank}(\widetilde{\mathbf{C}}) = QL_\mathrm{a}+L_\mathrm{c}$.

However, it must be observed that the rank of $\widetilde{\mathbf{C}}$ is often not sufficient to obtain a consistent system and correctly synthesize the equalizer; in Sec. 4.5 we explain how to tackle this problem by reducing the number of Laurent's pulses used for the synthesis.

4.3.2 LTV-MMSE equalizer

It is well known that, for ill-conditioned channel matrices, ZF equalization can introduce moderate-to-high amount of noise enhancement. To counteract

this phenomenon, we resort here to the *minimum mean-square error* (MMSE) equalizer, whose expression is obtained by minimizing the output mean-square error objective function $\mathrm{MSE}[\widetilde{\mathbf{F}}(k)] \triangleq \mathbb{E}\left[\|\mathbf{y}(k)-\mathbf{s}(k-d)\|^2\right]$, for all $k \in \mathbb{Z}$, which can also be expressed as

$$\begin{aligned}\mathrm{MSE}[\widetilde{\mathbf{F}}(k)] &= \mathbb{E}\left[\mathrm{tr}\left\{[\mathbf{y}(k)-\mathbf{s}(k-d)][\mathbf{y}(k)-\mathbf{s}(k-d)]^{\mathrm{H}}\right\}\right] \\ &= \mathrm{tr}\left[\widetilde{\mathbf{F}}^{\mathrm{H}}(k)\mathbf{R}_{\tilde{\mathbf{z}}\tilde{\mathbf{z}}}(k)\widetilde{\mathbf{F}}(k) - \widetilde{\mathbf{F}}^{\mathrm{H}}(k)\mathbf{R}_{\tilde{\mathbf{z}}\mathbf{s}}(k) - \mathbf{R}^{\mathrm{H}}_{\tilde{\mathbf{z}}\mathbf{s}}(k)\widetilde{\mathbf{F}}(k) + \mathbf{R}_{\mathbf{ss}}\right]\end{aligned} \tag{4.18}$$

It can be shown (see [39]) that

$$\begin{aligned}\widetilde{\mathbf{F}}^{\mathrm{H}}_{\mathrm{MMSE}}(k) &\triangleq \underset{\widetilde{\mathbf{F}}^{\mathrm{H}}(k)}{\arg\min}\left\{\mathrm{MSE}[\widetilde{\mathbf{F}}(k)]\right\} \\ &= \underset{\widetilde{\mathbf{F}}^{\mathrm{H}}(k)}{\arg\min}\left\{\mathrm{tr}\left[\widetilde{\mathbf{F}}^{\mathrm{H}}(k)\mathbf{R}_{\tilde{\mathbf{z}}\tilde{\mathbf{z}}}(k)\widetilde{\mathbf{F}}(k) - \widetilde{\mathbf{F}}^{\mathrm{H}}(k)\mathbf{R}_{\tilde{\mathbf{z}}\mathbf{s}}(k) - \mathbf{R}^{\mathrm{H}}_{\tilde{\mathbf{z}}\mathbf{s}}(k)\widetilde{\mathbf{F}}(k)\right]\right\} \\ &= \mathbf{R}^{\mathrm{H}}_{\tilde{\mathbf{z}}\mathbf{s}}(k)\mathbf{R}^{-1}_{\tilde{\mathbf{z}}\tilde{\mathbf{z}}}(k)\end{aligned} \tag{4.19}$$

where $\mathbf{R}_{\tilde{\mathbf{z}}\tilde{\mathbf{z}}}(k) \triangleq \mathbb{E}\left[\tilde{\mathbf{z}}(k)\tilde{\mathbf{z}}^{\mathrm{H}}(k)\right] \in \mathbb{C}^{N(L_{\mathrm{e}}+1)\times N(L_{\mathrm{e}}+1)}$ denotes the statistical time-varying correlation matrix of $\tilde{\mathbf{z}}(k)$, and $\mathbf{R}_{\tilde{\mathbf{z}}\mathbf{s}}(k) \triangleq \mathbb{E}\left[\tilde{\mathbf{z}}(k)\mathbf{s}^{\mathrm{H}}(k-d)\right] \in \mathbb{C}^{N(L_{\mathrm{e}}+1)\times Q}$.

It can be readily obtained from (4.11) and assumptions **(a-4.2)** and **(a-4.3)** that

$$\mathbf{R}_{\tilde{\mathbf{z}}\tilde{\mathbf{z}}}(k) = \widetilde{\mathbf{H}}(k)\widetilde{\mathbf{C}}\mathbf{R}_{\tilde{\mathbf{b}}\tilde{\mathbf{b}}}\widetilde{\mathbf{C}}^{\mathrm{T}}\widetilde{\mathbf{H}}^{\mathrm{H}}(k) + \sigma_v^2\mathbf{I}_{N(L_{\mathrm{e}}+1)} \tag{4.20}$$

where $\mathbf{R}_{\tilde{\mathbf{b}}\tilde{\mathbf{b}}} \triangleq \mathbb{E}\left[\tilde{\mathbf{b}}(k)\tilde{\mathbf{b}}^{\mathrm{H}}(k)\right] \in \mathbb{C}^{(QL_{\mathrm{a}}+L_{\mathrm{c}})\times(QL_{\mathrm{a}}+L_{\mathrm{c}})}$, and

$$\mathbf{R}_{\tilde{\mathbf{z}}\mathbf{s}}(k) = \widetilde{\mathbf{H}}(k)\widetilde{\mathbf{C}}\mathbf{R}_{\tilde{\mathbf{b}}\mathbf{s}} \tag{4.21}$$

where $\mathbf{R}_{\tilde{\mathbf{b}}\mathbf{s}} \triangleq \mathbb{E}\left[\tilde{\mathbf{b}}(k)\mathbf{s}^{\mathrm{H}}(k-d)\right] \in \mathbb{C}^{(QL_{\mathrm{a}}+L_{\mathrm{c}})\times Q}$. Note that the exact expression of the entries of the statistical correlation matrix $\mathbf{R}_{\tilde{\mathbf{b}}\tilde{\mathbf{b}}}$, as well as those of $\mathbf{R}_{\tilde{\mathbf{b}}\mathbf{s}}$, do not depend on k and can be calculated by using the known correlation properties of pseudo-symbols derived in Chap. 2 [see (2.13) and (2.16)].

4.4 WLTV equalization

It has been shown in Chap. 2 that CPM signals for $h = 1/2+k$, with $k \in \mathbb{Z}$, are *noncircular* or *improper* (see [59],[63]), since they exhibit non-vanishing

conjugate correlation features (see Sec. 2.3). In this case, it is well known (see [12, 10, 76, 27, 26, 30, 31, 49, 64, 80, 11, 46, 14, 13]) that employing *widely-linear* signal processing, which jointly elaborate the received signal and its complex conjugate version, allows one to improve performances.

Thus, we consider here a front-end causal *widely-linear time-varying* (WLTV) equalizer of order $L_{\rm e} > 0$, whose input-output relationship is given by

$$\mathbf{y}(k) = \mathbf{F}_1^{\rm H}\tilde{\mathbf{z}}(k) + \mathbf{F}_2^{\rm H}(k)\tilde{\mathbf{z}}^*(k) = \mathbf{F}^{\rm H}(k)\mathbf{z}(k) \tag{4.22}$$

for $k \in \mathbb{Z}$, where $\mathbf{F}_1(k), \mathbf{F}_2(k) \in \mathbb{C}^{N(L_{\rm e}+1)\times Q}$ collect all the equalizer parameters, $\mathbf{F}(k) \triangleq [\mathbf{F}_1^{\rm T}(k), \mathbf{F}_2^{\rm T}(k)]^{\rm T} \in \mathbb{C}^{2N(L_{\rm e}+1)\times Q}$ and $\mathbf{z}(k) \triangleq [\tilde{\mathbf{z}}^{\rm T}(k), \tilde{\mathbf{z}}^{\rm H}(k)]^{\rm T} \in \mathbb{C}^{2N(L_{\rm e}+1)}$, whereas from (4.9) the input vector $\tilde{\mathbf{z}}(k)$ is given by (4.11).

On the basis of (4.11), $\mathbf{z}(k)$ can also be expressed as

$$\mathbf{z}(k) = \mathbf{H}(k)\mathbf{C}\mathbf{b}(k) + \mathbf{w}(k) \tag{4.23}$$

where $\mathbf{H}(k) \in \mathbb{C}^{2N(L_{\rm e}+1)\times 2N(L_{\rm a}+1)}$ is the augmented channel matrix, defined as

$$\mathbf{H}(k) \triangleq \begin{bmatrix} \widetilde{\mathbf{H}}(k) & \mathbf{O}_{N(L_{\rm e}+1)\times N(L_{\rm a}+1)} \\ \mathbf{O}_{N(L_{\rm e}+1)\times N(L_{\rm a}+1)} & \widetilde{\mathbf{H}}^*(k) \end{bmatrix} \tag{4.24}$$

wheraes $\mathbf{C} \triangleq \mathbf{I}_2 \otimes \widetilde{\mathbf{C}} \in \mathbb{R}^{2N(L_{\rm a}+1)\times 2(QL_{\rm a}+L_{\rm c})}$, $\mathbf{b}(k) \triangleq [\tilde{\mathbf{b}}^{\rm T}(k), \tilde{\mathbf{b}}^{\rm H}(k)]^{\rm T} \in \mathbb{C}^{2(QL_{\rm a}+L_{\rm c})}$, and $\mathbf{w}(k) \triangleq [\tilde{\mathbf{w}}^{\rm T}(k), \tilde{\mathbf{w}}^{\rm H}(k)]^{\rm T} \in \mathbb{C}^{2N(L_{\rm e}+1)}$. Synthesis of ZF and MMSE widely-linear equalizers is described in the following.

4.4.1 WLTV-ZF equalizer

Similarly to the LTV case, in the absence of noise, perfect or *zero-forcing* (ZF) recovery can be obtained by using a widely-linear time-varying ZF equalizer (see [28]). To this end, by considering the deterministic relationship (2.19) between the pseudo-symbols and their complex conjugate versions shown in Chap. 2 [see (2.19)], we can express the conjugate vector $\tilde{\mathbf{b}}^*(k)$ as

$$\tilde{\mathbf{b}}^*(k) = (-1)^{k+1}\widetilde{\mathbf{J}}\tilde{\mathbf{b}}(k) \tag{4.25}$$

where $\widetilde{\mathbf{J}} \triangleq \operatorname{diag}\left[(-1)^{N_0^{(1)}}\mathbf{J}_{L_{\rm a}+L_0}, (-1)^{N_1^{(1)}}\mathbf{J}_{L_{\rm a}+L_1}, \ldots, (-1)^{N_{Q-1}^{(1)}}\mathbf{J}_{L_{\rm a}+L_{Q-1}}\right] \in \mathbb{Z}^{(QL_{\rm a}+L_{\rm c})\times(QL_{\rm a}+L_{\rm c})}$. Then, imposing the ZF condition $\mathbf{y}(k) = \mathbf{s}(k-d)$ to the equalizer output leads to the following system of linear equations:

$$\mathbf{F}^{\rm H}(k)\mathbf{H}(k)\mathbf{C}\mathbf{D}(k) = \mathbf{E}_d^{\rm T} \tag{4.26}$$

where $\mathbf{D}(k) \triangleq [\mathbf{I}_{QL_a+L_c}, (-1)^{k+1}\widetilde{\mathbf{J}}]^T \in \mathbb{Z}^{2(QL_a+L_c)\times(QL_a+L_c)}$.

The system of linear equation in (4.26) is consistent (see [7]) if and only if $\mathbf{D}^T(k)\mathbf{C}^T\mathbf{H}^H(k)[\mathbf{D}^T(k)\mathbf{C}^T\mathbf{H}^H(k)]^-\mathbf{E}_d = \mathbf{E}_d$, for all $k \in \mathbb{Z}$.

If the matrix $\mathbf{H}(k)\mathbf{CD}(k) \in \mathbb{C}^{2N(L_e+1)\times(QL_a+L_c)}$ is full-column rank, i.e., $\text{rank}[\mathbf{H}(k)\mathbf{CD}(k)] = QL_a + L_c$, for all $k \in \mathbb{Z}$, it results that $\mathbf{D}^T(k)\mathbf{C}^T\mathbf{H}^H(k)[\mathbf{D}^T(k)\mathbf{C}^T\mathbf{H}^H(k)]^- = \mathbf{I}_{QL_a+L_c}$, for all $k \in \mathbb{Z}$, and, then, the system in (4.26) turns out to be consistent independently of the equalization delay d. In this case, the *minimal norm* solution of the system in (4.26) is given (see, e.g., [7]) by

$$\mathbf{F}_{ZF}(k) = \mathbf{H}(k)\mathbf{CD}(k)\left[\mathbf{D}^T(k)\mathbf{C}^T\mathbf{H}^H(k)\mathbf{H}(k)\mathbf{CD}(k)\right]^{-1}\mathbf{E}_d \tag{4.27}$$

Since condition $\text{rank}[\mathbf{H}(k)\mathbf{CD}(k)] = QL_a + L_c$, for all $k \in \mathbb{Z}$, assures the consistency of the system in (4.26) and, thus, the existence of the WLTV-ZF equalizer, it seems natural to investigate the rank properties of $\mathbf{H}(k)\mathbf{CD}(k)$.

A necessary condition to achieve consistency is that $QL_a + L_c = Q(L_e + L_h) + L_c \leq 2N(L_e+1)$, from which

$$L_e \geq \frac{QL_h + L_c - 2N}{2N - Q} \tag{4.28}$$

Using the so-called *derotation* approach (see [20]), one can simplify the expression of $\mathbf{D}(k)$ by removing the inherent time-variability. This approach consists in multiplying first the vector $\tilde{\mathbf{z}}^*(k)$ by the alternating signal $(-1)^{k+1}$, with $k \in \mathbb{Z}$, and then applying the WLTV-ZF equalization to the input vector

$$\mathbf{z}_{DR}(k) \triangleq \begin{bmatrix} \tilde{\mathbf{z}}(k) \\ (-1)^{k+1}\tilde{\mathbf{z}}^*(k) \end{bmatrix} = \mathbf{H}(k)\mathbf{C}\begin{bmatrix} \tilde{\mathbf{b}}(k) \\ (-1)^{k+1}\tilde{\mathbf{b}}^*(k) \end{bmatrix} + \mathbf{w}_{DR}(k) \tag{4.29}$$

where $\mathbf{w}_{DR}(k) \triangleq [\mathbf{w}^T(k), (-1)^{k+1}\mathbf{w}^H(k)]^T$. Considering (4.25), one obtains $(-1)^{k+1}\tilde{\mathbf{b}}^*(k) = \widetilde{\mathbf{J}}\tilde{\mathbf{b}}(k)$, thus

$$\mathbf{z}_{DR}(k) = \mathbf{H}(k)\mathbf{CD}_{DR}\tilde{\mathbf{b}}(k) + \mathbf{w}_{DR}(k) \tag{4.30}$$

where $\mathbf{D}_{DR} \triangleq [\mathbf{I}_{QL_a+L_c}, \widetilde{\mathbf{J}}]^T \in \mathbb{Z}^{2(QL_a+L_c)\times(QL_a+L_c)}$.

Finally, the WLTV-ZF equalizer operating with the derotation approach is given by

$$\mathbf{F}_{ZF,DR}(k) = \mathbf{H}(k)\mathbf{CD}_{DR}\left[\mathbf{D}_{DR}^T\mathbf{C}^T\mathbf{H}^H(k)\mathbf{H}(k)\mathbf{CD}_{DR}\right]^{-1}\mathbf{E}_d \tag{4.31}$$

4.4.2 WLTV-MMSE equalizer

To counteract the noise enhancement typical of the ZF approach, we synthesize here the widely-linear version of the MMSE receiver, which minimizes the same objective function of Sec. 4.3.2, $\mathrm{MSE}[\widetilde{\mathbf{F}}(k)] \triangleq \mathbb{E}\left[\|\mathbf{y}(k)-\mathbf{s}(k-d)\|^2\right]$, for all $k \in \mathbb{Z}$, which can also be expressed now as

$$\begin{aligned}\mathrm{MSE}[\mathbf{F}(k)] &= \mathbb{E}\left[\mathrm{tr}\left\{[\mathbf{y}(k)-\mathbf{s}(k-d)][\mathbf{y}(k)-\mathbf{s}(k-d)]^{\mathrm{H}}\right\}\right] \\ &= \mathrm{tr}\left[\mathbf{F}^{\mathrm{H}}(k)\mathbf{R}_{\mathbf{zz}}(k)\mathbf{F}(k)-\mathbf{F}^{\mathrm{H}}(k)\mathbf{R}_{\mathbf{zs}}(k)-\mathbf{R}_{\mathbf{zs}}^{\mathrm{H}}(k)\mathbf{F}(k)+\mathbf{R}_{\mathbf{ss}}\right]\end{aligned} \tag{4.32}$$

It can be shown (see [39]) that

$$\begin{aligned}\mathbf{F}_{\mathrm{MMSE}}^{\mathrm{H}}(k) &\triangleq \underset{\mathbf{F}^{\mathrm{H}}(k)}{\arg\min}\left\{\mathrm{MSE}[\mathbf{F}(k)]\right\} \\ &= \underset{\mathbf{F}^{\mathrm{H}}(k)}{\arg\min}\left\{\mathrm{tr}\left[\mathbf{F}^{\mathrm{H}}(k)\mathbf{R}_{\mathbf{zz}}(k)\mathbf{F}(k)-\mathbf{F}^{\mathrm{H}}(k)\mathbf{R}_{\mathbf{zs}}(k)-\mathbf{R}_{\mathbf{zs}}^{\mathrm{H}}(k)\mathbf{F}(k)\right]\right\} \\ &= \mathbf{R}_{\mathbf{zs}}^{\mathrm{H}}(k)\mathbf{R}_{\mathbf{zz}}^{-1}(k)\end{aligned} \tag{4.33}$$

where $\mathbf{R}_{\mathbf{zz}}(k) \triangleq \mathbb{E}\left[\mathbf{z}(k)\mathbf{z}^{\mathrm{H}}(k)\right] \in \mathbb{C}^{2N(L_{\mathrm{e}}+1)\times 2N(L_{\mathrm{e}}+1)}$ denotes the statistical time-varying correlation matrix of $\mathbf{z}(k)$, and $\mathbf{R}_{\mathbf{zs}}(k) \triangleq \mathbb{E}\left[\mathbf{z}(k)\mathbf{s}^{\mathrm{H}}(k-d)\right] \in \mathbb{C}^{2N(L_{\mathrm{e}}+1)\times Q}$.

It can be readily obtained from (4.11) and assumptions **(a-4.2)** and **(a-4.3)** that

$$\mathbf{R}_{\mathbf{zz}}(k) = \mathbf{H}(k)\mathbf{C}\mathbf{R}_{\mathbf{bb}}(k)\mathbf{C}^{\mathrm{T}}\mathbf{H}^{\mathrm{H}}(k) + \sigma_v^2\mathbf{I}_{2N(L_{\mathrm{e}}+1)} \tag{4.34}$$

with $\mathbf{R}_{\mathbf{bb}}(k) \triangleq \mathbb{E}\left[\mathbf{b}(k)\mathbf{b}^{\mathrm{H}}(k)\right] \in \mathbb{C}^{2(QL_{\mathrm{a}}+L_{\mathrm{c}})\times 2(QL_{\mathrm{a}}+L_{\mathrm{c}})}$, and

$$\mathbf{R}_{\mathbf{zs}}(k) = \mathbf{H}(k)\mathbf{C}\mathbf{R}_{\mathbf{bs}}(k) \tag{4.35}$$

with $\mathbf{R}_{\mathbf{bs}} \triangleq \mathbb{E}\left[\mathbf{b}(k)\mathbf{s}^{\mathrm{H}}(k-d)\right] \in \mathbb{C}^{2(QL_{\mathrm{a}}+L_{\mathrm{c}})\times Q}$. Note that the exact expression of the entries of the statistical correlation matrix $\mathbf{R}_{\mathbf{bb}}(k)$, as well as those of $\mathbf{R}_{\mathbf{bs}}(k)$, now depend on k due to the time varying conjugate cross-correlation of the pseudo-symbols [see (2.16)]. In particular, one has:

$$\begin{aligned}\mathbf{R}_{\mathbf{bb}}(k) = \mathbb{E}\left[\mathbf{b}(k)\mathbf{b}^{\mathrm{H}}(k)\right] &= \begin{bmatrix}\mathbb{E}\left[\tilde{\mathbf{b}}(k)\tilde{\mathbf{b}}^{\mathrm{H}}(k)\right] & \mathbb{E}\left[\tilde{\mathbf{b}}(k)\tilde{\mathbf{b}}^{\mathrm{T}}(k)\right] \\ \mathbb{E}\left[\tilde{\mathbf{b}}^{*}(k)\tilde{\mathbf{b}}^{\mathrm{H}}(k)\right] & \mathbb{E}\left[\tilde{\mathbf{b}}^{*}(k)\tilde{\mathbf{b}}^{\mathrm{T}}(k)\right]\end{bmatrix} \\ &= \begin{bmatrix}\mathbf{R}_{\tilde{\mathbf{b}}\tilde{\mathbf{b}}} & \mathbf{R}_{\tilde{\mathbf{b}}\tilde{\mathbf{b}}^{*}}(k) \\ \mathbf{R}_{\tilde{\mathbf{b}}\tilde{\mathbf{b}}^{*}}^{*}(k) & \mathbf{R}_{\tilde{\mathbf{b}}\tilde{\mathbf{b}}}^{*}\end{bmatrix}\end{aligned} \tag{4.36}$$

$$\mathbf{R}_{\mathbf{bs}}(k) = \mathbb{E}\left[\mathbf{b}(k)\mathbf{s}^{\mathrm{H}}(k)\right] = \begin{bmatrix} \mathbb{E}\left[\tilde{\mathbf{b}}(k)\mathbf{s}^{\mathrm{H}}(k)\right] \\ \mathbb{E}\left[\tilde{\mathbf{b}}^{*}(k)\mathbf{s}^{\mathrm{H}}(k)\right] \end{bmatrix} = \begin{bmatrix} \mathbf{R}_{\tilde{\mathbf{b}}\mathbf{s}} \\ \mathbf{R}^{*}_{\tilde{\mathbf{b}}\mathbf{s}^{*}}(k) \end{bmatrix} \tag{4.37}$$

where the entries of $\mathbf{R}_{\tilde{\mathbf{b}}\tilde{\mathbf{b}}}$ and $\mathbf{R}_{\tilde{\mathbf{b}}\tilde{\mathbf{b}}^{*}}(k)$, as well as $\mathbf{R}_{\tilde{\mathbf{b}}\mathbf{s}}$ and $\mathbf{R}_{\tilde{\mathbf{b}}\mathbf{s}^{*}}(k)$ can be calculated using the expressions of cross-correlation and conjugate cross-correlation functions shown in Chap. 2 [see (2.13) and (2.16)].

4.5 Low-complexity receiving structures

In Sec. 4.2 we have shown that the CPM signal can be expressed as the sum of amplitude modulated signals (see [50]) (Laurent representation); such a representation has been employed to obtain the expression (4.9) for the received vector. However, the same representation can be used to synthesize simplified versions of both LTV and WLTV equalizers.

The key to achieve such a complexity reduction is to *approximate* the CPM signal by a sum of $Q_{\mathrm{r}} < Q = 2^{L-1}$ PAM components, so as to recover only a subset of $Q_{\mathrm{e}} \leq Q_{\mathrm{r}}$ corresponding pseudo-symbols, from which finally the transmitted symbols can be extracted (see [47]). This represents a viable strategy because it is well known that the first Laurent pulse $c_{\mathrm{a},0}(t)$, which represents the pulse of longest duration, i.e., $(L+1)T$, also happens to have the main energy and is the most important component of the signal (see [50]).

Such a feature is extremely clear when particular frequency shape pulse are used, with $h = 0.5$. Indeed, computer calculations [3] show that for CPM-GMSK signaling depicted in Fig. 2.2, with $h = 0.5$, $BT = 0.25$ and $L = 4$, a fraction 0.991944 of the signal energy is contained in the first PAM component, and a fraction 0.00803 of energy is carried by the second one (see [47]). Only a fraction 2.63×10^{-5} of the signal energy (-46 dB) is contained into the remaining six pulses, thus the signal can be well represented by using only the first pulse, and at most the second one (see [47]).

It is worthwhile to note that using only a subset of Laurent's pulses might not be sufficient to represent partial-response CPM signals having modulation indices other than one-half, for which the so-called *main pulse* [60] could be used. Nevertheless, the fact that high-order Laurent's pulses have low energy influences the rank of $\widetilde{\mathbf{C}}$ in (4.14) and makes the problem inherently ill-conditioned, thus to obtain a consistent system and correctly synthesize the

equalizers, we have to discard the contribution of high-order pulses. In this way, eq. (4.11) becomes

$$\tilde{\mathbf{z}}(k) \triangleq \begin{bmatrix} \mathbf{r}(k) \\ \mathbf{r}(k-1) \\ \vdots \\ \mathbf{r}(k-L_{\mathrm{e}}) \end{bmatrix} = \widetilde{\mathbf{H}}(k) \sum_{q=0}^{Q_{\mathrm{r}}-1} \widetilde{\mathbf{C}}_q \tilde{\mathbf{b}}_q(k) + \tilde{\mathbf{w}}(k) = \widetilde{\mathbf{H}}(k) \widetilde{\mathbf{C}}_{(\mathrm{r})} \tilde{\mathbf{b}}_{(\mathrm{r})}(k) + \tilde{\mathbf{w}}(k) \tag{4.38}$$

where $\widetilde{\mathbf{C}}_{(\mathrm{r})} \triangleq [\widetilde{\mathbf{C}}_0, \widetilde{\mathbf{C}}_1, \ldots, \widetilde{\mathbf{C}}_{Q_{\mathrm{r}}-1}] \in \mathbb{R}^{N(L_{\mathrm{a}}+1)\times(Q_{\mathrm{r}}L_{\mathrm{a}}+\tilde{L}_{\mathrm{c}})}$ and $\tilde{\mathbf{b}}_{(\mathrm{r})} \triangleq [\tilde{\mathbf{b}}_0^{\mathrm{T}}(k), \tilde{\mathbf{b}}_1^{\mathrm{T}}(k), \ldots, \tilde{\mathbf{b}}_{Q_{\mathrm{r}}-1}^{\mathrm{T}}(k)]^{\mathrm{T}} \in \mathbb{C}^{Q_{\mathrm{r}}L_{\mathrm{a}}+\tilde{L}_{\mathrm{c}}}$, with $Q_{\mathrm{r}} < Q$ chosen so as to obtain a full-column rank $\widetilde{\mathbf{C}}$, i.e., $\mathrm{rank}(\widetilde{\mathbf{C}}) = Q_{\mathrm{r}}L_{\mathrm{a}} + \tilde{L}_{\mathrm{c}}$, and $\tilde{L}_{\mathrm{c}} \triangleq \sum_{q=0}^{Q_{\mathrm{r}}-1} L_q$. The new necessary condition to be satisfied to have a consistent system is $N(L_{\mathrm{e}}+1) \geq Q_{\mathrm{r}}L_{\mathrm{a}} + \tilde{L}_{\mathrm{c}}$, from which

$$L_{\mathrm{e}} \geq \frac{Q_{\mathrm{r}}L_{\mathrm{h}} + \tilde{L}_{\mathrm{c}} - N}{N - Q_{\mathrm{r}}} \tag{4.39}$$

The maximum number of pseudo-symbols that could be recovered using this approach is Q_{r}. The resulting pseudo-symbols could be used to rebuild an equalized version of the CPM signal at the receiver, so as to apply further processing (see [47]).

We propose in Sec. 4.6 a simple recursive decision strategy that uses only two consecutive pseudo-symbols $s_{0,k}, s_{0,k-1}$, corresponding to the first Laurent's pulse to extract the information-bearing symbol a_k: in this case, to further reduce the equalizer complexity, we equalize only the first pseudo-symbol. In this way, the input-output relationships of the equalizers boil down to

$$y(k) = \tilde{\mathbf{f}}^{\mathrm{H}}(k)\tilde{\mathbf{z}}(k) \tag{4.40}$$

with $\tilde{\mathbf{f}}(k) \in \mathbb{C}^{N(L_{\mathrm{e}}+1)}$ for LTV equalizers, and

$$y(k) = \mathbf{f}_1^{\mathrm{H}}(k)\tilde{\mathbf{z}}(k) + \mathbf{f}_2^{\mathrm{H}}(k)\tilde{\mathbf{z}}^*(k) = \mathbf{f}^{\mathrm{H}}(k)\mathbf{z}(k) \tag{4.41}$$

with $\mathbf{f}_1(k), \mathbf{f}_1(k) \in \mathbb{C}^{N(L_{\mathrm{e}}+1)}$ and $\mathbf{f}(k) \in \mathbb{C}^{2N(L_{\mathrm{e}}+1)}$, for WLTV ones.

Bearing in mind eqs. (4.38), (4.40) and (4.41), with straightforward manipulation of the equations in Sec. 4.3 and Sec. 4.4, one can obtain new expressions for all the considered equalizers.

Giving as example the LTV-ZF synthesis, the problem (4.14) becomes

$$\tilde{\mathbf{f}}^{\mathrm{H}}(k)\widetilde{\mathbf{H}}\widetilde{\mathbf{C}}_{(\mathrm{r})} = \mathbf{e}_d^{\mathrm{T}} \tag{4.42}$$

where $\mathbf{e}_d \triangleq [\mathbf{e}_{d,0}^{\mathrm{T}}, \mathbf{0}_{L_1+L_a}^{\mathrm{T}}, \ldots, \mathbf{0}_{L_{Q_\mathrm{r}}+L_a}^{\mathrm{T}}]^{\mathrm{T}} \in \mathbb{B}^{Q_\mathrm{r}L_\mathrm{a}+\tilde{L}_\mathrm{c}}$.

The system of linear equation in (4.42) is consistent (see [7]) if and only if $\widetilde{\mathbf{C}}_{(\mathrm{r})}^{\mathrm{T}}\widetilde{\mathbf{H}}^{\mathrm{H}}(k)[\widetilde{\mathbf{C}}_{(\mathrm{r})}^{\mathrm{T}}\widetilde{\mathbf{H}}^{\mathrm{H}}(k)]^{-}\mathbf{e}_d = \mathbf{e}_d$, for all $k \in \mathbb{Z}$. If the matrix $\widetilde{\mathbf{H}}(k)\widetilde{\mathbf{C}}_{(\mathrm{r})} \in \mathbb{C}^{N(L_\mathrm{e}+1)\times(Q_\mathrm{r}L_\mathrm{a}+\tilde{L}_\mathrm{c})}$ is full-column rank, i.e., $\mathrm{rank}[\widetilde{\mathbf{H}}(k)\widetilde{\mathbf{C}}_{(\mathrm{r})}] = Q_\mathrm{r}L_\mathrm{a} + \tilde{L}_\mathrm{c}$, for all $k \in \mathbb{Z}$, it results that $\widetilde{\mathbf{C}}_{(\mathrm{r})}^{\mathrm{T}}\widetilde{\mathbf{H}}^{\mathrm{H}}(k)[\widetilde{\mathbf{C}}_{(\mathrm{r})}^{\mathrm{T}}\widetilde{\mathbf{H}}^{\mathrm{H}}(k)]^{-} = \mathbf{I}_{Q_\mathrm{r}L_\mathrm{a}+\tilde{L}_\mathrm{c}}$, for all $k \in \mathbb{Z}$, and, then, the system in (4.42) turns out to be consistent independently of the equalization delay d. In this case, the *minimal norm* solution of the system in (4.42) is (see, e.g., [7]) given by

$$\tilde{\mathbf{f}}_{\mathrm{ZF}}(k) = \widetilde{\mathbf{H}}(k)\widetilde{\mathbf{C}}_{(\mathrm{r})}\left[\widetilde{\mathbf{C}}_{(\mathrm{r})}^{\mathrm{T}}\widetilde{\mathbf{H}}^{\mathrm{H}}(k)\widetilde{\mathbf{H}}(k)\widetilde{\mathbf{C}}_{(\mathrm{r})}\right]^{-1}\mathbf{e}_d \tag{4.43}$$

4.6 Simplified recursive symbol detection

The second stage of the proposed receiver processes the pseudo-symbols estimates at the output of the first stage to recover the transmitted binary sequence a_k, with $k \geq 0$.

Based on (2.11), the generic qth pseudo-symbol in the interval $t \in [kT, (k+1)T]$ can be expressed as

$$s_{q,k} = s_{0,k-L}e^{j\pi h a_k}\prod_{\ell=1}^{L-1} e^{j\pi h[1-\beta_q(\ell)]a_{k-\ell}} \tag{4.44}$$

from which one obtains

$$\mathbf{s}(k) = \begin{bmatrix} s_{0,k} \\ s_{1,k} \\ \vdots \\ s_{Q-1,k} \end{bmatrix} = s_{0,k-L}e^{j\pi h a_k}\underbrace{\begin{bmatrix} \rho_0[\mathbf{a}_\mathrm{s}(k)] \\ \rho_1[\mathbf{a}_\mathrm{s}(k)] \\ \vdots \\ \rho_{Q-1}[\mathbf{a}_\mathrm{s}(k)] \end{bmatrix}}_{\boldsymbol{\rho}[\mathbf{a}_\mathrm{s}(k)]\in\mathbb{C}^Q} \tag{4.45}$$

where $\rho_q[\mathbf{a}_\mathrm{s}(k)] = \prod_{\ell=1}^{L-1} e^{j\pi h[1-\beta_q(\ell)]a_{k-\ell}}$, with $\mathbf{a}_\mathrm{s}(k) \triangleq [a_{k-1}, a_{k-2}, \ldots, a_{k-L+1}]^{\mathrm{T}} \in \{-1,1\}^{L-1}$.

It is clear from (4.44) that, in general, the pseudo-symbol $s_{q,k}$, with $q \in \{0,1,\ldots,Q-1\}$, depends on the pseudo-symbol $s_{0,k-L}$ and the last $L-1$ symbols $\{a_{k-1}, a_{k-2}, \ldots, a_{k-L+1}\}$, as well as the symbol a_k.

Let $\mathbf{y}(k)$ be the output of the equalizer, this suggests that one can use the VA, albeit with colored noise, to extract an estimate $\hat{a}_{k-d}$ of a_{k-d} from each entry of $\mathbf{y}(k) \approx \mathbf{s}(k-d)$, for high signal-to-noise ratio (SNR), and give somehow a weighted result (e.g. one can think to use a weighted mean based on the energy of each Laurent pulse). Let $h = m/p$, with $m, p \in \mathbb{Z}$, in this case the number of states to be considered in VA would be $p2^{L-1}$ if m is even, otherwise $p2^L$ if m is odd; e.g. if $L = 3$ and $h = 0.7$, we could have 80 states.

In order to reduce the number of states, i.e., the complexity of the decision, one can extract only the pseudo-symbol $s_{0,k-d}$, as shown in Sec. 4.5. In this case, note that (4.45) boils down to

$$s_{0,k} = s_{0,k-1} e^{j\pi h a_k} \tag{4.46}$$

Looking at (4.46), it is clear that the pseudo-symbol $s_{0,k}$ only depends on the previous pseudo-symbol $s_{0,k-1}$, as well as the symbol a_k. Also in this case one could use VA to extract an estimate $\hat{a}_{k-d}$ of a_{k-d} from the output of the equalizer $y(k) \approx s_{0,k-d}$, for high SNR. Let $h = m/p$, with $m, p \in \mathbb{Z}$, now the amount of states to be considered would be p if m is even, otherwise $2p$ if m is odd, with a significant complexity reduction.

Although more complicated strategies can be considered, we resort herein to a simple CPM demodulator that exploits the recursive representation (4.46) of the pseudo-symbols. Thus, we obtain an estimate $\hat{a}_{k-d}$ of a_{k-d} as

$$\hat{a}_{k-d} = \frac{1}{\pi h} \arg\{y(k) y^*(k-1)\} \tag{4.47}$$

Note that when $h = 0.5$ one has:

$$s_{0,k} = s_{0,k-1} e^{j\frac{\pi}{2} a_k} = j a_k s_{0,k-1} \tag{4.48}$$

from which it can be inferred that

$$\hat{a}_{k-d} = \Im\{y(k) y^*(k-1)\} \tag{4.49}$$

The value $\hat{a}_{k-d}$ is finally compared to a threshold to obtain an hard estimate of the transmitted symbol.

4.7 FRESH implementation

The synthesis of the first stage of the receiver described in Sec. 4.3 and Sec. 4.4 has been carried out without assuming a particular model for the LTV channel. In this section, instead, we exploit the parsimonious CE-BEM representation [32, 5, 52] of the LTV channel, described in Chap. 3 to obtain an alternative form of the receivers in the frequency domain, so-called *FRESH representation*.

The starting point is to express the discrete-time channel $h(k,\ell)$ in (4.5) via the CE-BEM as

$$h(k,\ell) = \sum_{q=-Q_{\rm h}/2}^{Q_{\rm h}/2} h_q(\ell) e^{j\frac{2\pi}{P}qk} \tag{4.50}$$

with $\ell \in \{0,1,\ldots,NL_{\rm h}\}$ and $k \in \mathscr{K}$, where the set $\mathscr{K} \triangleq \{k_0N, k_0N+1,\ldots,k_0N+N-1,(k_0+1)N,(k_0+1)N+1,\ldots,(k_0+K-1)N+N-1\}$ is the observation window of finite length $K>1$ (expressed in symbols), with $k_0 \in \mathbb{Z}$, $L_{\rm h}$ is the channel length (expressed in symbols), $P \geq KN$, $Q_{\rm h} \triangleq 2\lceil f_{\rm Dmax} PT_{\rm c}\rceil$, and $f_{\rm Dmax}$ denotes the Doppler spread of the channel. Hereafter, we assume that:

(a-4.5) the coefficients $\{h_q(\ell)\}_{q=-Q_{\rm h}/2}^{Q_{\rm h}/2}$ are perfectly known at the receiver, $\forall \ell \in \{0,1,\ldots,NL_{\rm h}\}$, since they can be estimated blindly (see [32, 75, 74, 77]) or by means of training sequences (see [56, 51]).

By employing (4.50), matrix $\widetilde{\mathbf{H}}(k)$ in (4.11) and (4.24) can be written as

$$\widetilde{\mathbf{H}}(k) = \sum_{q=-Q_{\rm h}/2}^{Q_{\rm h}/2} \widetilde{\mathbf{H}}_q e^{j\frac{2\pi}{P}qkN} \tag{4.51}$$

where

$$\widetilde{\mathbf{H}}_q \triangleq \begin{bmatrix} \mathbf{I}_N & \mathbf{O}_N & \cdots & \mathbf{O}_N \\ \mathbf{O}_N & e^{-j\frac{2\pi}{P}qN}\mathbf{I}_N & \cdots & \mathbf{O}_N \\ \vdots & \ddots & \ddots & \vdots \\ \mathbf{O}_N & \cdots & \mathbf{O}_N & e^{-j\frac{2\pi}{P}qL_{\rm e}N}\mathbf{I}_N \end{bmatrix} \mathbf{H}_q \in \mathbb{C}^{N(L_{\rm e}+1)\times N(L_{\rm a}+1)} \tag{4.52}$$

with $\mathbf{H}_q \in \mathbb{C}^{N(L_{\rm e}+1)\times N(L_{\rm a}+1)}$ representing an upper-triangular block Toeplitz matrix, whose the first N rows are given by $[\mathbf{H}_{0,q},\mathbf{H}_{1,q},\ldots,\mathbf{H}_{L_{\rm h},q},\overbrace{\mathbf{O}_N,\ldots,\mathbf{O}_N}^{L_{\rm e}}]$, where $\{\mathbf{H}_{\ell,q}\}_{i_1,i_2} = h_q(\ell N+i_1-i_2)e^{j\frac{2\pi}{P}qi_1}$, $\forall i_1,i_2 \in \{0,1,\ldots,N-1\}$.

If we define $R = P/N$, then (4.51) can be equivalently rewritten as[4]

$$\widetilde{\mathbf{H}}(k) = \sum_{p=0}^{R-1} \widetilde{\mathscr{H}}_p e^{j\frac{2\pi}{R}pk} \tag{4.53}$$

where

$$\widetilde{\mathscr{H}}_p \triangleq \begin{cases} \widetilde{\mathbf{H}}_p, & 0 \le p \le Q_{\mathrm{h}}/2; \\ \mathbf{O}_{N(L_{\mathrm{e}}+1)\times N(L_{\mathrm{a}}+1)}, & Q_{\mathrm{h}}/2+1 \le p \le R-Q_{\mathrm{h}}/2-1; \\ \widetilde{\mathbf{H}}_{p-R}, & R-Q_{\mathrm{h}}/2 \le p \le R-1. \end{cases} \tag{4.54}$$

It should be noted that (4.53) is the *discrete Fourier series* (DFS) expansion, with period R, of the periodically time-varying (PTV) matrix $\widetilde{\mathbf{H}}(k)$, with $\widetilde{\mathscr{H}}_p$ representing the DFS coefficients, with $p \in \{0,1,\ldots,R-1\}$.

Furthermore, substituting (4.53) and exploiting the DFS properties[5], the overall channel matrix (4.24) can be expressed as

$$\mathbf{H}(k) = \sum_{p=0}^{R-1} \mathscr{H}_p e^{j\frac{2\pi}{R}pk} \tag{4.55}$$

It should be noted that (4.55) is the DFS expansion, with period R, of the PTV matrix $\mathbf{H}(k)$, and the DFS coefficients $\mathscr{H}_p$, with $p \in \{0,1,\ldots,R-1\}$, can be expressed as

$$\mathscr{H}_p \triangleq \begin{bmatrix} \widetilde{\mathscr{H}}_p & \mathbf{O}_{N(L_{\mathrm{e}}+1)\times N(L_{\mathrm{a}}+1)} \\ \mathbf{O}_{N(L_{\mathrm{e}}+1)\times N(L_{\mathrm{a}}+1)} & \widetilde{\mathscr{H}}^*_{(-p)_R} \end{bmatrix} \tag{4.56}$$

As a consequence, all the proposed LTV and WLTV equalizers turn out to be also PTV with period R and, thus, they can be expressed by means of their DFS representation over R points:

$$\widetilde{\mathbf{F}}(k) = \sum_{p=0}^{R-1} \widetilde{\mathbf{F}}_p e^{j\frac{2\pi}{R}pk} \tag{4.57}$$

$$\mathbf{F}(k) = \sum_{p=0}^{R-1} \mathbf{F}_p e^{j\frac{2\pi}{R}pk} \tag{4.58}$$

[4] In the sequel, for sake of simplicity, we assume that P/N is an even integer.

[5] Let $X_p = \mathrm{DFS}[x(n)]$, $Y_p = \mathrm{DFS}[y(n)]$, and $y(n) = x^*(n)$, with $x(n)$ and $y(n)$ periodic sequences with period R, it can be shown that $Y_p = X^*_{(-p)_R}$.

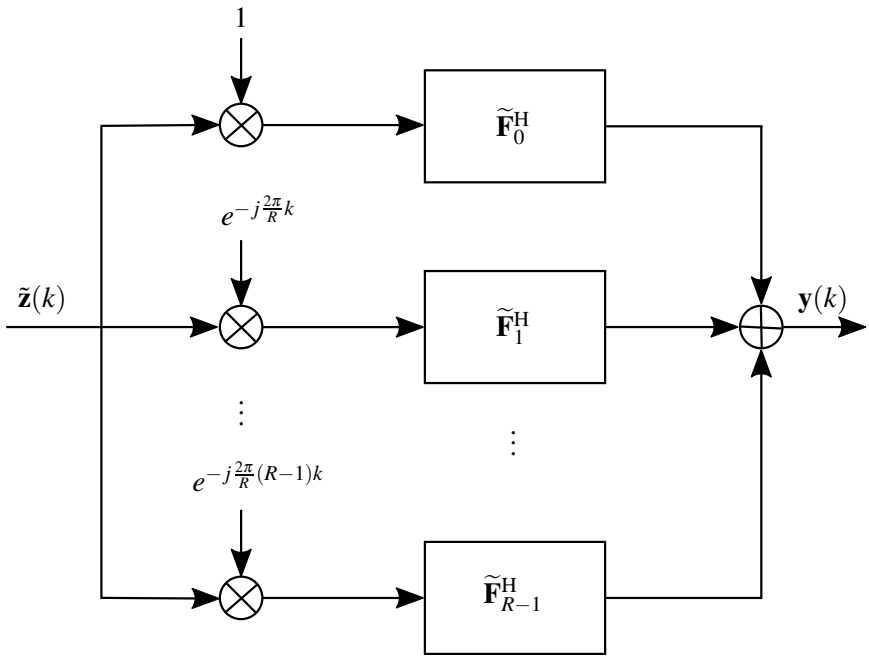

Figure 4.1: FRESH representation of the LTV-ZF equalizer.

where $\widetilde{\mathbf{F}}_p$ and $\mathbf{F}_p$ are, respectively, the DFS coefficients of $\widetilde{\mathbf{F}}(k)$ and $\mathbf{F}(k)$. To obtain more compact forms,, we define the following matrices:

$$\widetilde{\mathbf{\Psi}} \triangleq [\widetilde{\mathbf{F}}_0^{\mathrm{T}}, \widetilde{\mathbf{F}}_1^{\mathrm{T}}, \ldots, \widetilde{\mathbf{F}}_{R-1}^{\mathrm{T}}]^{\mathrm{T}} \in \mathbb{C}^{RN(L_{\mathrm{e}}+1)\times Q} \tag{4.59}$$

$$\mathbf{\Psi} \triangleq [\mathbf{F}_0^{\mathrm{T}}, \mathbf{F}_1^{\mathrm{T}}, \ldots, \mathbf{F}_{R-1}^{\mathrm{T}}]^{\mathrm{T}} \in \mathbb{C}^{2RN(L_{\mathrm{e}}+1)\times Q} \tag{4.60}$$

collecting all the equalization parameters.

Substituting (4.57) in the input-output relationship (4.10) of the LTV equalizers one obtains

$$\mathbf{y}(k) = \sum_{p=0}^{R-1} \widetilde{\mathbf{F}}_p^{\mathrm{H}} e^{-j\frac{2\pi}{R}pk} \tilde{\mathbf{z}}(k) = \widetilde{\mathbf{\Psi}}^{\mathrm{H}} [\boldsymbol{\zeta}(k) \otimes \tilde{\mathbf{z}}(k)] \tag{4.61}$$

where $\boldsymbol{\zeta}(k) \triangleq [1, e^{-j\frac{2\pi}{R}k}, \ldots, e^{-j\frac{2\pi}{R}(R-1)k}]^{\mathrm{T}} \in \mathbb{C}^R$. That is, the LTV equalizer can be regarded as a parallel bank of R LTI equalizers, each driven by a different frequency-shifted version of $\tilde{\mathbf{z}}(k)$ (see Fig. 4.1).

4.7.1 FRESH-LTV-ZF equalizer

By substituting (4.57) and (4.53), the ZF condition (4.14) can be rewritten as

$$\widetilde{\mathbf{C}}^{\mathrm{T}}\left[\sum_{p=0}^{R-1}\widetilde{\mathscr{H}}_p e^{j\frac{2\pi}{R}pk}\right]^{\mathrm{H}}\left[\sum_{p=0}^{R-1}\widetilde{\mathbf{F}}_p e^{j\frac{2\pi}{R}pk}\right]=\mathbf{E}_d \tag{4.62}$$

It can be noticed that the first term is the product of two periodic sequences with period R. Considering again the properties[5] of DFS and that the DFS of the product of two periodic sequences is the circular convolution of their respective DFSs, eq. (4.62) can be expressed as

$$\sum_{p=0}^{R-1}\left[\sum_{m=0}^{R-1}\widetilde{\mathbf{C}}^{\mathrm{T}}\widetilde{\mathscr{H}}^{\mathrm{H}}_{(m-p)_R}\widetilde{\mathbf{F}}_m\right]e^{j\frac{2\pi}{R}pk}=\mathbf{E}_d \tag{4.63}$$

Since identity (4.63) must hold for all $k\in\mathbb{Z}$ and $\mathbf{E}_d$ is time-invariant, one obtains

$$\sum_{m=0}^{R-1}\widetilde{\mathbf{C}}^{\mathrm{T}}\widetilde{\mathscr{H}}^{\mathrm{H}}_{(m-p)_R}\widetilde{\mathbf{F}}_m=\begin{cases}\mathbf{E}_d, & \text{for } p=0;\\ \mathbf{O}_{(QL_{\mathrm{a}}+L_{\mathrm{c}})\times Q}, & \text{for } p\in\{1,2,\ldots,R-1\};\end{cases} \tag{4.64}$$

which, using (4.59) can be compactly rewritten as

$$\widetilde{\mathscr{C}}^{\mathrm{T}}\widetilde{\mathscr{H}}^{\mathrm{H}}_{\mathrm{circ}}\widetilde{\mathbf{\Psi}}=\mathscr{E}_d \tag{4.65}$$

where $\widetilde{\mathscr{C}}\triangleq\mathbf{I}_R\otimes\widetilde{\mathbf{C}}\in\mathbb{R}^{RN(L_{\mathrm{a}}+1)\times R(QL_{\mathrm{a}}+L_{\mathrm{c}})}$ and the matrix $\widetilde{\mathscr{H}}_{\mathrm{circ}}\in\mathbb{C}^{RN(L_{\mathrm{e}}+1)\times RN(L_{\mathrm{a}}+1)}$ is block circulant (see [40]) whose $(i+1,j+1)$ block, for $0\le i,j\le R-1$, is given by $\widetilde{\mathscr{H}}_{(i-j)_R}\in\mathbb{C}^{N(L_{\mathrm{e}}+1)\times N(L_{\mathrm{a}}+1)}$, i.e.,

$$\widetilde{\mathscr{H}}_{\mathrm{circ}}\triangleq\begin{bmatrix}\widetilde{\mathscr{H}}_0 & \widetilde{\mathscr{H}}_{R-1} & \cdots & \widetilde{\mathscr{H}}_2 & \widetilde{\mathscr{H}}_1\\ \widetilde{\mathscr{H}}_1 & \widetilde{\mathscr{H}}_0 & \cdots & \widetilde{\mathscr{H}}_3 & \widetilde{\mathscr{H}}_2\\ \vdots & \vdots & \ddots & \vdots & \vdots\\ \widetilde{\mathscr{H}}_{R-1} & \widetilde{\mathscr{H}}_{R-2} & \cdots & \widetilde{\mathscr{H}}_1 & \widetilde{\mathscr{H}}_0\end{bmatrix} \tag{4.66}$$

whereas $\mathscr{E}_d\triangleq[\mathbf{E}_d^{\mathrm{T}},\mathbf{O}_{Q\times(QL_{\mathrm{a}}+L_{\mathrm{c}})},\ldots,\mathbf{O}_{Q\times(QL_{\mathrm{a}}+L_{\mathrm{c}})}]^{\mathrm{T}}\in\mathbb{B}^{R(QL_{\mathrm{a}}+L_{\mathrm{c}})\times Q}$.

Under the same conditions reported in Sec. 4.3.1, the solution of (4.65) in the minimal-norm sense is given by

$$\widetilde{\mathbf{\Psi}}_{\mathrm{ZF}}=\widetilde{\mathscr{H}}_{\mathrm{circ}}\widetilde{\mathscr{C}}\left(\widetilde{\mathscr{C}}^{\mathrm{T}}\widetilde{\mathscr{H}}^{\mathrm{H}}_{\mathrm{circ}}\widetilde{\mathscr{H}}_{\mathrm{circ}}\widetilde{\mathscr{C}}\right)^{-1}\mathscr{E}_d. \tag{4.67}$$

4.7.2 FRESH-LTV-MMSE equalizer

The expression (4.33) can be interpreted as the solution of the following linear system:

$$\mathbf{R}_{\tilde{\mathbf{z}}\tilde{\mathbf{z}}}(k)\widetilde{\mathbf{F}}(k) = \mathbf{R}_{\tilde{\mathbf{z}}\mathbf{s}}(k) \tag{4.68}$$

Taking into account (4.20) and (4.53), it can be proven that $\mathbf{R}_{\tilde{\mathbf{z}}\tilde{\mathbf{z}}}(k)$ admits the DFS expansion

$$\mathbf{R}_{\tilde{\mathbf{z}}\tilde{\mathbf{z}}}(k) = \sum_{p=0}^{R-1} \mathscr{R}_{\tilde{\mathbf{z}}\tilde{\mathbf{z}}}^{[p]} e^{j\frac{2\pi}{R}pk} \tag{4.69}$$

where the DFS coefficients $\{\mathscr{R}_{\tilde{\mathbf{z}}\tilde{\mathbf{z}}}^{[p]}\}_{p=0}^{R-1}$ can be interpreted as the *cyclic correlation matrices* (CCMs, see [23]) of $\tilde{\mathbf{z}}(k)$. By substituting (4.53), (4.57), and (4.69), eq. (4.68) can be expressed as

$$\widetilde{\mathscr{R}}_{\text{circ}}\widetilde{\mathbf{\Psi}} = \widetilde{\mathbf{\Xi}}\widetilde{\mathbf{C}}\mathbf{R}_{\tilde{\mathbf{b}}\mathbf{s}} \tag{4.70}$$

where $\widetilde{\mathbf{\Xi}} \triangleq [\widetilde{\mathscr{H}}_0^{\mathrm{T}}, \widetilde{\mathscr{H}}_1^{\mathrm{T}}, \ldots, \widetilde{\mathscr{H}}_{R-1}^{\mathrm{T}}]^{\mathrm{T}} \in \mathbb{C}^{RN(L_e+1)\times N(L_a+1)}$ and $\widetilde{\mathscr{R}}_{\text{circ}} \in \mathbb{C}^{RN(L_e+1)\times RN(L_e+1)}$ is a block circulant matrix (see [40]) whose $(i+1, j+1)$ block, for $0 \le i, j \le R-1$, is given by $\mathscr{R}_{\tilde{\mathbf{z}}\tilde{\mathbf{z}}}^{[(i-j)_R]} \in \mathbb{C}^{N(L_e+1)\times N(L_e+1)}$, i.e.,

$$\widetilde{\mathscr{R}}_{\text{circ}} \triangleq \begin{bmatrix} \mathscr{R}_{\tilde{\mathbf{z}}\tilde{\mathbf{z}}}^{[0]} & \mathscr{R}_{\tilde{\mathbf{z}}\tilde{\mathbf{z}}}^{[R-1]} & \cdots & \mathscr{R}_{\tilde{\mathbf{z}}\tilde{\mathbf{z}}}^{[2]} & \mathscr{R}_{\tilde{\mathbf{z}}\tilde{\mathbf{z}}}^{[1]} \\ \mathscr{R}_{\tilde{\mathbf{z}}\tilde{\mathbf{z}}}^{[1]} & \mathscr{R}_{\tilde{\mathbf{z}}\tilde{\mathbf{z}}}^{[0]} & \cdots & \mathscr{R}_{\tilde{\mathbf{z}}\tilde{\mathbf{z}}}^{[3]} & \mathscr{R}_{\tilde{\mathbf{z}}\tilde{\mathbf{z}}}^{[2]} \\ \vdots & \vdots & \ddots & \vdots & \vdots \\ \mathscr{R}_{\tilde{\mathbf{z}}\tilde{\mathbf{z}}}^{[R-1]} & \mathscr{R}_{\tilde{\mathbf{z}}\tilde{\mathbf{z}}}^{[R-2]} & \cdots & \mathscr{R}_{\tilde{\mathbf{z}}\tilde{\mathbf{z}}}^{[1]} & \mathscr{R}_{\tilde{\mathbf{z}}\tilde{\mathbf{z}}}^{[0]} \end{bmatrix}. \tag{4.71}$$

Solution of (4.70) is given by

$$\widetilde{\mathbf{\Psi}}_{\text{MMSE}} = \widetilde{\mathscr{R}}_{\text{circ}}^{-1}\widetilde{\mathbf{\Xi}}\widetilde{\mathbf{C}}\mathbf{R}_{\tilde{\mathbf{b}}\mathbf{s}} \tag{4.72}$$

4.7.3 FRESH-WLTV-ZF equalizer

Considering the synthesis of the LTV-ZF equalizer using the de-rotation approach, the expression of the equalizer (4.31) represents the solution, in the minimal-norm sense, of the following linear system:

$$\mathbf{D}^{\mathrm{T}}\mathbf{C}^{\mathrm{T}}\mathbf{H}^{\mathrm{H}}(k)\mathbf{F}(k) = \mathbf{E}_d \tag{4.73}$$

By substituting (4.58) and (4.55), the ZF condition (4.14) can be rewritten as

$$\mathbf{D}^{\mathrm{T}}\mathbf{C}^{\mathrm{T}}\left[\sum_{p=0}^{R-1}\boldsymbol{\mathscr{H}}_p e^{j\frac{2\pi}{R}pk}\right]^{\mathrm{H}}\left[\sum_{p=0}^{R-1}\mathbf{F}_p e^{j\frac{2\pi}{R}pk}\right]=\mathbf{E}_d \tag{4.74}$$

Following the same steps in Sec. 4.7.1 one obtains the linear system

$$\boldsymbol{\mathscr{C}}^{\mathrm{T}}\boldsymbol{\mathscr{H}}_{\mathrm{circ}}^{\mathrm{H}}\boldsymbol{\Psi}=\boldsymbol{\mathscr{E}}_d \tag{4.75}$$

where $\boldsymbol{\mathscr{C}} \triangleq \mathbf{I}_R \otimes (\mathbf{CD}) \in \mathbb{R}^{2RN(L_{\mathrm{a}}+1)\times R(QL_{\mathrm{a}}+L_{\mathrm{c}})}$ and the matrix $\boldsymbol{\mathscr{H}}_{\mathrm{circ}} \in \mathbb{C}^{2RN(L_{\mathrm{e}}+1)\times 2RN(L_{\mathrm{a}}+1)}$ is block circulant (see [40]) whose $(i+1,j+1)$ block, for $0\leq i,j\leq R-1$, is given by $\boldsymbol{\mathscr{H}}_{(i-j)_R} \in \mathbb{C}^{2N(L_{\mathrm{e}}+1)\times 2N(L_{\mathrm{a}}+1)}$, i.e.,

$$\boldsymbol{\mathscr{H}}_{\mathrm{circ}} \triangleq \begin{bmatrix} \boldsymbol{\mathscr{H}}_0 & \boldsymbol{\mathscr{H}}_{R-1} & \cdots & \boldsymbol{\mathscr{H}}_2 & \boldsymbol{\mathscr{H}}_1 \\ \boldsymbol{\mathscr{H}}_1 & \boldsymbol{\mathscr{H}}_0 & \cdots & \boldsymbol{\mathscr{H}}_3 & \boldsymbol{\mathscr{H}}_2 \\ \vdots & \vdots & \ddots & \vdots & \vdots \\ \boldsymbol{\mathscr{H}}_{R-1} & \boldsymbol{\mathscr{H}}_{R-2} & \cdots & \boldsymbol{\mathscr{H}}_1 & \boldsymbol{\mathscr{H}}_0 \end{bmatrix} \tag{4.76}$$

Under the same conditions reported in Sec. 4.4.1, the solution of (4.75) in the minimal-norm sense is given by

$$\boldsymbol{\Psi}_{\mathrm{ZF}} = \boldsymbol{\mathscr{H}}_{\mathrm{circ}}\boldsymbol{\mathscr{C}}\left(\boldsymbol{\mathscr{C}}^{\mathrm{T}}\boldsymbol{\mathscr{H}}_{\mathrm{circ}}^{\mathrm{H}}\boldsymbol{\mathscr{H}}_{\mathrm{circ}}\boldsymbol{\mathscr{C}}\right)^{-1}\boldsymbol{\mathscr{E}}_d. \tag{4.77}$$

4.7.4 FRESH-WLTV-MMSE equalizer

To extend the derivation of the FRESH version of the WLTV-MMSE solution one starts from the following linear system:

$$\mathbf{R}_{\mathbf{zz}}(k)\mathbf{F}(k)=\mathbf{R}_{\mathbf{zs}}(k) \tag{4.78}$$

Taking into account (4.34), (4.35), and (4.55), it can be proven that $\mathbf{R}_{\mathbf{zz}}(k)$ and $\mathbf{R}_{\mathbf{zs}}(k)$ admit the DFS expansions

$$\mathbf{R}_{\mathbf{zz}}(k)=\sum_{p=0}^{R-1}\boldsymbol{\mathscr{R}}_{\mathbf{zz}}^{[p]}e^{j\frac{2\pi}{R}pk} \tag{4.79}$$

$$\mathbf{R}_{\mathbf{zs}}(k)=\sum_{p=0}^{R-1}\boldsymbol{\mathscr{R}}_{\mathbf{zs}}^{[p]}e^{j\frac{2\pi}{R}pk} \tag{4.80}$$

where $\{\boldsymbol{\mathscr{R}}_{\mathbf{zz}}^{[p]}\}_{P=0}^{R-1}$ and $\{\boldsymbol{\mathscr{R}}_{\mathbf{zs}}^{[p]}\}_{P=0}^{R-1}$ are, respectively, the DFS coefficients of $\mathbf{R}_{\mathbf{zz}}(k)$ and $\mathbf{R}_{\mathbf{zs}}(s)$.

Following the same steps of Sec. 4.7.2 we obtain from (4.78) the linear system

$$\boldsymbol{\mathscr{R}}_{\text{circ}}\boldsymbol{\Psi} = \boldsymbol{\mathscr{R}}_{\text{vec}} \tag{4.81}$$

where $\boldsymbol{\mathscr{R}}_{\text{circ}} \in \mathbb{C}^{2RN(L_e+1)\times 2RN(L_e+1)}$ is a block circulant matrix (see [40]) whose $(i+1, j+1)$ block, for $0 \le i, j \le R-1$, is given by $\boldsymbol{\mathscr{R}}_{\mathbf{zz}}^{[(i-j)_R]} \in \mathbb{C}^{2N(L_e+1)\times 2N(L_e+1)}$, i.e.,

$$\boldsymbol{\mathscr{R}}_{\text{circ}} \triangleq \begin{bmatrix} \boldsymbol{\mathscr{R}}_{\mathbf{zz}}^{[0]} & \boldsymbol{\mathscr{R}}_{\mathbf{zz}}^{[R-1]} & \cdots & \boldsymbol{\mathscr{R}}_{\mathbf{zz}}^{[2]} & \boldsymbol{\mathscr{R}}_{\mathbf{zz}}^{[1]} \\ \boldsymbol{\mathscr{R}}_{\mathbf{zz}}^{[1]} & \boldsymbol{\mathscr{R}}_{\mathbf{zz}}^{[0]} & \cdots & \boldsymbol{\mathscr{R}}_{\mathbf{zz}}^{[3]} & \boldsymbol{\mathscr{R}}_{\mathbf{zz}}^{[2]} \\ \vdots & \vdots & \ddots & \vdots & \vdots \\ \boldsymbol{\mathscr{R}}_{\mathbf{zz}}^{[R-1]} & \boldsymbol{\mathscr{R}}_{\mathbf{zz}}^{[R-2]} & \cdots & \boldsymbol{\mathscr{R}}_{\mathbf{zz}}^{[1]} & \boldsymbol{\mathscr{R}}_{\mathbf{zz}}^{[0]} \end{bmatrix} \tag{4.82}$$

and $\boldsymbol{\mathscr{R}}_{\text{vec}} \in \mathbb{C}^{2RN(L_e+1)\times Q}$ is defined as

$$\boldsymbol{\mathscr{R}}_{\text{vec}} \triangleq \begin{bmatrix} \boldsymbol{\mathscr{R}}_{\mathbf{zs}}^{[0]} \\ \boldsymbol{\mathscr{R}}_{\mathbf{zs}}^{[1]} \\ \vdots \\ \boldsymbol{\mathscr{R}}_{\mathbf{zs}}^{[R-1]} \end{bmatrix} \tag{4.83}$$

Finally, solution of (4.81) is given by

$$\boldsymbol{\Psi}_{\text{MMSE}} = \boldsymbol{\mathscr{R}}_{\text{circ}}^{-1}\boldsymbol{\mathscr{R}}_{\text{vec}} \tag{4.84}$$

4.7.5 Complexity issues

All the FRESH implementations presented so far require inversion of large matrices:

- $\widetilde{\boldsymbol{\mathscr{C}}}^{\text{T}}\widetilde{\boldsymbol{\mathscr{H}}}_{\text{circ}}^{\text{H}}\widetilde{\boldsymbol{\mathscr{H}}}_{\text{circ}}\widetilde{\boldsymbol{\mathscr{C}}} \in \mathbb{C}^{R(QL_a+L_c)\times R(QL_a+L_c)}$ [see (4.67)],
- $\widetilde{\boldsymbol{\mathscr{R}}}_{\text{circ}} \in \mathbb{C}^{RN(L_e+1)\times RN(L_e+1)}$ [see (4.72)],
- $\boldsymbol{\mathscr{C}}^{\text{T}}\boldsymbol{\mathscr{H}}_{\text{circ}}^{\text{H}}\boldsymbol{\mathscr{H}}_{\text{circ}}\boldsymbol{\mathscr{C}} \in \mathbb{C}^{R(QL_a+L_c)\times R(QL_a+L_c)}$ [see (4.77)],
- $\boldsymbol{\mathscr{R}}_{\text{circ}} \in \mathbb{C}^{2RN(L_e+1)\times 2RN(L_e+1)}$ [see (4.84)].

However, it is possible to reduce the complexity of the synthesis. Reasoning as in [79, 78], it can be shown that, due to the block circulant nature of such matrices, a much simpler inversion can be carried out operating on the smaller component blocks; moreover, the number of block inverses can be reduced by exploiting the Hermitian symmetry of the overall matrix.

Moreover, low-complexity suboptimal implementations of the FRESH receivers can be obtained as in [79, 78] by truncating the DFS series of (4.57) and (4.58) to $Q_c + 1 \ll R$ frequency shifts. The resulting FRESH implementation consists of a bank of only $Q_c + 1$ LTI equalizers instead of R ones.

Even though the complexity of FRESH implementation can be significantly reduced by the above-mentioned approaches, the related synthesis still requires a large number of matrix inversions. Thus, future investigations will be focused on further reducing the complexity of the proposed equalizers, by using iterative approaches.

4.8 Numerical results

In this section, Monte Carlo computer simulation results are presented to assess the effectiveness of the proposed equalizers, that is, the LTV-ZF, LTV-MMSE, WLTV-ZF, and WLTV-MMSE ones.

We consider two system configurations: the first employs a PCM/FM modulation format, largely used for the CNPC data-links of medium-to-large dimension UASs; the second one employs a GMSK modulation scheme, often used on smaller unmanned vehicles (see Sec. 1.2). The performances of both systems have been evaluated over two typical aeronautical doubly-selective channel: the takeoff/landing (TL) scenario and the en-route scenario (ER) (see Chap. 3), characterized by maximum delay spread values equal to 7 μs and 33 μs, respectively.

The oversampling factor is $N = 8$ for both the configurations, the channel length is $L_h = 2$ and $L_h = 8$ for the TL and ER scenarios, respectively, the equalizer length and delay are $L_e = L_h + 1$ and $d = 0$, respectively. Moreover, we considered values of the Doppler spread roughly equal to 1.2 kHz and 3.5 kHz for the TL and ER scenarios, respectively.

The parameters of the oversampled BEM model are $K = 1000$ and $P = 2KN = 16000$, resulting in $R = 2K = 2000$, whereas $Q_h + 1 = 25$ and 71 for

the TL and ER scenarios, respectively.

As a performance measure, we adopt the *average* (over 10 channel realizations) *bit-error rate* (ABER), which is reported as function of $\mathscr{E}_\mathrm{b}/N_0$ in dB; it is worthwhile to note that for each channel realization we generated 10^5 binary symbols and hence evaluate the BER over a large number of Monte Carlo trials. ABER performances of the proposed equalizers (LTV-ZF, LTV-MMSE, WLTV-ZF, and WLTV-MMSE), synthesized assuming perfect knowledge of the channel, are compared with those of LTI-ZF and LTI-MMSE, which are obtained considering a time-averaged version of the same channel, in the same BEM observation window (K symbols). As a reference, we evaluate by simulation also the performances of the receiver implementing only the second-stage, without performing any equalization ("w/o EQ" in the plots).

It should be noted that in most cased the BER values obtained by simulations will not be compliant with the typical requirements for aeronautical telemetry link; this is due to the fact that we did not take into account the effect of diversity and coding (which are always present in a real telemetry link) and, moreover, we considered rather small values of $\mathscr{E}_\mathrm{b}/N_0$ (from 4 to 12 dB) in order to keep the number of Monte Carlo trials small. Our aim was mainly to compare the performances between the different techniques, taking as reference the LTI equalizer and the scheme without equalization.

4.8.1 PCM/FM configuration

First we consider a $R_b = 200$ kb/s data link employing CPM-1REC ($L = 1$), that is, PCM/FM or CPFSK, with $h = 0.7$. It is well known that for $h \neq 1/2 + k$, with $k \in \mathbb{Z}$, the one-sided CPM signal is asymptotically circular or proper (see Chap. 2) and (4.25) cannot be used to synthesize the WLTV-ZF equalizer; therefore, simulating performances of the WLTV-ZF equalizer in this configuration would not make sense.

Fig. 4.2 reports the ABER values versus $\mathscr{E}_\mathrm{b}/N_0$ ranging from 4 to 12 dB into the TL scenario. First we observe that, in this scenario, both LTV-ZF and LTV-MMSE equalization strategies exhibit the same performances, wheraes the LTI-ZF and LTI-MMSE equalizers fail completely due to ill-conditioning of the time-averaged channel. Moreover, the proposed equalizers largely outperform the "w/o EQ" receiver, especially for moderate-to-high values of

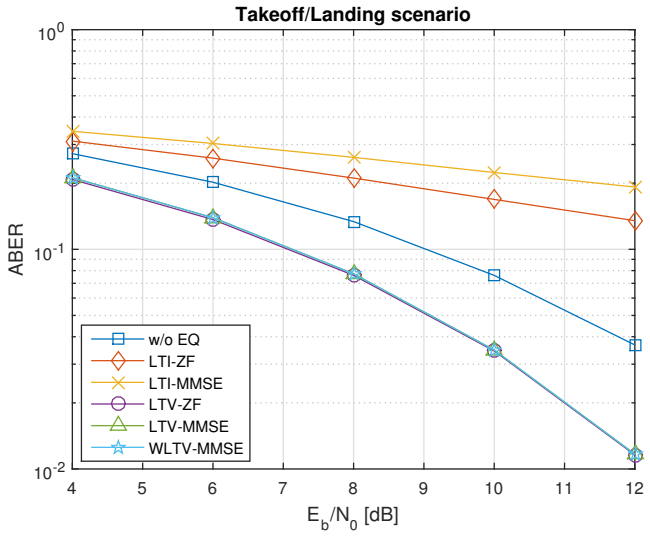

Figure 4.2: Average BER versus energy contrast for PCM/FM configuration into takeoff/landing (TL) scenario.

$\mathscr{E}_b/N_0$, where the performance gap of LTV equalizers approaches 2 dB over the "w/o EQ". Note that, since for $h = 0.7$ the CPM signal is circular or proper, the WLTV-MMSE equalizer exactly converges to its LTV counterpart, exhibiting therefore the same performances.

In Fig. 4.3, we consider the ER scenario, which is characterized by higher delay and Doppler spread values. Also in this case the proposed equalizers significantly outperform the "w/o EQ" receiver and their LTI counterparts. However, it can be observed that, in this more challenging scenario, the LTV-MMSE equalizer exhibits better performances than the LTV-ZF one. In particular, the advantage of the MMSE approach is apparent in this case, since the LTV-ZF equalizer performs comparably to the LTI-MMSE one. Also in this case it can be noted that, due to the circular properties of the CPM signal for $h = 0.7$, the WLTV-MMSE equalizer converges to the LTV-MMSE, exhibiting the same performances.

By comparing results of Fig. 4.2 and Fig. 4.3, it can be observed that the LTV-MMSE or WLTV-MMSE equalizers always provide the best performances; in general, when the modulation index $h \neq 1/2 + k$, with $k \in \mathbb{Z}$, i.e.,

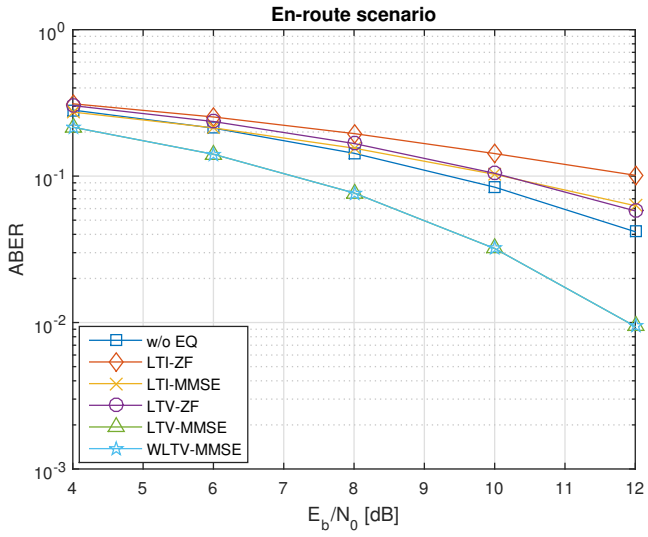

Figure 4.3: Average BER versus energy contrast for PCM/FM configuration into en-route (ER) scenario.

when the CPM signal does not exhibit noncircular or improper features, the LTV-MMSE should be used because it has a lower complexity than its WLTV counterpart.

4.8.2 GMSK configuration

In the second configuration, we consider a 200 kb/s data link employing a binary full-response ($L = 1$) GMSK modulation format with $h = 0.5$. In this case, the CPM signal exhibits noncircular or improper cyclic features (see Chap. 2), therefore, one can resort to the WLTV equalizers to obtain better performances (see Sec. 4.4).

Fig. 4.4 reports the ABER values versus $\mathscr{E}_\mathrm{b}/N_0$ ranging from 4 to 12 dB for the TL scenario. First, we observe that, in this scenario, the WLTV-ZF and WLTV-MMSE equalization strategies exhibit the same performances, and the same roughly happens for the LTV-ZF and LTV-MMSE ones. Once again, the LTI-ZF and LTI-MMSE equalizers completely fail due to ill-conditioning of the time-averaged channel. Moreover, the proposed equalizers largely outperform the "w/o EQ" receiver, especially for moderate-to-high values of $\mathscr{E}_\mathrm{b}/N_0$,

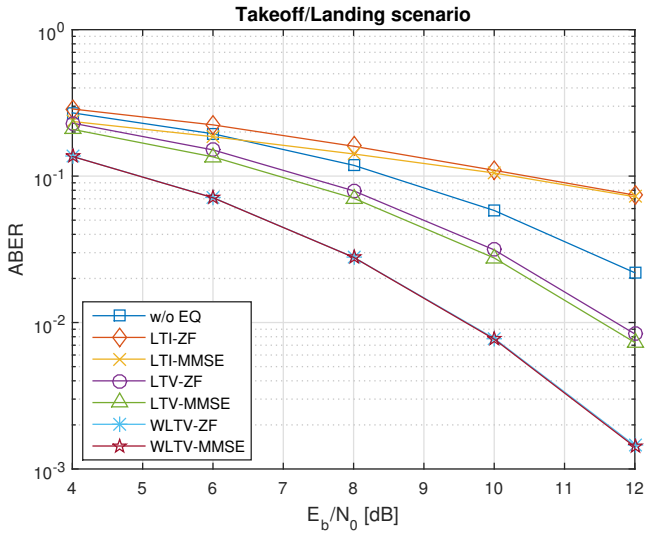

Figure 4.4: Average BER versus energy contrast for GMSK configuration into takeoff/landing (TL) scenario.

where the performance gap of LTV equalizers approaches 2 dB over the "w/o EQ", whereas the performance gap between WLTV equalizers and "w/o EQ" approaches reaches almost 4 dB. Note that, by exploiting the noncircular or improper features of the CPM signal, the WLTV equalizers always gain about 2 dB with respect to their LTV counterparts.

In Fig. 4.5, we consider the ER scenario, which is characterized by higher delay and Doppler spread values. Also in this case the proposed equalizers significantly outperform the "w/o EQ" receiver and their LTI counterparts. Once again, in this scenario, the MMSE versions of both the LTV and WLTV equalizers exhibit better performances than the LTV-ZF.

By comparing results of Fig. 4.4 and Fig. 4.5, it can be observed that the WLTV-MMSE equalizer always provides the best performance in both the TL and ER scenarios. We can conclude that, when the modulation index $h = 1/2 + k$, with $k \in \mathbb{Z}$, using widely-linear signal processing always provide better performances when compared with linear approaches.

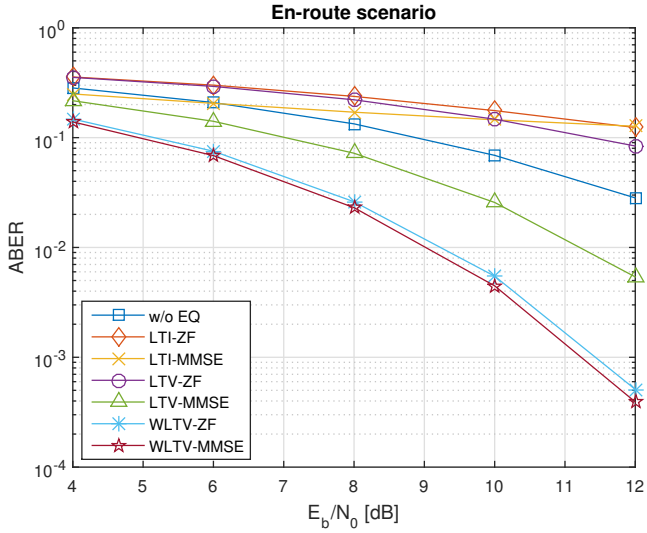

Figure 4.5: Average BER versus energy contrast for GMSK configuration into en-route (ER) scenario.

Conclusions

Communication systems are one of the fundamental milestones of the aeronautical environment, as well as one of its biggest challenges. Despite the constant growing of applications requiring high communication performances, the aviation context is reluctant to move toward new technologies. Common communication strategies (e.g., PCM/FM and GMSK) are not suitable to transmit at very high data rates over time- and/or frequency-dispersive air-ground channels, therefore, new requirements have to be fulfilled by an incremental approach, that is, by updating some parts of the legacy systems.

In this thesis, after introducing some open problems in aeronautical communications, we focused on signal and channel modeling and receiver synthesis for aeronautical communication data-links employing CPM modulations over doubly-selective wireless communication channels.

In particular, second-order statistical characterization of the pseudo-symbols arising from Laurent representation of CPM signals has been given, showing that some mathematical inconsistencies can be overcome by adopting a one-sided signal model.

As to channel modeling, the BEM model has been applied to typical aeronautical communication channels, and computer simulation results have shown that it gives a very good representation for all of the considered environment scenarios.

Dealing with receiver synthesis, we proposed efficient and low-complexity time-varying equalizers that exploit the CPM signal features, in order to compensate for the effects produced by rapidly time-varying aeronautical channels. In particular, LTV-ZF, MMSE-LTV, WLTV-ZF, and WLTV-MMSE receiver structures for CPM signals operating over doubly-selective channels have been proposed. Moreover, by using the BEM model, we have been able to obtain a

FRESH version for all of the proposed equalizers, that is, all of the equalizers can be described as a filter-bank composed by time-invariant equalizers.

With regard to computational complexity, we proposed a low-complexity approach to extract the information bearing symbols from pseudo-symbols; furthermore, the FRESH equalizers have been implemented by using well known methods that exploit the block circulant structure of the matrices involved .

The performances of the proposed equalizers have been assessed by computer simulations in two commonly used modulation strategies (PCM/FM and GMSK) operating over two challenging environments: takeoff/landing scenario and en-route scenario. The simulation results showed that time-varying equalization always provides better performances if compared with time-invariant strategies. Furthermore, the gap becomes huge when noncircular or improper features of the CPM signal are exploited for processing.

Although we noticed that the amount of time-invariant equalizers involved in FRESH equalization can be simply reduced by truncating the DFS series, the synthesis process needs anyway a large number of matrix inversions. Thus, future developments will be focused on further reducing complexity of the synthesis using iterative approaches. Furthermore, all of the proposed equalizers have been synthesized assuming perfect knowledge of the channel; future research will be aimed at estimating the BEM channel parameters from data in order to validate the proposed approaches in a real context.

Bibliography

[1] "NextGen homepage," http://www.faa.gov/nextgen.

[2] "SESAR homepage," http://www.sesarju.eu/.

[3] J. B. Anderson, T. Aulin, and C. E. Sundberg, *Digital Phase Modulation*. Springer, 1986.

[4] C. A. Balanis, *Advanced Engineering Electromagnetics*, 2nd ed. Wiley, 2012.

[5] I. Barhumi, G. Leus, and M. Moonen, "Time-varying FIR equalization for doubly selective channels," *IEEE Transactions on Wireless Communications*, vol. 4, no. 1, pp. 202–214, Jan. 2005.

[6] P. Bello, "Characterization of randomly time-variant linear channels," *IEEE Transactions on Communications Systems*, vol. 11, no. 4, pp. 360–393, Dec. 1963.

[7] A. Ben-Israel and T. N. E. Greville, *Generalized Inverses*. Springer, 2003.

[8] S. Bonter, D. R. Dunty, J. Greene, and D. W. Duff, "Predator UAV line-of-sight datalink terminal radio frequency test report (JSC-CR-04-066)," Tech. Rep., Sep. 2004.

[9] M. A. Boujelben, F. Bellili, S. Affes, and A. Stephenne, "SNR estimation over SIMO channels from linearly modulated signals," *IEEE Transactions on Signal Processing*, vol. 58, no. 12, pp. 6017–6028, Dec. 2010.

[10] S. Buzzi and M. Lops, "Performance analysis for the improved linear multiuser detectors in BPSK-modulated DS-CDMA systems," *IEEE Transactions on Communications*, vol. 51, no. 1, pp. 37–42, Jan. 2003.

[11] S. Buzzi, M. Lops, and S. Sardellitti, "Widely linear reception strategies for layered space-time wireless communications," *IEEE Transactions on Signal Processing*, vol. 54, no. 6, pp. 2252–2262, Jun. 2006.

[12] S. Buzzi, M. Lops, and A. M. Tulino, "A generalized minimum-mean-output-energy strategy for CDMA systems with improper MAI," *IEEE Transactions on Information Theory*, vol. 48, no. 3, pp. 761–767, Mar. 2002.

[13] A. S. Cacciapuoti, G. Gelli, and F. Verde, "FIR zero-forcing multiuser detection and code designs for downlink MC-CDMA," *IEEE Transactions on Signal Processing*, vol. 55, no. 10, pp. 4737–4751, Oct. 2007.

[14] P. Chevalier and F. Pipon, "New insights into optimal widely linear array receivers for the demodulation of BPSK, msk, and GMsk signals corrupted by noncircular interferences-application to saic," *IEEE Transactions on Signal Processing*, vol. 54, no. 3, pp. 870–883, Mar. 2006.

[15] E. Conte, *Lezioni di teoria dei segnali*, ser. Manuali per l'università Liguori. Liguori, 1996.

[16] A. V. Dandawate and G. B. Giannakis, "Nonparametric polyspectral estimators for kth-order (almost) cyclostationary processes," *IEEE Transactions on Information Theory*, vol. 40, no. 1, pp. 67–84, Jan. 1994.

[17] D. Darsena, G. Gelli, I. Iudice, and F. Verde, "Widely-linear transceiver design for amplify-and-forward MIMO relaying," in *2016 IEEE Sensor Array and Multichannel Signal Processing Workshop (SAM)*, Jul. 2016, pp. 1–5.

[18] D. Darsena, G. Gelli, F. Verde, and I. Iudice, "Blind LTV shortening of doubly selective OFDM channels for UAS applications," in *Metrology for Aerospace (MetroAeroSpace), 2015 IEEE*, Jun. 2015, pp. 557–561.

[19] ——, "LTV equalization of CPM signals over doubly-selective aeronautical channels," in *2016 IEEE Metrology for Aerospace (MetroAeroSpace)*, Jun. 2016, pp. 75–80.

[20] Z. Ding and G. Li, "Single-channel blind equalization for GSM cellular systems," *IEEE Journal on Selected Areas in Communications*, vol. 16, no. 8, pp. 1493–1505, Oct. 1998.

[21] F. Eurocontrol, "Communications operating concept and requirements for the future radio system (cocr)," *Eurocontrol/FAA*, 2007.

[22] K. Feher, "FQPSK-B, revision A1, digcom-feher patented technology transfer document," Jan. 1999.

[23] L. E. Franks, "Polyperiodic linear filtering," in *Cyclostationarity in Communications and Signal Processing*, W. A. Gardner, Ed. IEEE Press, 1994, pp. 240–266.

[24] F. Friedlander and M. Joshi, *Introduction to the Theory of Distributions*, 2nd ed. Cambridge University Press, 2008.

[25] W. A. Gardner, "Cyclic Wiener filtering: theory and method," *IEEE Transactions on Communications*, vol. 41, no. 1, pp. 151–163, Jan. 1993.

[26] G. Gelli, L. Paura, and A. R. P. Ragozini, "Blind widely linear multiuser detection," *IEEE Communications Letters*, vol. 4, no. 6, pp. 187–189, Jun. 2000.

[27] G. Gelli, L. Paura, and A. M. Tulino, "Cyclostationarity-based filtering for narrowband interference suppression in direct-sequence spread-spectrum systems," *IEEE Journal on Selected Areas in Communications*, vol. 16, no. 9, pp. 1747–1755, Dec. 1998.

[28] G. Gelli, L. Paura, and F. Verde, "On the existence of FIR zero-forcing equalizers for nonredundantly precoded transmissions through FIR channels," *IEEE Signal Processing Letters*, vol. 12, no. 3, pp. 202–205, Mar. 2005.

[29] M. Geoghegan, "Implementation and performance results for trellis detection of SOQPSK," in *Proceedings of the International Telemetering Conference*, Las Vegas, Nevada, Oct. 2001.

[30] H. Gerstacker, R. Schober, and A. Lampe, "Receivers with widely linear processing for frequency-selective channels," *IEEE Transactions on Communications*, vol. 51, no. 9, pp. 1512–1523, Sep. 2003.

[31] W. H. Gerstacker, F. Obernosterer, R. Schober, A. Lehmann, A. Lampe, and P. Gunreben, "Widely linear equalization for space-time block-coded transmission over fading ISI channels," in *Proceedings IEEE 56th Vehicular Technology Conference*, vol. 1, 2002, pp. 238–242 vol.1.

[32] G. B. Giannakis and C. Tepedelenlioglu, "Basis expansion models and diversity techniques for blind identification and equalization of time-varying channels," *Proceedings of the IEEE*, vol. 86, no. 10, pp. 1969–1986, Oct. 1998.

[33] A. Goldsmith, *Wireless Communications*. New York, NY, USA: Cambridge University Press, 2005.

[34] R. M. Gray, *Probability, Random Processes, and Ergodic Properties*. Springer-Verlag GmbH, 2009.

[35] E. Haas, "Aeronautical channel modeling," *IEEE Transactions on Vehicular Technology*, vol. 51, no. 2, pp. 254–264, Mar. 2002.

[36] T. J. Hill, "An enhanced, constant envelope, interoperable shaped offset QPSK (SOQPSK) waveform for improved spectral efficiency," in *Proceedings of the International Telemetering Conference*, Oct. 2000.

[37] F. Hlawatsch and G. Matz, Eds., *Wireless Communications Over Rapidly Time-Varying Channels*. Elsevier Science Publishing Co Inc, 2011.

[38] P. Hoeher, "A statistical discrete-time model for the wssus multipath channel," *IEEE Transactions on Vehicular Technology*, vol. 41, no. 4, pp. 461–468, Nov. 1992.

[39] M. Honig, U. Madhow, and S. Verdú, "Blind adaptive multiuser detection," *IEEE Transactions on Information Theory*, vol. 41, no. 4, pp. 944–960, Jul. 1995.

[40] R. A. Horn and C. R. Johnson, *Matrix analysis*, 2nd ed. New York, NY, USA: Cambridge University Press, 2012.

[41] K. Huang, "Supplementary proof for "exact and approximate construction of digital phase modulations by superposition of AMp" by p. a. laurent," *IEEE Transactions on Communications*, vol. 53, no. 2, pp. 234–237, Feb. 2005.

[42] X. Huang and Y. Li, "The PAM decomposition of CPM signals with integer modulation index," *IEEE Transactions on Communications*, vol. 51, no. 4, pp. 543–546, Apr. 2003.

[43] H. L. Hurd, "Nonparametric time series analysis for periodically correlated processes," *IEEE Transactions on Information Theory*, vol. 35, no. 2, pp. 350–359, Mar. 1989.

[44] R. Jain and F. Templin, "Requirements, challenges and analysis of alternatives for wireless datalinks for unmanned aircraft systems," *IEEE Journal on Selected Areas in Communications*, vol. 30, no. 5, pp. 852–860, Jun. 2012.

[45] W. C. Jakes and D. C. Cox, Eds., *Microwave Mobile Communications*. Wiley-IEEE Press, 1994.

[46] J.-J. Jeon, J. G. Andrews, and K.-M. Sung, "The blind widely linear minimum output energy algorithm for DS-CDMA systems," *IEEE Transactions on Signal Processing*, vol. 54, no. 5, pp. 1926–1931, May 2006.

[47] G. K. Kaleh, "Simple coherent receivers for partial response continuous phase modulation," *IEEE Journal on Selected Areas in Communications*, vol. 7, no. 9, pp. 1427–1436, Dec. 1989.

[48] S. Kato and K. Feher, "Correlated signal processor," Jan. 28 1986, US Patent 4,567,602. [Online]. Available: https://www.google.com/patents/US4567602

[49] A. Lampe, R. Schober, W. Gerstacker, and J. Huber, "A novel iterative multiuser detector for complex modulation schemes," *IEEE Journal on Selected Areas in Communications*, vol. 20, no. 2, pp. 339–350, Feb. 2002.

[50] P. Laurent, "Exact and approximate construction of digital phase modulations by superposition of amplitude modulated pulses (AMP)," *IEEE Transactions on Communications*, vol. 34, no. 2, pp. 150–160, Feb. 1986.

[51] G. Leus, "On the estimation of rapidly time-varying channels," in *2004 12th European Signal Processing Conference*, Sep. 2004, pp. 2227–2230.

[52] G. Leus, I. Barhumi, and M. Moonen, "Low-complexity serial equalization of doubly-selective channels," in *Proceedings of Sixth Baiona Workshop on Signal Processing in Communications*, 2003, pp. 69–74.

[53] M. Luise and G. M. Vitetta, *Teoria dei segnali*. McGraw-Hill Education, 2009.

[54] D. W. Matolak, "Air-ground channels & models: Comprehensive review and considerations for unmanned aircraft systems," in *2012 IEEE Aerospace Conference*, Mar. 2012, pp. 1–17.

[55] D. W. Matolak, I. Sen, and W. Xiong, "The 5-GHz airport surface area channel — Part I: Measurement and modeling results for large airports," *IEEE Transactions on Vehicular Technology*, vol. 57, no. 4, pp. 2014–2026, Jul. 2008.

[56] X. Meng and J. K. Tugnait, "Semi-blind time-varying channel estimation using superimposed training," in *2004 IEEE International Conference on Acoustics, Speech, and Signal Processing*, vol. 3, May 2004, pp. iii–797–800 vol.3.

[57] U. Mengali and M. Morelli, "Decomposition of M-ary CPM signals into PAM waveforms," *IEEE Transactions on Information Theory*, vol. 41, no. 5, pp. 1265–1275, Sep. 1995.

[58] A. Napolitano and C. M. Spooner, "Cyclic spectral analysis of continuous-phase modulated signals," *IEEE Transactions on Signal Processing*, vol. 49, no. 1, pp. 30–44, Jan. 2001.

[59] F. D. Neeser and J. L. Massey, "Proper complex random processes with applications to information theory," *IEEE Transactions on Information Theory*, vol. 39, no. 4, pp. 1293–1302, Jul. 1993.

[60] S. P. Neugebauer and Z. Ding, "Blind SIMO channel estimation for CPM using the laurent approximation," in *2004 IEEE International Symposium on Circuits and Systems (IEEE Cat. No.04CH37512)*, vol. 5, May 2004, pp. V–676–V–679 Vol.5.

[61] F. Pancaldi and G. M. Vitetta, "Equalization algorithms in the frequency domain for continuous phase modulations," *IEEE Transactions on Communications*, vol. 54, no. 4, pp. 648–658, Apr. 2006.

[62] M. Patzold, *Mobile Fading Channels*. New York, NY, USA: John Wiley & Sons, Inc., 2003.

[63] B. Picinbono, "On circularity," *IEEE Transactions on Vehicular Technology*, vol. 42, no. 12, pp. 3473–3482, Dec. 1994.

[64] B. Picinbono and P. Chevalier, "Widely linear estimation with complex data," *IEEE Transactions on Signal Processing*, vol. 43, no. 8, pp. 2030–2033, Aug. 1995.

[65] J. G. Proakis and M. Salehi, *Digital Communications*, 5th ed. McGraw-Hill Education - Europe, 2007.

[66] S. Saleem and G. L. Stüber, "Frequency-domain equalization for multi-h CPM — an application to aeronautical telemetry," in *2013 IEEE 24th Annual International Symposium on Personal, Indoor, and Mobile Radio Communications (PIMRC)*, Sep. 2013, pp. 1462–1466.

[67] H. Schulze, "Stochastic models and digital simulation of mobile channels," in *URSI/ITG Conf. in Kleinheubach*, 1988, pp. 473–483.

[68] I. Sen and D. W. Matolak, "The 5-GHz airport surface area channel — Part II: Measurement and modeling results for small airports," *IEEE Transactions on Vehicular Technology*, vol. 57, no. 4, pp. 2027–2035, Jul. 2008.

[69] L. Song and J. K. Tugnait, "Doubly-selective fading channel equalization: A comparison of the Kalman filter approach with the basis expansion model-based equalizers," *IEEE Transactions on Wireless Communications*, vol. 8, no. 1, pp. 60–65, Jan. 2009.

[70] J. Tan and G. L. Stuber, "Frequency-domain equalization for continuous phase modulation," *IEEE Transactions on Wireless Communications*, vol. 4, no. 5, pp. 2479–2490, Sep. 2005.

[71] R. C. C. Telemetry Group, "Telemetry standards. IRIG standard 106-15 Part 1," Tech. Rep., Jul. 2015. [Online]. Available: http://www.irig106.org/

[72] W. V. Thillo, F. Horlin, J. Nsenga, V. Ramon, A. Bourdoux, and R. Lauwereins, "Low-complexity linear frequency domain equalization for continuous phase modulation," *IEEE Transactions on Wireless Communications*, vol. 8, no. 3, pp. 1435–1445, Mar. 2009.

[73] M. K. Tsatsanis and G. B. Giannakis, "Adaptive methods for equalization of rapidly fading channels," in *Military Communications Conference, 1993. MILCOM '93. Conference record. Communications on the Move., IEEE*, vol. 2, Oct. 1993, pp. 639–643 vol.2.

[74] J. K. Tugnait and W. Luo, "Blind identification of time-varying channels using multistep linear predictors," *IEEE Transactions on Signal Processing*, vol. 52, no. 6, pp. 1739–1749, Jun. 2004.

[75] ——, "Linear prediction error method for blind identification of periodically time-varying channels," *IEEE Transactions on Signal Processing*, vol. 50, no. 12, pp. 3070–3082, Dec. 2002.

[76] A. M. Tulino and S. Verdú, "Asymptotic analysis of improved linear receivers for BPSK-CDMA subject to fading," *IEEE Journal on Selected Areas in Communications*, vol. 19, no. 8, pp. 1544–1555, Aug. 2001.

[77] F. Verde, "Subspace-based blind multiuser detection for quasi-synchronous MC-CDMA systems," *IEEE Signal Processing Letters*, vol. 11, no. 7, pp. 621–624, Jul. 2004.

[78] ——, "Low-complexity time-varying frequency-shift equalization for doubly selective channels," in *ISWCS 2013; The Tenth International Symposium on Wireless Communication Systems*, Aug. 2013, pp. 1–5.

[79] ——, "Frequency-shift zero-forcing time-varying equalization for doubly selective SIMO channels," *EURASIP Journal on Advances in Signal Processing*, vol. 2006, no. 1, pp. 1–14, 2006.

[80] Y. C. Yoon and H. Leib, "Maximizing SNR in improper complex noise and applications to CDMA," *IEEE Communications Letters*, vol. 1, no. 1, pp. 5–8, Jan. 1997.

[81] B. Younes, J. Brase, C. Patel, and J. Wesdock, "An assessment of shaped offset QPSK for use in NASA space network and ground network systems," in *Meetings of Consultative Committee for Space Data Systems*, Toulouse, France, Oct. 2000.

[82] T. Zemen and C. F. Mecklenbrauker, "Time-variant channel estimation using discrete prolate spheroidal sequences," *IEEE Transactions on Signal Processing*, vol. 53, no. 9, pp. 3597–3607, Sep. 2005.